

# UNCLASSIFIED

<b>AD NUMBER</b>
AD909773
<b>NEW LIMITATION CHANGE</b>
<b>TO</b> Approved for public release, distribution unlimited
<b>FROM</b> Distribution authorized to U.S. Gov't. agencies only; T&E; Apr 73. Other requests shall be referred to AFAL, Wright-Patterson AFB, OH 45433
<b>AUTHORITY</b>
AFWAL Ltr., 30 Sep 83

THIS PAGE IS UNCLASSIFIED

# STUDIES IN OPTICS

Brian J. Thompson, Principal Investigator, 716-275-2314

**Project Scientists:**

Brian J. Thompson

Michael Harcher

James M. Forsyth

Douglas C. Sinclair

N. Balasubramanian

The Institute of Optics  
The University of Rochester  
Rochester, N.Y. 14627

TECHNICAL REPORT AFAL-TR-73-112

April, 1973



Sponsored by  
Advanced Research Projects Agency

ARPA Order No. 745, Amend. 6

Program Code No. 62703-D

Contract No. F33615-70-C-1451, P00006

Effective Date of Contract: 70 Feb 13

Contract Expiration Date: 72 Dec 15

Amount of Contract: \$191,050

This document is subject to special export controls and each transmission to foreign countries must be made only with prior approval of the Air Force Avionics Laboratory.

The views and conclusions contained in this document are those of the authors and should not be interpreted as necessarily representing the official policies, either expressed or implied, of the Advanced Research Projects Agency or the U.S. Government.

Air Force Avionics Laboratory  
Air Force Systems Command  
Wright-Patterson Air Force Base, Ohio

WITH: AFAL/750

Distribution limited to U.S. Gov't. agencies only.  
Test and Evaluation: 11 Feb 1973  
For this document must be referred to other requests

# **NOTICE**

When Government drawings, specifications, or other data are used for any purpose other than in connection with a definitely related Government procurement operation, the United States Government thereby incurs no responsibility nor any obligation whatsoever; and the fact that the government may have formulated, furnished, or in any way supplied the said drawings, specifications, or other data, is not to be regarded by implication or otherwise as in any manner licensing the holder or any other person or corporation, or conveying any rights or permission to manufacture, use, or sell any patented invention that may in any way be related thereto.

Copies of this report should not be returned unless return is required by security considerations, contractual obligations, or notice on a specific document.

## STUDIES IN OPTICS

Brian J. Thompson  
Michael Hercher  
James M. Forsyth  
Douglas C. Sinclair  
N. Balasubramanian

TECHNICAL REPORT AFAL-TR-73-112

April 1973

This research was supported by the Advanced Research Projects Agency of the Department of Defense and was monitored by the AF Avionics Laboratory under Contract F33615-70-C-1451.

This document is subject to special export controls and each transmittal to foreign governments or foreign nationals may be made only with prior approval of the Air Force Avionics Laboratory.

Air Force Avionics Laboratory  
Air Force Systems Command  
Wright-Patterson Air Force Base, Ohio

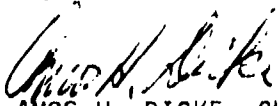
## FOREWORD

This study was conducted by members of The Institute of Optics, The University of Rochester, Rochester, New York 14627, under the sponsorship of the Advanced Research Projects Agency, Project No. 745, Contract F33615-70-C-1451. The Air Force program monitors were Capt. Robert B. Bell and Dr. Michael Heil, Air Force Avionics Laboratory, Air Force Systems Command, Wright-Patterson Air Force Base, Ohio 45433.

Portions of the study were performed by Institute of Optics graduate students Shui-Lin Chao, Jean Louis Meyzonnette, and Chand Roychoudhuri.

Inclusive dates of the project are 13 February 1970 to 15 December 1972. This technical report was submitted on 30 January 1973 and approved as of 4 April 1973.

This technical report has been reviewed and is approved for publication.



AMOS H. DICKE, Chief  
Electro-Optics Device Branch  
Electronic Technology Division

## ABSTRACT

These studies in optics relate to a variety of interconnected problems in the evaluation and controlled improvement of the output characteristics of lasers and the design of laser systems. Four major areas of endeavor are focussed upon in the sections of this report. Section II is a study of techniques for assessing laser beam propagation characteristics for both cw and pulsed lasers using holography in conjunction with interferometry. Section III concerns itself with some design problems of efficient solid state laser systems with high average power and low beam divergence with particular reference to the measurement and correction of optical distortion in solid laser rods. Section IV has as its objective a means of producing high-speed continuously scanning laser beams by use of intra-cavity beam deflection. The final portion is an evaluation of the techniques of ac interferometry.

## TABLE OF CONTENTS

	Page
SECTION I. REPORT SUMMARY .....	1
SECTION II. STUDY OF TECHNIQUES FOR ASSESSING AND IMPROVING LASER BEAM PROPAGATION CHARACTERISTICS Studying Beam Parameters of CW and Pulse Lasers using Holography in Conjunction with Interferometry.....	3
1. Introduction.....	3
2. Possible Methods.....	4
3. Early Local Reference Beam Techniques.....	8
a. Interferometric Techniques.....	8
b. Holographic Techniques.....	11
4. Test Experiments.....	14
a. Local Reference Beam Holography to Reconstruct Intensity Distribution....	14
b. Local Reference Beam Holography to Reconstruct Phase Structure and Sub- sequent Interferometry to Study Phase and Amplitude of a Wavefront.....	20
5. Application of the Method to Known Laser Wavefront ( $TEM_{01}$ CW He-Ne).....	23
6. Application of the Method to Ruby Pulse Laser.....	33
7. Application of the Method to Nd-Glass Laser.....	39
8. Conclusion.....	44
References.....	45

## CONTENTS (Continued)

	Page
SECTION III. THE DESIGN OF EFFICIENT SOLID STATE LASER SYSTEMS WITH HIGH AVERAGE POWER AND LOW BEAM DIVERGENCE	
The Measurement and Correction of Optical Distortion in Solid Laser Rods.....	49
1. Introduction.....	49
2. Measurement of Optical Distortion in Laser Rods.....	51
a. Mach-Zehnder Interferometer.....	53
b. Holographic Wavefront Recording.....	57
c. In-Line Hologram.....	60
3. Correction of Optical Distortion in Laser Rods.....	64
a. Introduction.....	64
b. Production of Scaled Correction Plates	65
4. Summary.....	76
SECTION IV. A STUDY OF LASER BEAM-STEERING TECHNIQUES LEADING TO BEAM-STEERING DEVICES IN THE MULTI-MHz RANGE.....	79
1. Introduction.....	79
2. Modulator Design.....	81
3. Modulator Construction.....	83
4. Additional Studies.....	85
5. Conclusion.....	86
Appendix: Construction of Large-Bore Ion Laser	87
References.....	89



## CONTENTS (Continued)

	Page
SECTION V. FURTHER RESEARCH IN IMAGE-FORMING OPTICS.....	91
1. Introduction.....	91
2. Theory.....	92
3. Experiment.....	117
References.....	123
Appendix .....	125

## LIST OF ILLUSTRATIONS

Figure		Page
1.	Local reference beam interferometry .	6
2.	Local reference beam holography .	6
3.	LRB holography to record a simulated "multimode" laser wavefront and its subsequent study through interferometry after reconstruction.	9
4.	Simple set up to test LRB holographic technique with "multimode" laser wavefront simulated from a TEM <sub>00</sub> CW He-Ne laser beam.	15
5.	Noisy laser wavefront simulated by an amplitude Ronchi mask. Direct record and reconstructions with original and "different" laser.	18
6.	Noisy laser wavefront simulated by a phase Ronchi mask. Direct record and reconstructions by original and "different" laser.	19
7.	Constant and variable frequency phase reconstruction through LRB holography. Verification by interferometric fringes.	22
8.	LRB holographic record of a real TEM <sub>01</sub> He-Ne CW laser wavefront.	26
9.	Pure and impure TEM <sub>01</sub> modes from a He-Ne laser.	27,28
10.	Reconstruction of the laser wavefront from the LRB hologram and its subsequent interferometric study.	30
11.	Reconstruction of the TEM <sub>01</sub> laser wavefront from the LRB hologram record and its interferogram.	31,32

Figure		Page
12.	LRB holography to record a ruby pulse laser wavefront and its subsequent study through interferometry after reconstruction.	34
13.	Intensity pattern of a ruby laser pulse reconstructed from a LRB holographic record.	35
14.	"Horizontal" fringes. Interferograms of the pulse laser wavefront reconstructed in continuous mode.	37
15.	"Vertical" fringes. Interferogram of the pulse laser wavefront reconstructed in continuous mode.	38
16.	LRB holography to record a Nd-glass pulse laser wavefront.	40
17.	Studying Nd-glass laser wavefront by LRB holography using 4Z film.	42
18.	Mach-Zehnder interferometer arrangement for testing laser rods.	54
19.	Mach-Zehnder interferometer arrangement for measuring distortion in laser wavefronts.	54
20.	Interferogram of a ruby laser rod during repetitive operation at one pulse per second.	55
21.	Twyman-Green interferometer arrangement for testing laser rods.	58
22.	Method for obtaining holographic records of distorted wavefronts from lasers.	58
23.	Method for obtaining in-line holograms of distorted laser wavefronts.	62
24.	Illustration of a scaled-up correction plate.	68

Figure		Page
25.	Machining of a scaled-up correction plate, using a spherical-tipped tool with bonded diamond grit.	68
26.	Digitization of data contained in a wavefront interferogram.	75
27.	Relation of object wave and deformed object wave in a holographic interferometer.	93
28.	Illustrating variables used to describe homologous rays.	97
29.	Illustrating homologous rays.	99
30.	Illustrating the wave vectors used to describe object displacements.	101
31.	Intensity variation versus object displacement.	107
32.	Experimental arrangement for a heterodyne holographic system.	109
33.	Experimental arrangement for full-field viewing of a heterodyne interferogram.	115
34.	Experimental arrangement for the position sensing heterodyne interferometer.	118
35.	Apparatus used for the position sensing heterodyne interferometer.	119
36.	Interferogram corresponding to probe beam displacement	120
37.	Interferogram corresponding to probe beam coincidence.	121
38.	AC interferometer configuration.	126

Figure		Page
39.	Mechanical design for an ac grating interferometer.	130
40.	Arrangement for making photographic grating using a Strobotac.	131
41.	Arrangement for making photographic gratings using a modulated laser.	132
42.	Arrangement for making photographic gratings using an interferometer.	134
43.	Fringe geometry with the arrangement of figure 42.	135
44.	1.8 lines/mm grating.	137
45.	5 lines/mm grating.	138
46.	18 lines/mm grating.	139

## SECTION I

### REPORT SUMMARY

The results of research into a number of interrelated problems in laser beam generation, evaluation, control, and propagation are the subject of this report. Because of the breadth of the work considered, the study was divided into four parts that are clearly related but require different disciplines. Each of these four areas was under the direction of a separate principal investigator with a responsible investigator coordinating the related efforts.

Section II is a study of techniques for assessing laser beam characteristics of both cw and pulsed lasers using holography in conjunction with interferometry. The local reference beam holographic methods were established and implemented in a variety of situations including cw helium-neon laser, pulsed ruby laser, and pulsed Nd:glass laser. For the Nd:glass lasers, methods were developed for doing infra-red holography using the new experimental 4-Z film.

Methods are described for measuring the dynamic optical distortion in a laser rod (section III) and for manufacturing the necessary correction plates to compensate for the measured distortions. The scaled-up correction plates are made with

ground glass and then appropriately scaled down by immersing the plate in a liquid whose index nearly matches that of the correction plate. Scattering losses from these indexed-matched correction plates are negligible.

Scanning laser systems have an important role to play in a variety of applications. Thus one portion of the work reported here (section IV) is concerned with a means of producing a high-speed continuously scanning laser beam by appropriate use of an intra-cavity beam deflector that locks a set of transverse modes of the laser. Transverse mode-locking in a large-bore argon ion laser was satisfactorily demonstrated. This mode-locking leads to the production of a scanning beam from the output of the laser. The resolution of the scanning beam is limited by the optical quality of the intra-cavity modulators.

The final section of the report is concerned with problems relating to the peripheral optical elements that may be used for the propagation of laser beams. The particular problem attacked is that of the use of ac interferometry for optical testing. A theoretical analysis of a number of interferometers which utilize moving fringe patterns has been carried out and preliminary experimental data generated, particularly for heterodyne interferometry for vibration analysis and position sensing.

## SECTION II

### STUDY OF TECHNIQUES FOR ASSESSING AND IMPROVING LASER BEAM PROPAGATION CHARACTERISTICS Studying Beam Parameters of CW and Pulse Lasers Using Holography in Conjunction with Interferometry

C. Royhoudhuri and B. J. Thompson

#### 1. INTRODUCTION

In many applications of laser beam technology including coherent optical processing, coherent light ranging, laser beam scanning, etc., a knowledge of the complex amplitude distribution over the output wavefront is often essential. In the precision shop techniques of micro etching and welding, or in initiating controlled fusion by high energy laser beams, the knowledge of the spot size and the energy distribution of the focused laser beam is extremely important. These parameters can be determined very easily from the knowledge of the near field complex amplitude distribution if the beam is fully coherent or in general by knowledge of the mutual coherence function. For certain optical techniques the information about the far field distribution may be the more relevant quantity; this can also be determined from the knowledge



of the near field distribution, using the diffraction integral if the beam is coherent or the mutual intensity propagation integral if the beam is partially coherent. The objective of this study is to develop a method by which the complex amplitude distribution and/or the mutual intensity function of a laser beam near field can be determined.

## 2. POSSIBLE METHODS

In principle the determination of the intensity distribution across a wavefront is straightforward since an optical detector responds to the light intensity. But the problem of recording the phase distribution of an unknown wavefront is of fundamental nature, especially if the wavefront is not a very simple one.

One may apply the Fourier transform technique: record the square modulus of the Fourier transform of the unknown wavefront and then the inverse Fourier transform may be used to find out a partial knowledge (autocorrelation) of the original wavefront. The problem of complete phase retrieval<sup>(1)</sup> is still there when we only gather a knowledge of the modulus of the Fourier transform instead of the complex Fourier transform.

Interferometry offers a better method of recording the complex amplitude, since interference gives rise to modulation in the resultant intensity. The modulation is directly affected by the degree of coherence and the amplitude of the interfering beams. In applying this technique to study laser beam wavefronts, especially if they are pulsed, the required reference beam will have to be generated from the very wavefront to be studied.

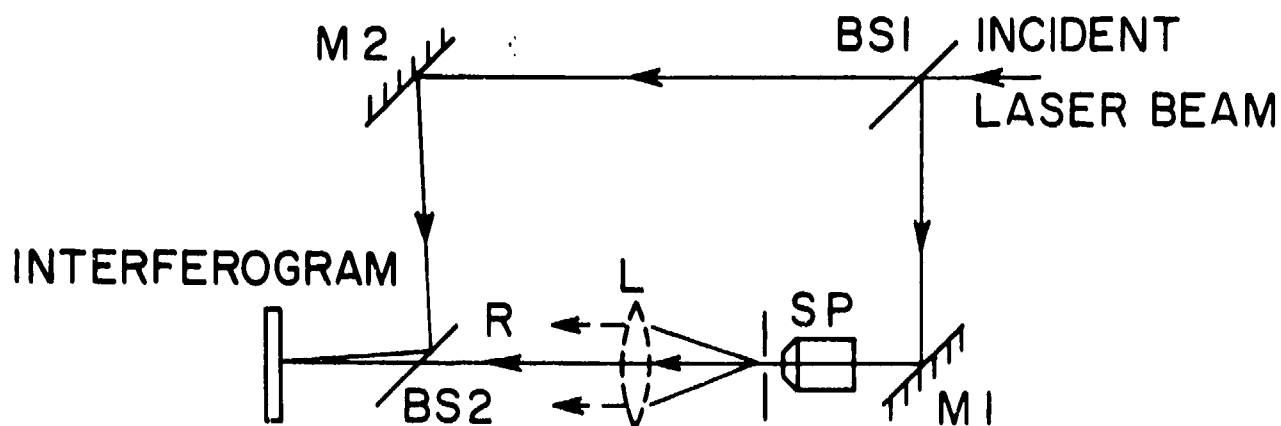
The simplest application of the interference technique is to record a shearing interferogram<sup>(2)</sup> of the wavefront. But the interpretation of the interferogram may not be trivial, especially for complicated wavefronts. The reason is that both of the interfering wavefronts are unknown. A simple and elegant solution to this problem is to generate a known local reference beam (L.R.B.) by splitting off a part of the wavefront to be studied and focusing it onto a small pinhole aperture generating an approximately spherical wavefront or a plane wavefront with the help of an auxiliary lens, L, as shown in fig. 1.\*

For a complete knowledge of the relative phase and amplitude distribution of a wavefront, we also need to know the intensity distribution of the two wavefronts.

For pulsed laser systems it may be very difficult to get

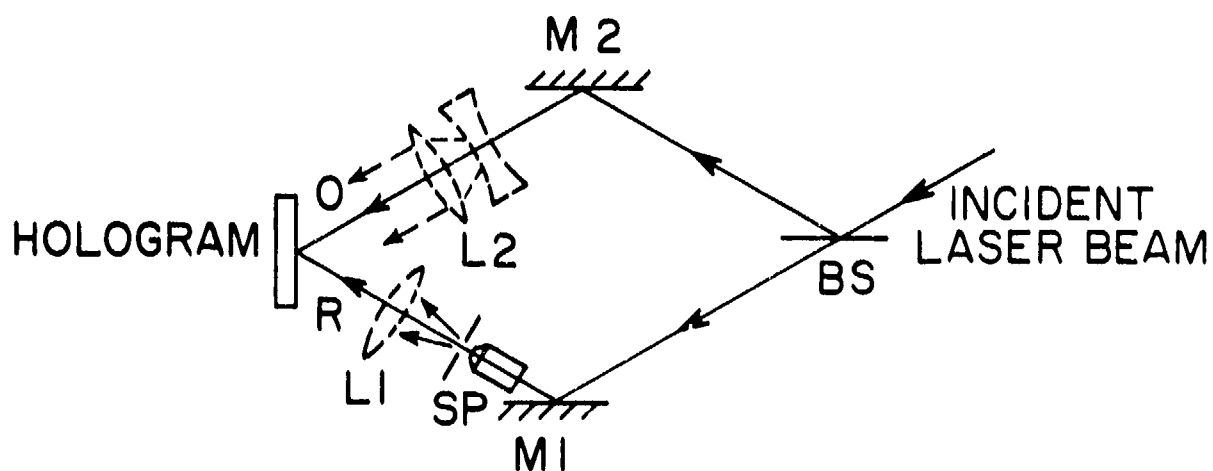
---

\*Figures 1-7 represent work reported on earlier<sup>(25)</sup>, the essential features of which are covered here for completeness.



## LOCAL REFERENCE BEAM INTERFEROMETRY

Fig. 1



## LOCAL REFERENCE BEAM HOLOGRAPHY

Fig. 2

a simultaneous record of the intensity pattern of the two interfering beams along with the interferogram. An obvious solution to this problem is to record the wavefront holographically and to study the reconstructed beam at leisure using a steady continuous laser for reconstruction.

Here it is worth recognizing that the interferogram of fig. 1 is already a hologram but only of limited value since it is an "on-axis" hologram and in the reconstruction the desired wavefront will be mixed up with unwanted wavefronts traveling in the same direction. However using an off-axis hologram arrangement<sup>(3)</sup> overcomes the problem. The basic method described here is the holographic arrangement as shown in fig. 2. If necessary, the "object" beam could be expanded using a suitable lens system.

There is one important point to be emphasized regarding the local reference beam method: it is useful to have a uniform wavefront both in phase and amplitude to insure a faithful reconstruction. A suitable spatial filter (a pinhole of suitable size with or without a matching microscope objective) serves this purpose very well generating an easily reproducible spherical wavefront.

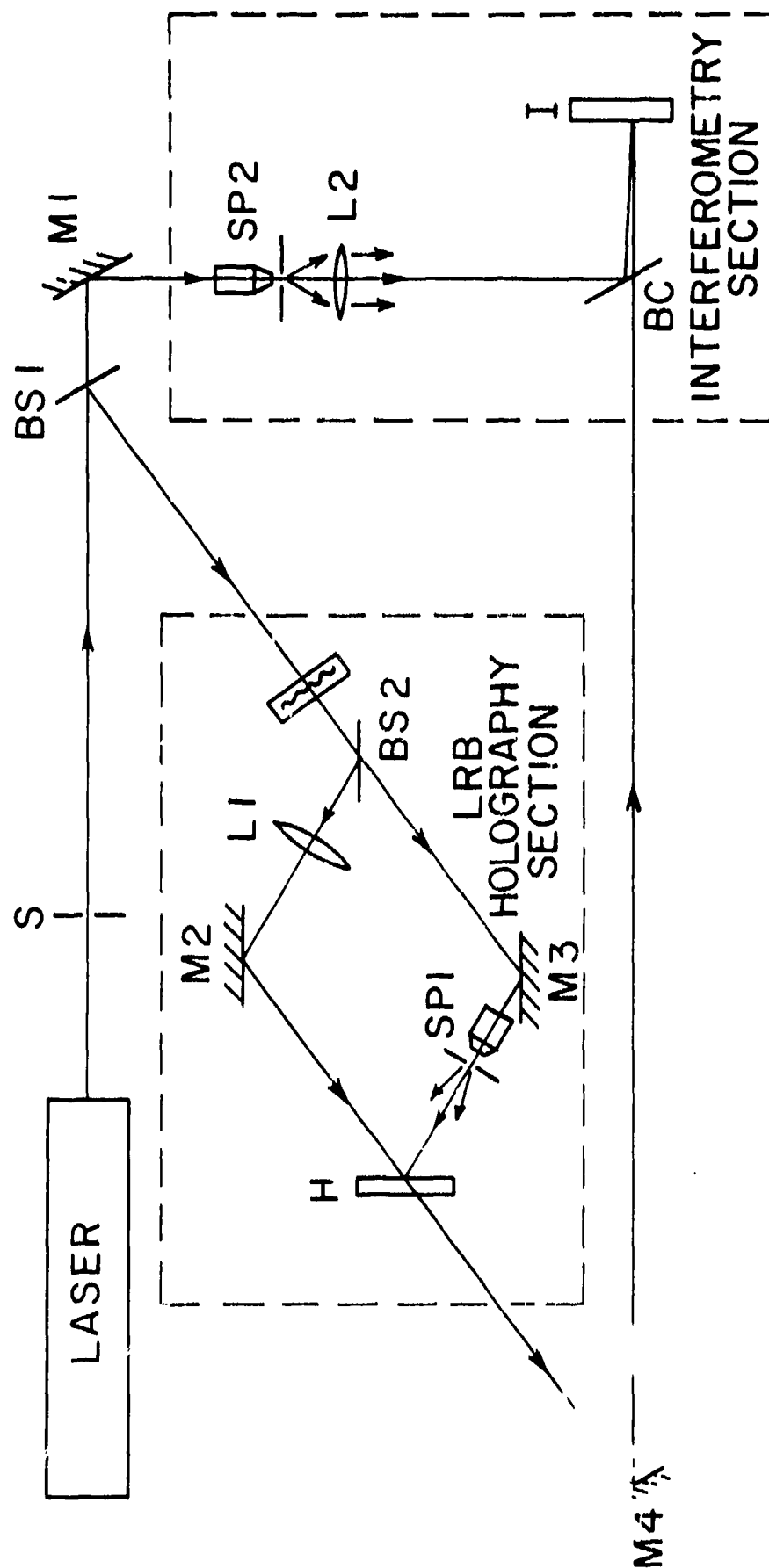
In this method of determining both the phase and the amplitude distribution of a pulse multimode laser wavefront

both local reference beam holography and interferometry are exploited, but in two independent steps. The first step is to record a hologram of the pulse wavefront by local reference beam holography with an arrangement shown in simplified form in fig. 2. Then the wavefront is reconstructed using a continuous  $TEM_{00}$  mode laser beam; and the reconstructed wavefront is made to interfere with a uniform plane wavefront. The coherent plane wavefront can be easily derived from a part of the same laser beam used to generate the reconstruction wavefront, as shown in fig. 3. The interferogram gives complete information about the phase and amplitude distribution of the multimode laser wavefront. This method offers a powerful flexible method to study a pulse multimode laser wavefront, since the pulsed laser wavefront can be regenerated as a stationary one. Its parameters can be studied by a variety of methods.

### 3. EARLY LOCAL REFERENCE BEAM TECHNIQUES

#### (a) Interferometric Techniques

This local reference beam method is related to a method first suggested by Korobkin and Leontovich <sup>(4)</sup> in



LRB HOLOGRAPHY TO RECORD A SIMULATED "MULTIMODE"  
LASER WAVEFRONT AND ITS SUBSEQUENT STUDY THROUGH  
INTERFEROMETRY AFTER RECONSTRUCTION.

Fig.3

early 1963. They studied the degree of spatial coherence of a ruby laser by recording the interference produced by light from separate sections of the wavefront. Their experiments indicated a high degree of spatial coherence between the different parts of the wavefront, but did not (and can not) give the structure of the entire phase front.

Bondarenko et al<sup>(5)</sup> carried out an experiment in late 1963 in which the output of a ruby laser was studied; a spherical wavefront was generated by scattering a small central part of the main beam through a transparent dielectric nonuniformity which was then made to interfere with remainder of the beam. Related studies were subsequently carried out by Davis<sup>(6)</sup>. He used an appropriately coated plano-concave lens to produce the axially symmetric primary "object" beam reflected from the plane surface and the spherical local reference beam reflected from the concave surface.

For more convenient and quantitative mapping of a complicated phase structure, the reference wavefront should preferably be a plane and uniform one. Miyamoto and Yasuura<sup>(7)</sup> demonstrated a simplified version of such an experiment. They measured the phase and amplitude distribution of a laser wavefront from a continuous He-Ne type running in a single transverse and single longitudinal

mode. The reference wave was produced by splitting off a part of the laser beam; it was then expanded and collimated by a pair of positive lenses.

None of the above methods produces a local reference beam that gives rise to a uniform wavefront from a general wavefront. This severely limits the usefulness of these methods to study multimode laser beams.

#### (b) Holographic Techniques

It appears from the patent literature that Cathey<sup>(8)</sup> was the first to invent the idea of generating a local reference beam for holography. Instead of using a separate external reference beam, he passed a part of the object beam through a lens and pinhole assembly to the hologram. Since Cathey's idea occurred in the patent literature, it was not well known to the scientific community.

In early 1967, Rosen and Clark<sup>(9)</sup> experimented with holography without any external reference beam; but their idea was not as versatile as that of Cathey's. Their object was very close to the hologram plane and interference between the different parts of the object gave rise to the hologram; reconstruction of one part of the object was carried out by illuminating the hologram by the appropriate



part of the object beam.

In late 1967, Caulfield et al <sup>(10,11)</sup> apparently reinvented Cathey's idea of generating an easily reproducible local reference beam. Their original goal was to avoid the problem of path matching between the object beam from an unknown distance and the external reference beam in the conventional off-axis holography. Caulfield <sup>(12)</sup> then realized that this idea of local reference beam holography can be extended further to make holograms of any object of any extent and distance, and suggested the construction of a holographic camera with a laser as the "flash".

All the above mentioned works are very much confined to the realm of pictorial holography. As mentioned in the previous section, the present technique started with the idea of recording the pulsed laser wavefront by local reference beam holography and then studying all the beam parameters at leisure by using a continuous  $TEM_{00}$  laser beam for reconstruction. To test the resolution capabilities both in amplitude and phase of the method, we ran three sets of experiments with a  $TEM_{00}$  He-Ne laser and simulating the nonuniform wavefront by using suitable masks in the laser beam. Then the method was applied to

study TEM<sub>01</sub> CW He-Ne (.6328 $\mu$ m) as also ruby (.6943 $\mu$ m) and Nd-glass (1.06 $\mu$ m) pulse laser wavefronts.

Before concluding this section we should mention some of the publications which have some relationship to our work. Lurie<sup>(13)</sup>, Murata et al<sup>(14,15)</sup>, Ross<sup>(16)</sup> and Aleksoff<sup>(17,18)</sup> have done some work on holographic measurements of coherence.

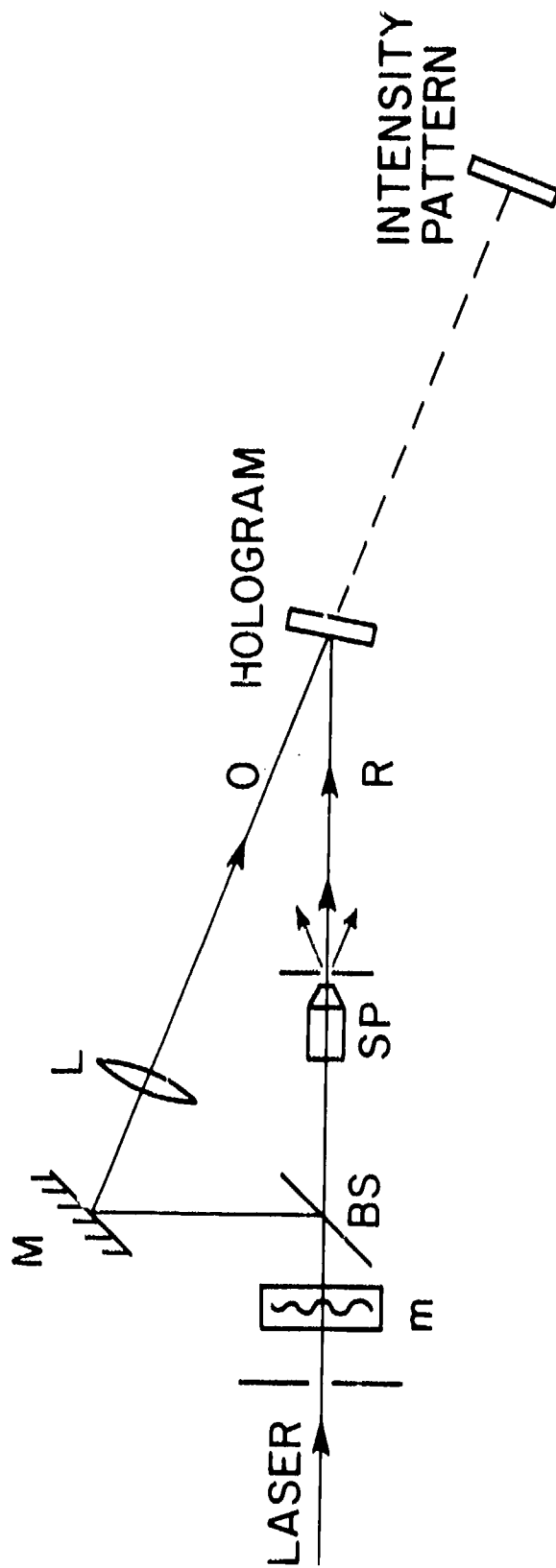
The first two contribute to the analytic understanding of the role of degree of coherence in holography and hence its measurements, and are supported by experimental illustrations. Only Ross's work directly refers to the measurement of both temporal and spatial coherence of ruby pulse lasers; but because the use of ground glass to produce the 'object beam' completely randomizes the phase information, only the modulus of the coherence function can be measured. Aleksoff's work<sup>(18)</sup> reports displaying the different transverse modes corresponding to the different longitudinal modes. But he used only a CW He-Ne laser, and he also uses phase randomizing ground glass.

#### 4. TEST EXPERIMENTS

##### (a) Local Reference Beam Holography to Reconstruct Intensity Distribution

In this preliminary series of experiments we have successfully demonstrated that local reference beam holography can reconstruct quite rapidly spatially intensity distributions. This establishes two fundamental requirements of any local reference beam for holography. That there is a reconstruction at all, establishes the essential requirement that the local reference beam is satisfactory. The faithfulness in the reconstruction demonstrates the reproducibility criterion of the local reference beam. This is an important point since we are going to make holograms of a pulse laser wavefront with local reference beam from the same pulse and then reconstruct the wavefront regenerating the reference beam from a different laser.

Since the test experiment was performed with a continuous He-Ne laser running in the  $TEM_{00}$  mode, the rapidly varying (spatially) intensity distribution was simulated by inserting known masks in the beam. The experimental arrangement is shown in fig. 4. The He-Ne laser beam is diffracted by the known mask  $m$ , and the diffracted beam is divided into



SIMPLE SET UP TO TEST LRB HOLOGRAPHIC  
TECHNIQUE WITH "MULTIMODE" LASER WAVEFRONT  
SIMULATED FROM A TEM<sub>00</sub> CW He-Ne LASER BEAM.

Fig.4

two parts with the help of the beam splitter BS. The part which goes straight through is used to generate the local reference beam with the help of the spatial filter SP. The reflected part constitutes the simulated rapidly varying amplitude variation of a "multimode" pulsed laser; this is our object beam. By choosing different focal lengths for the lens L we can control the frequency of amplitude variation at the recording plane I and the relation between the mask M and diffracted beam received by the hologram.

Two sets of records were taken using two different masks: an amplitude Ronchi ruling and a phase Ronchi ruling. In each case holograms were recorded under three different conditions using lenses of appropriate focal lengths for L (fig. 4) such that the hologram appeared to be successively in (i) the Fraunhofer plane, (ii) the Fresnel plane and (iii) the image plane with respect to the diffracting mask M. The reason for recording in three different hologram planes is to test the precise reproducibility of the reconstructing local reference beam. For example, it is established <sup>(19)</sup> that the quality of the reconstructed image from an image plane hologram is least sensitive to deviations in the reconstructing beam from that of the

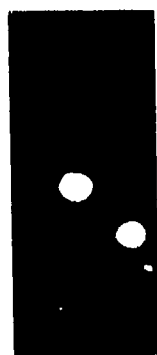
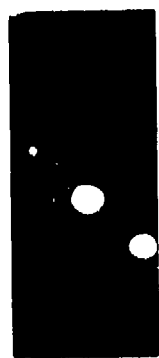
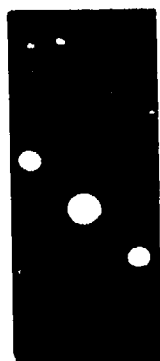
original reference beam; it is a little more sensitive for a Fresnel plane hologram. The highest sensitivity is for the Fraunhofer plane hologram. This is because the amplitude corresponding to the frequency spectrum of an object is spatially dispersed in a regular fashion over the entire Fraunhofer plane; consequently any distortion in any part of the reconstructing beam would lead to a distortion all over the object which corresponds to those spatial frequencies that are modified. Whereas for image plane holograms, a local distortion in the reconstructing beam will produce, at best, a corresponding local distortion in the object.

The recorded results shown in figures 5 and 6 are arranged in an identical sequence; the only difference is that fig. 5 corresponds to the amplitude Ronchi ruling mask and fig. 6 corresponds to the phase Ronchi mask. In both the diagrams the three successive columns correspond to (i) the Fraunhofer plane, (ii) the Fresnel plane and (iii) the image plane holographic arrangements as mentioned earlier. The pictures of the first row are the direct record of the object beam. The second row corresponds to the reconstruction by the original local reference beam and the third row represents records of the reconstruction by a local reference beam generated from a "different" laser beam.

FRAUNHOFER PLANE

FRESNEL PLANE

IMAGE PLANE

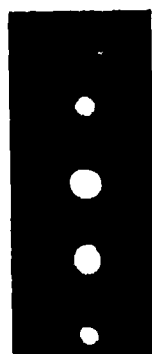
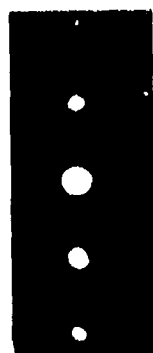
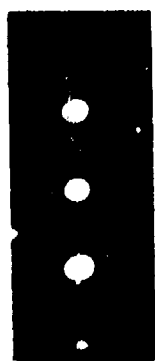


THE NOISY LASER WAVE FRONT WAS  
SIMULATED BY AN AMPLITUDE RONCHI MASK.  
FIRST ROW: DIRECT RECORD, SECOND ROW:  
RECONSTRUCTION WITH THE ORIGINAL LASER,  
THIRD ROW: RECONSTRUCTION WITH A  
"DIFFERENT" LASER.

FRAUNHOFER PLANE

FRESNEL PLANE

IMAGE PLANE



THE NOISY LASER WAVE FRONT WAS  
SIMULATED BY A PHASE RONCHI MASK.  
FIRST ROW: DIRECT RECORD, SECOND ROW:  
RECONSTRUCTION WITH THE ORIGINAL LASER,  
THIRD ROW: RECONSTRUCTION WITH A  
"DIFFERENT" LASER.



It can be noted, from a careful comparison of the last two rows of each column of both figures 5 and 6 that the reconstructions by the original local reference beam and by a beam generated from a different laser are remarkably similar. It may also be noted that all three columns show almost equal faithfulness in reconstruction. Apparently, the different holograms do not show different resolution capability. This establishes very strongly that the local reference beam generated from a different laser very closely resembles the original local reference beam. It is worth mentioning that our reconstructed images (2nd and 3rd rows) show a slight deviation from the directly recorded images (1st row). The amplitude variation of the "object" beam was apparently beyond the linear region of "transmittance vs. exposure" curve for the hologram. This can be taken care of by choosing a better beam balance ratio.

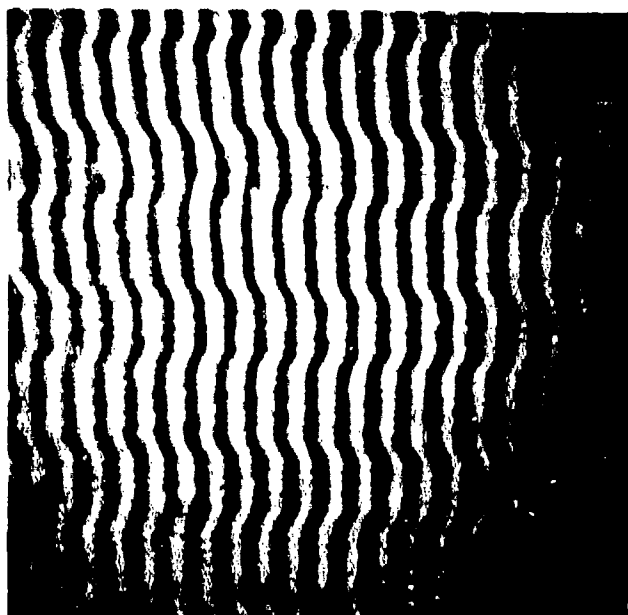
- (b) Local Reference Beam Holography to Reconstruct Phase Structure and Subsequent Interferometry to Study Phase and Amplitude of a Wavefront.

As in the previous experiment, the phase and amplitude variation of the laser wavefront was simulated by inserting a suitable phase mask in the beam. The experimental arrangement is shown in figure 3. The lens L1 images the phase mask on to the interferogram plane I where it interferes with

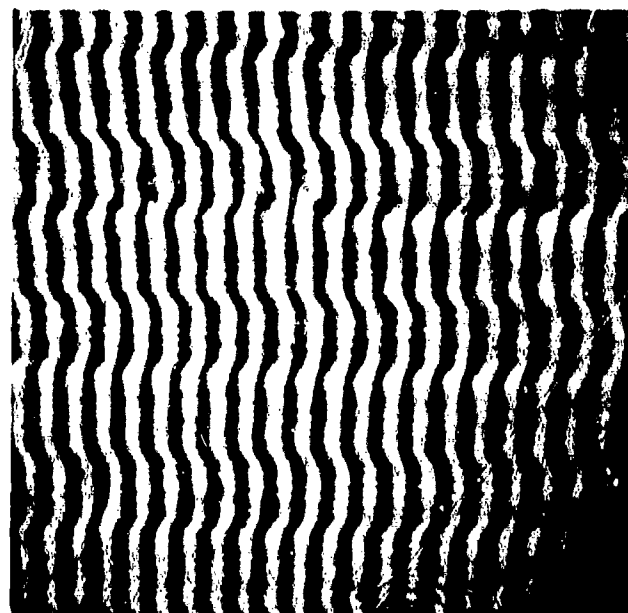
a uniform plane wavefront generated from a part of the original laser beam with help of the spatial filter SP2 and the collimating lens L2.

The first experiment was done with a Ronchi phase mask. Figure 7 shows the interferograms of the phase wavefront recorded directly and from the holographic reconstructions with local reference beam generated under different conditions. Interferogram (7a) was recorded from the direct object beam and (7b) was recorded from the reconstructed object beam.

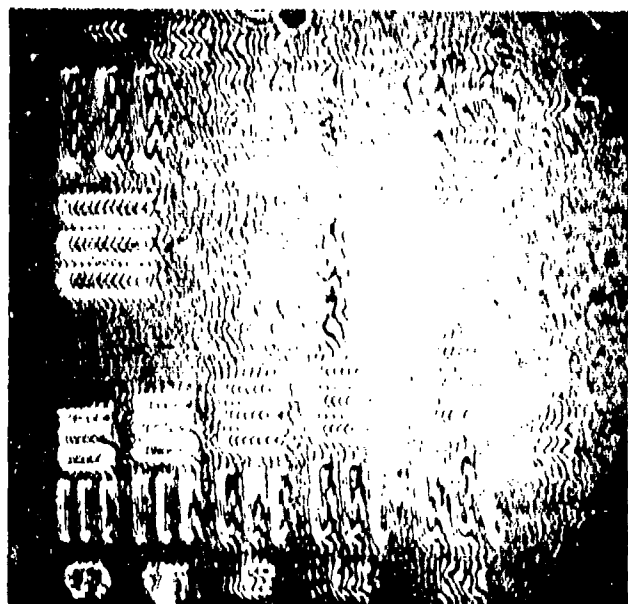
The second experiment was performed with a standard resolution testing phase bar-target. This mask introduces changes in amplitude and phase of varying frequency over the wavefront. The interferograms of the direct and reconstructed wavefronts are shown in 7(c) and 7 (d) respectively. As in the previous set of experiments the comparison of (b) with (a) and (d) with (c) of figure 7 establishes the faithfulness of the holographic process and the reproducibility of the local reference beam. Since high frequency bar sets have been reconstructed we can apply the local reference beam techniques to record even a very noisy laser wavefront like the "filamentary" output from a pulsed solid state laser.



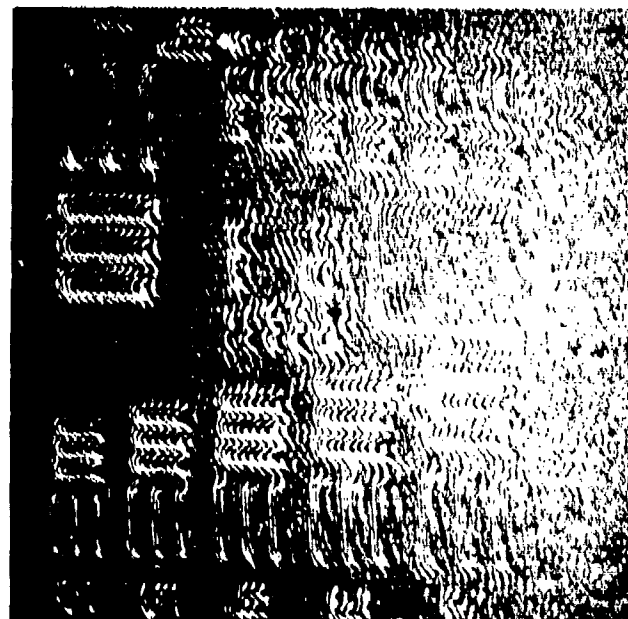
(a)



(b)



(c)



(d)

CONSTANT AND VARIABLE FREQUENCY  
PHASE RECONSTRUCTION THROUGH LRB  
HOLOGRAPHY. VERIFICATION BY INTERFERO-  
METRIC FRINGES.

Actually, for both of the above experiments, three different reconstructions were carried out under three different conditions; first, with the original local reference beam, the original interferogram; the second and third reconstructions were carried out with local reference beam generated from two laser beams of widely different wavefronts. These were also indistinguishably similar to the first reconstruction as well as the original (direct) interferogram; this establishes the reproducibility of the local reference beam.

The analysis of the interferograms of the above experiments offers the obvious possibility of studying both phase and amplitude of the reconstructed wavefronts from the contour and visibility of the fringes since the reference beam for interferometry is completely known.

#### 5. APPLICATION OF THE METHOD TO KNOWN LASER WAVEFRONT (TEM<sub>01</sub> CW He-Ne)

While we have established the applicability of the method with known simulated "multimode" from TEM<sub>00</sub> He-Ne beam, we have not, so far, applied it to the study of a real laser mode where the results are known so that useful

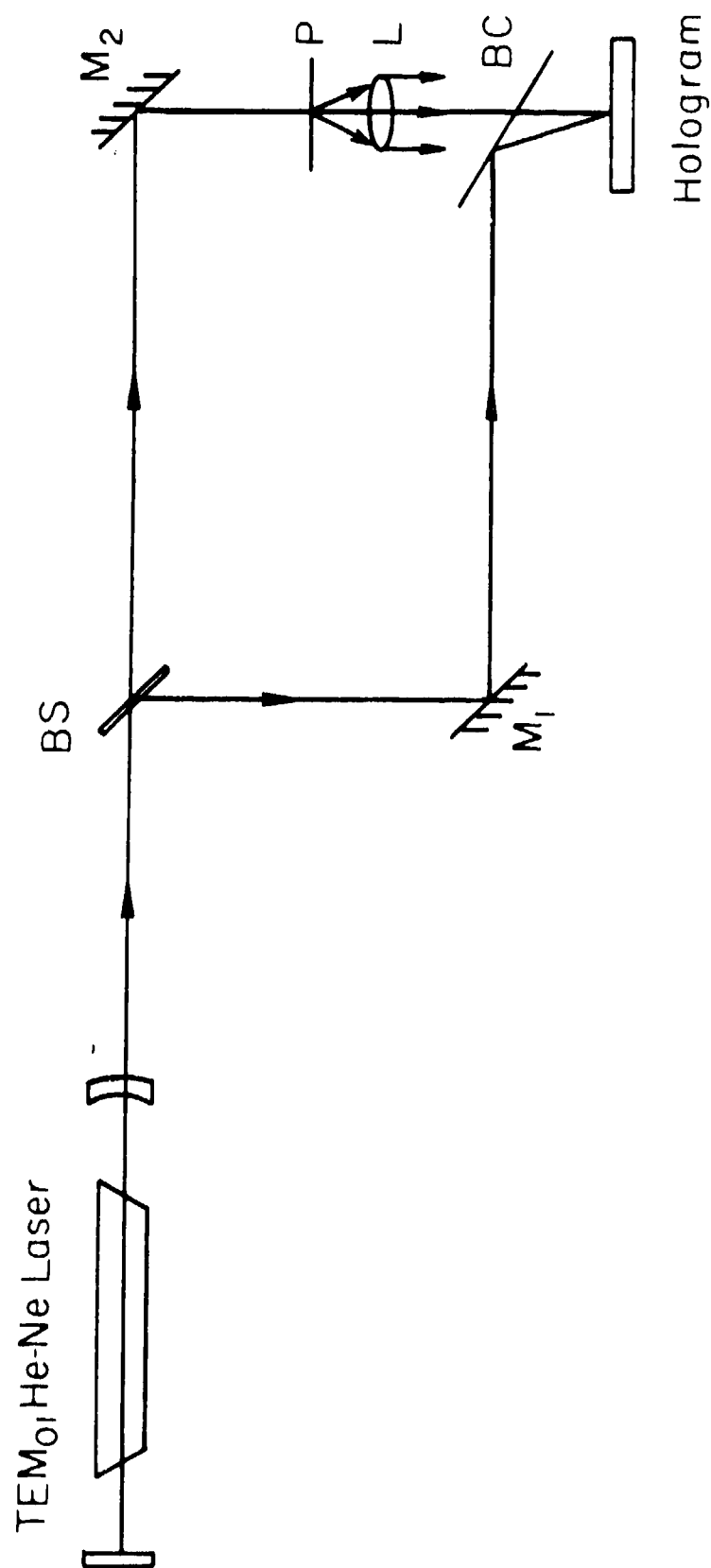
comparison can be made. Thus the results of reconstruction of the wavefront from the hologram will further establish the validity of our method.

In addition, the very idea of applying holography to study near-infrared Nd-glass laser pulses ( $1.06\mu\text{m}$ ) has some technical problems. One of the inherent characteristics of the Nd-glass laser is that when it is pumped strongly (around or above 100J), the spectral width<sup>(20)</sup> of the output pulse runs from 50 to  $100\text{\AA}$  ( $\sim 1000$  to around 3000 GHz). Correspondingly, the coherence length could be a small fraction of a mm. (The spectral width could be reduced down to  $.1\text{\AA}$ , i.e., around 30 GHz or coherence length  $\sim 1\text{cm}$  by introducing a prism<sup>(21)</sup> or tilted etalon<sup>(22,23)</sup> inside the laser cavity.) Thus the path difference between the two interfering beams of Nd-glass pulse will have to be kept accurately equal. For this reason a Mach-Zehnder interferometer was used as shown in figure 8.

Another problem occurs since there are no commercially available photographic plates of reasonably low grain size to do holographic work at  $1.06\mu\text{m}$ . Eastman Kodak Company has supplied us with some special experimental films (4-Z) sensitive to  $1.06\mu\text{m}$ . It has been claimed to have a spatial

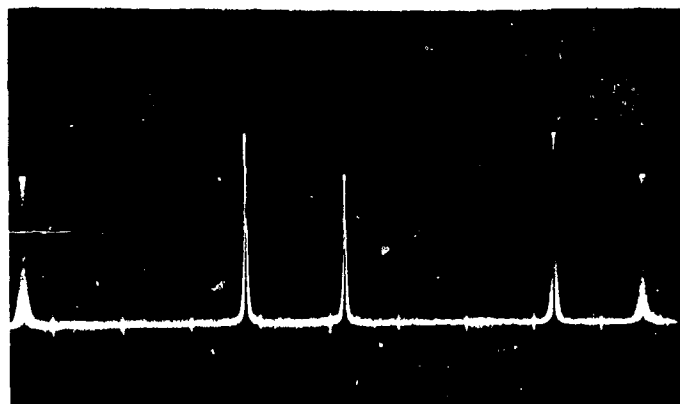
resolution capability of a few hundred lines/mm which is nearly an order of magnitude higher than 1-Z emulsion. Even then the angle between the interfering beams could not be more than  $15^\circ$  ( $\sim 400\ell/\text{mm}$ ). The set-up (fig. 8) of the Mach-Zehnder interferometer is ideal for use with these new films. But at low carrier fringe frequency, the very success of holography might become questionable if the frequency of the information is only an order of magnitude lower than the carrier. With this important point in mind, we have carried out some experiments to study some  $\text{TEM}_{01}$  modes from a He-Ne laser of beam diameter less than a mm with the local reference beam holographic method.

The He-Ne laser used was of hemispherical cavity (30cm) and the bore of the discharge tube was just large enough to allow the laser to run at some low order transverse mode. To keep the experiment simple, we chose to record a  $\text{TEM}_{01}$  mode under two slightly different circumstances. First, it was adjusted to run at a pure  $\text{TEM}_{01}$  mode as is verified by the oscilloscope trace of the longitudinal modes (fig 9a), the intensity pattern (9b), and the interferogram (9c). Secondly, it was made to run dominantly at  $\text{TEM}_{01}$  but with some undetermined "impurity"



LRB HOLOGRAPHIC RECORD OF A REAL  
TEM<sub>01</sub> He-Ne CW LASER WAVE FRONT

Fig.8



(a)



(b)

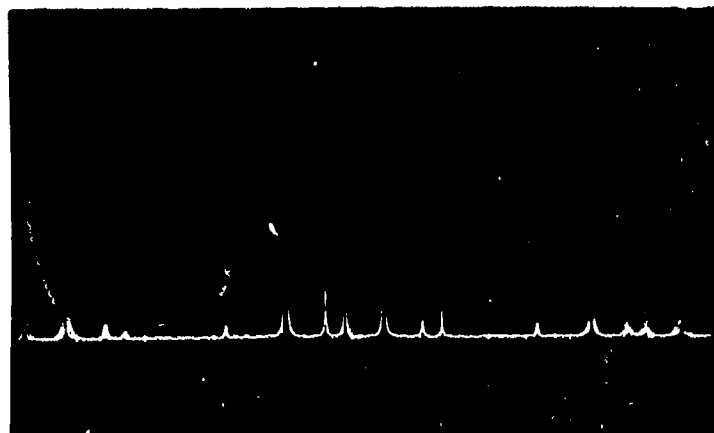


(c)

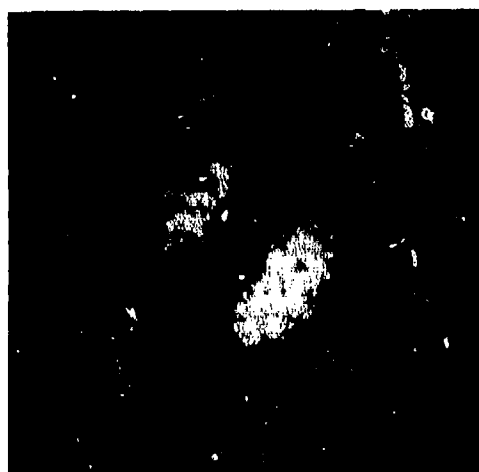
# PURE TEM<sub>01</sub> MODE FROM A He-Ne LASER

- (a) THE LONGITUDINAL MODES AS RECORDED THROUGH A SCANNING FABRY-PEROT INTERFEROMETER OF FREE SPECTRAL RANGE  $\sim 1.54$  GHz. INTERMODE SPACING :  $\Delta\nu$  LASER  $\sim .5$  GHz.
- (b) THE INTENSITY PATTERN.
- (c) THE INTERFEROGRAM.  $180^\circ$  PHASE DIFFERENCE BETWEEN THE TWO "LOBES" IS SELF-EVIDENT.

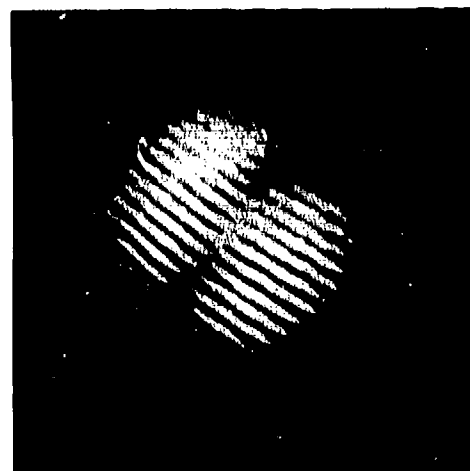




(d)



(e)



(f)

"IMPURE"  $TEM_{01}$  MODE FROM He-Ne LASER

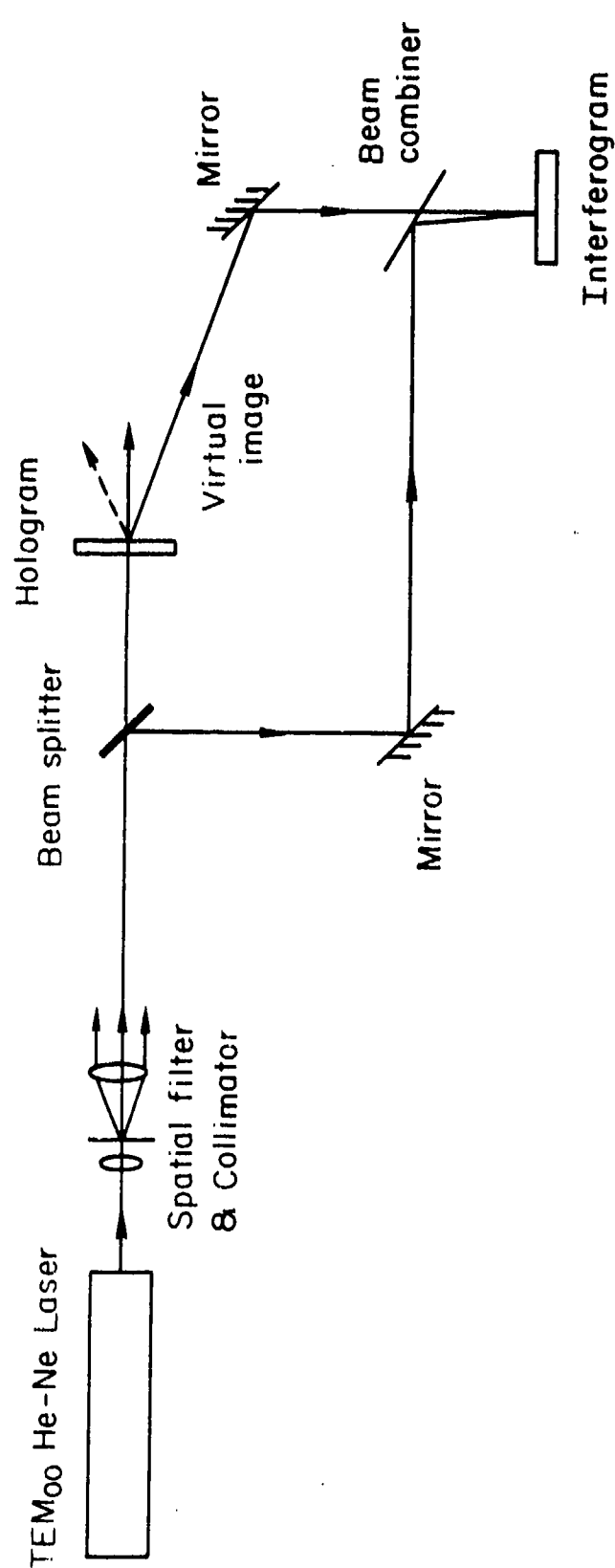
- (d) LONGITUDINAL MODES;
- (e) INTENSITY PATTERN;
- (f) INTERFEROGRAM.

Fig.9 (Continued)

which is demonstrated in the records of the spectrum (9d), the intensity distribution (9e), and the interferogram (9f).

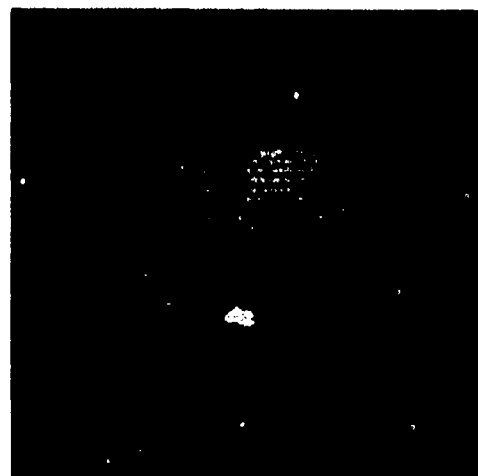
We recorded these two pure and impure  $TEM_{01}$  modes holographically on Agfa 10E75 plates at low carrier fringe frequency of about 400 lines/mm. The results of reconstruction through a separate Mach-Zehnder interferometer (fig. 10) are shown in fig. 11. Fig. 11a is the magnified hologram of pure  $TEM_{01}$  and 11b, 11c correspond to the reconstructed intensity and complex amplitude distribution respectively. Fig. 11d is the hologram of the impure  $TEM_{01}$  mode and the results of reconstruction are shown in 11e (intensity distribution) and 11f (complex amplitude distribution). The comparison of these pictures with the corresponding ones in fig. 9 establishes the local reference beam holographic method for relatively low frequency carrier fringes.

This modified experimental method should be well suited to study Nd-glass laser pulses, since it accommodates the restrictions imposed by this laser (very short coherence length) and by the new Kodak films sensitive to 1.06 $\mu$  radiation (low spatial resolution capability).

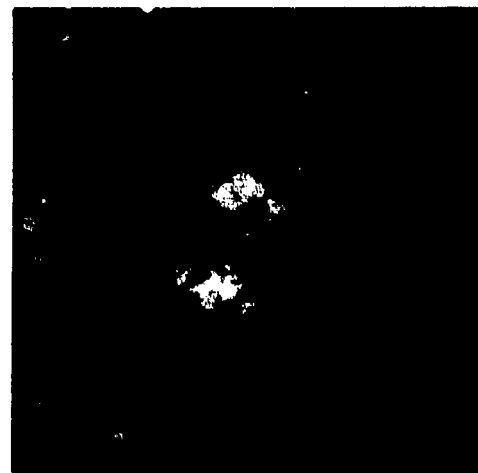


RECONSTRUCTION OF THE LASER WAVEFRONT FROM THE  
LRB-HOLOGRAM AND ITS SUBSEQUENT INTERFEROMETRIC STUDY

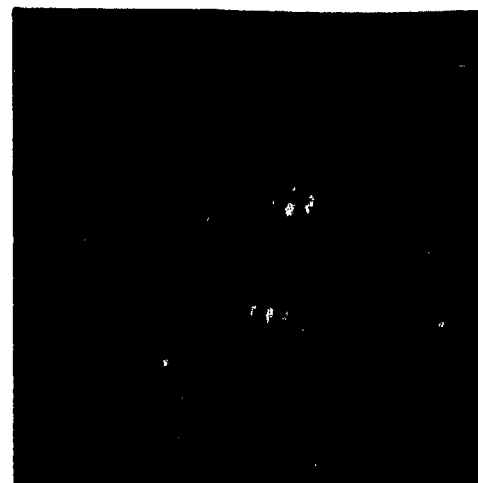
Fig.10



(a)



(b)



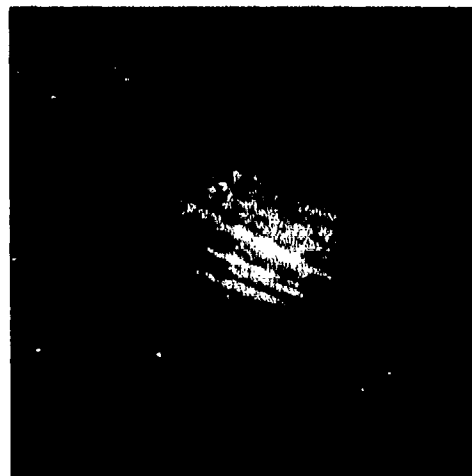
(c)

RECONSTRUCTION OF THE  $TEM_{01}$  LASER  
WAVEFRONT FROM THE LRB-HOLOGRAM  
RECORD AND ITS INTERFEROGRAM.

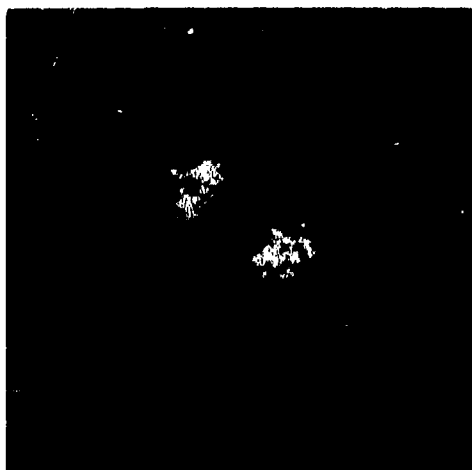
(a) A MAGNIFIED PORTION OF THE HOLOGRAM  
( $\sim 400 \text{ L/mm}$ )

(b) INTENSITY PATTERN; (c) INTERFEROGRAM

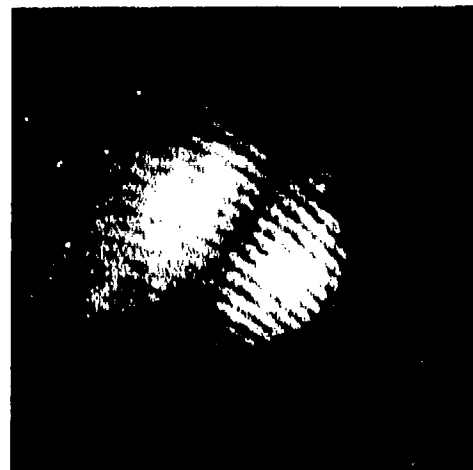
Fig.11



(d)



(e)



(f)

RECONSTRUCTION OF THE "IMPURE"  $TEM_{01}$   
LASER WAVEFRONT FROM THE LRB-HOLOGRAM  
RECORD AND ITS INTERFEROGRAM.

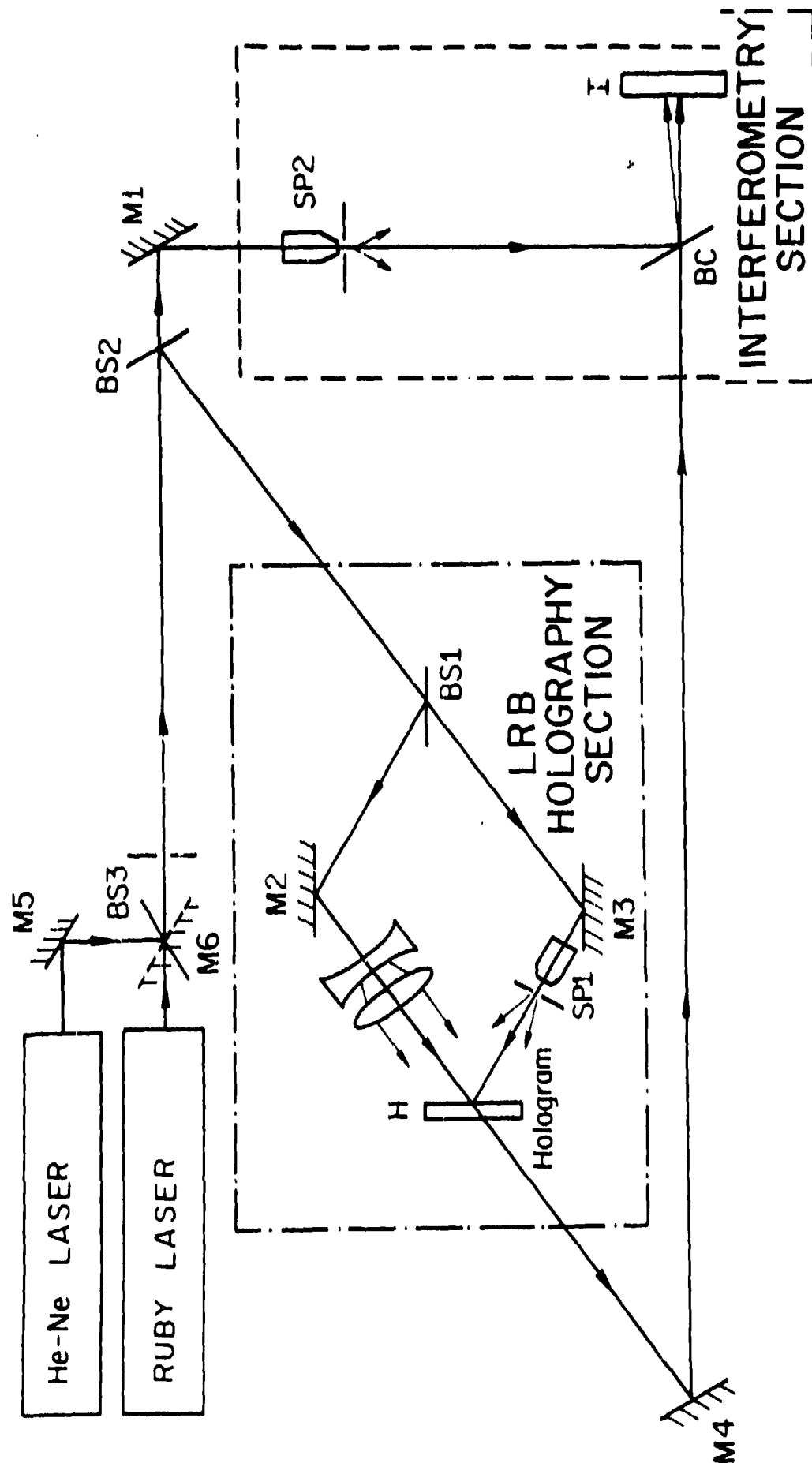
(d) HOLOGRAM ; (e) INTENSITY PATTERN ;  
(f) INTERFEROGRAM

## 6. APPLICATION OF THE METHOD TO RUBY PULSE LASER

In this section experiments with a multi-mode pulse laser wavefront generated by a conventional ruby laser are reported. The experimental arrangement is shown in Fig. 12. The continuous He-Ne laser serves two purposes. First, in conjunction with mirror, M5 and beam splitter, BS3, it is used to align the ruby laser cavity. The second purpose is to reconstruct the pulsed laser wavefront in continuous mode from the recorded hologram and study it interferometrically with the help of mirrors M5, M6 and the section following M1 and SP2; the hologram being recorded, without either BS3 or M6 in position, in the section following BS2 and BS1.

The cavity<sup>(24)</sup> for the ruby laser was formed by a roof prism (with the face at Brewster angle) in one end and in the other a partially transmitting resonating reflector (the output end). This gives a polarized output of reasonably narrow bandwidth radiation suitable for regular holographic work.

In this illustrative experiment, the ruby laser cavity was kept purposefully "misaligned" to give some higher order transverse modes. The intensity pattern of fig. 13 is a record of such a transverse mode reconstructed with the



LRB HOLOGRAPHY TO RECORD A RUBY PULSE LASER  
WAVEFRONT AND ITS SUBSEQUENT STUDY THROUGH  
INTERFEROMETRY AFTER RECONSTRUCTION.

Fig.12



(a)



(b)

INTENSITY PATTERN OF A RUBY LASER PULSE  
RECONSTRUCTED FROM A L R B HOLOGRAPHIC  
RECORD. TWO DIFFERENT EXPOSURES OF THE  
SAME WAVEFRONT.



He-Ne laser from a hologram record of the ruby pulse. Figures 14 and 15 show some of the interferograms of this wavefront with a large radius (50 cm) spherical wavefront generated by SP2 (fig. 12). Fig. 14 shows two sets of "horizontal" fringes. Because of the introduced tilt, the fringes are slightly curved upward in (a) and downward in (b). In fig. 14 there are distinct jumps in the fringe contour (phase contour) as one goes from one lobe to another which is the established characteristics of a laser mode. The "vertical" fringes of fig. 15 further establishes the fact that each lobe corresponds to "roughly" one and the same phase. But, still, it is very difficult to assign any particular mode numbers to it. Besides, the "diffraction fringes" in the intensity pattern (fig. 13) makes it more difficult to explain. It appears that the emission was a mixture of some "filamentary" modes and some higher order Hermite-Gaussian modes; and the different transverse modes could belong to different longitudinal modes. In case the experimenter is specifically interested in identifying the different transverse modes corresponding to different longitudinal modes, he should use Aleksoff's method<sup>(18)</sup> of putting a high resolution spherical Fabry-Perot (FPS) etalon in one beam and a diffuser in the other beam, where

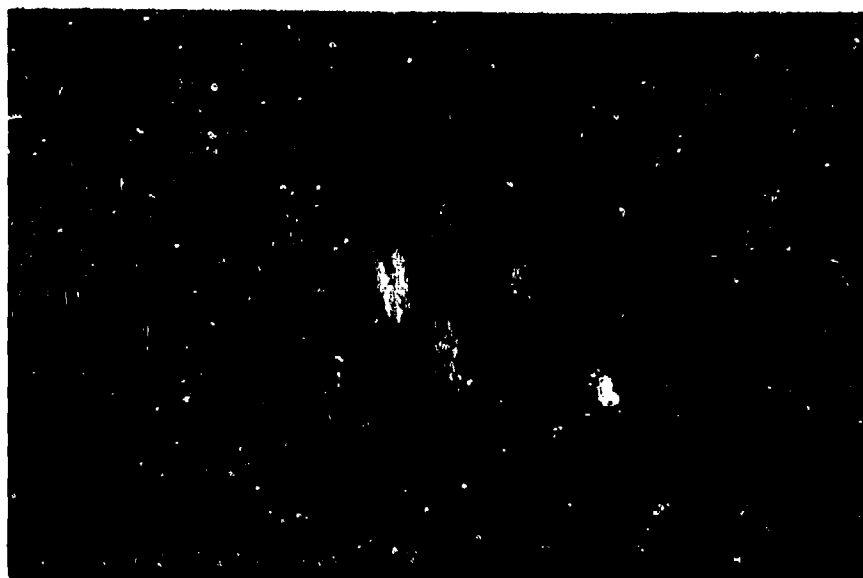


(a)

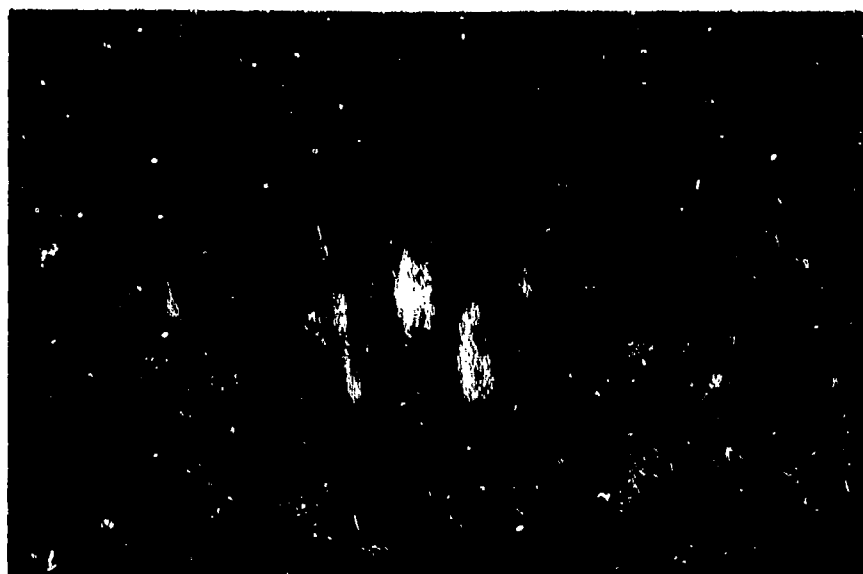


(b)

"HORIZONTAL" FRINGES. INTERFEROGRAMS OF THE PULSE-LASER-WAVEFRONT RECONSTRUCTED IN CONTINUOUS MODE. THE CENTER OF CURVATURE OF THE FRINGES IS ABOVE THE CENTER OF THE PICTURE IN (a) AND BELOW IN (b).



(a)



(b)

"VERTICAL" FRINGES. INTERFEROGRAMS OF THE PULSE-LASER-WAVEFRONT RECONSTRUCTED IN CONTINUOUS MODE. THE CENTER OF CURVATURE OF THE FRINGES IS TO THE LEFT OF THE CENTER OF THE PICTURE IN (a) AND TO RIGHT IN (b) .

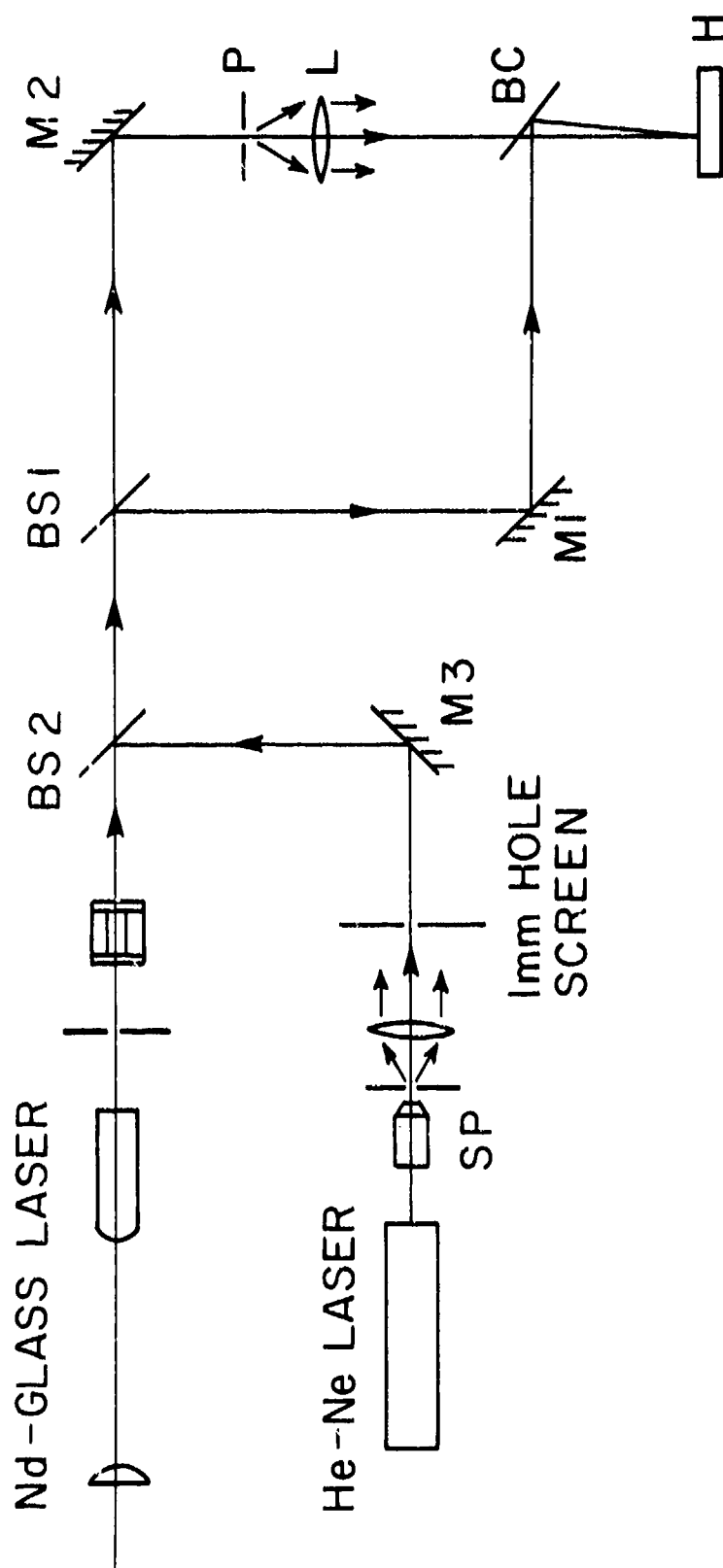
Fig.15

the reference beam consists of spatially separated longitudinal modes through FPS and the object is the diffuser illuminated by an unperturbed part of the laser pulse.

## 7. APPLICATION OF THE METHOD TO Nd-GLASS LASER

In this section we report the results of application of the local reference beam holography method to the study of a Nd-glass pulsed laser wavefront. It has been mentioned in section 5 that this laser poses two problems for holography: (a) Kodak 4-Z film (still in experimental stage) which is sensitive to  $1.06\mu\text{m}$  radiation, has a resolution capability of less than two hundred lines per mm. (b) The Nd-glass laser pulse has a very short temporal coherence length ( $\sim$  few mm) even with a resonating output mirror (top left part of fig. 16). Both these problems can be handled by a Mach-Zehnder interferometer type holographic arrangement (right hand portion of fig. 16).

It can be seen in fig. 16 that the laser rod is like a thick plano-convex lens and the totally reflecting mirror is a 'matching' convex mirror. The output 'mirror' is a tilted etalon <sup>(22,23)</sup> which is capable of forcing the cavity to lase in a spectral bandwidth narrow enough



LRB HOLOGRAPHY TO RECORD A Nd - GLASS  
PULSE LASER WAVEFRONT .

Fig.16

for holographic work. This arrangement with an appropriate aperture inside the cavity is capable of giving a  $TEM_{00}$  mode output of large beam diameter ( $\sim 3\text{mm}$ ). The CW He-Ne laser is used for aligning the laser cavity.

Initially the holographic fringe frequency was set for about 400 lines/mm as it was the initial claim on 4-Z film. Because of consistent failure to record any hologram, a shearing interferogram of fringe frequency of about one line per millimeter was first recorded on 1-Z film (Fig. 17b; Fig. 17a shows the intensity record). The shearing interference was produced by the two beams reflected from the front and back surfaces of about half a millimeter thick microscope coverglass. The shearing interferogram demonstrates that the radiation had at least several mm temporal coherence. So, the only reason for the failure of recording a hologram must have been due to having a fringe frequency of the order of or higher than the frequency response of the film.

Then the angle of interference of the hologram beams was reduced so as to have fringe frequency around 100 lines/mm and a successful hologram was recorded (fig. 17c). The reconstruction was carried out with a  $TEM_{00}$



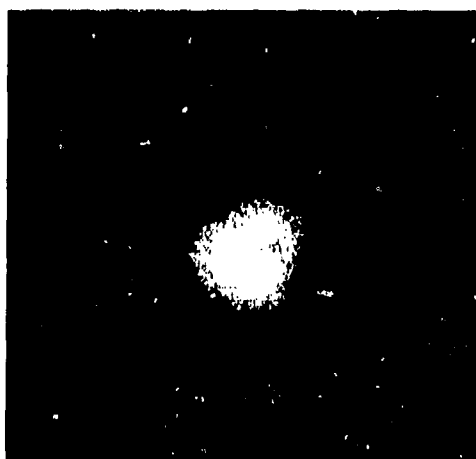
(a)



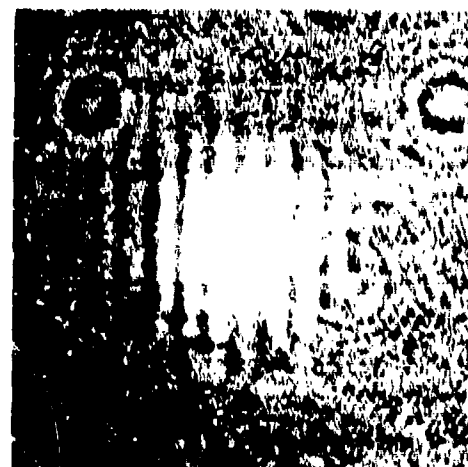
(b)



(c)



(d)



(e)

STUDYING Nd - GLASS PULSE LASER WAVE  
FRONT BY LRB - HOLOGRAPHY USING 4Z FILM.  
(a) DIRECT INTENSITY PATTERN (b) SHEARING INTER-  
FEROGRAM, (c) HOLOGRAM (~100 L/MM) (d) RECON-  
STRUCTED INTENSITY PATTERN, (e) INTERFEROGRAM  
OF THE RECONSTRUCTED WAVEFRONT.

He-Ne laser. The arrangement has been discussed in Sec. 5 (fig. 10). The reconstructed intensity pattern is shown in fig. 17d which is remarkably similar to the direct record (a). The interferogram formed with the reconstructed beam is shown in (e). Comparison of (b) and (e) demonstrates that both the direct and the reconstructed wavefront have uniform phase. But, the shape of the intensity pattern, slightly triangular (a and d) restrains one from concluding that the pulse was a  $TEM_{00}$  one. It is likely that the laser cavity was producing a  $TEM_{00}$  wavefront of beam diameter larger than the aperture set inside the cavity (fig. 16) and that the slight deviation of this aperture from perfect circular shape gave rise to the slightly triangular amplitude distribution with uniform phase.

Thus we can claim to have established our essential objective that even Nd-glass infrared laser wavefront can be studied by our method. At this point we may mention that, as far as literature is concerned, this is the first successful record of an infrared hologram on conventional photographic film sensitized to infrared radiation.



## 8. CONCLUSION

The main purpose of this work was to develop and establish a local reference beam holographic technique in conjunction with interferometry to study beam parameters of any laser wavefront (CW or pulsed). The complete information about any wavefront is known when its mutual intensity function is determined; and a hologram records this complete information. Then, following the role of coherence function in the visibility of interference fringes and its corresponding effect in holographic reconstruction, it is easy to see that the brightness in the holographically reconstructed image is proportional to the square modulus of the mutual coherence function between the object point and the reference wave point. So, with a knowledge of the reference wavefront, the modulus of the mutual coherence function can be mapped out from the photometric measurement of the intensity in the reconstructed image. The phase of the mutual coherence function can be unambiguously measured by our interferometric technique after holographic reconstruction.

## REFERENCES

1. Mehta, C.L., Nuovo Cimento, 36, 202-205 (1965)  
"Determination of Spectral Profiles from Correlation Measurements"
2. Hariharan, P., & Sen, D., JOSA 51, 1307 (1961)  
"Effects of Partial Coherence in Two-Beam Interference"
3. Leith, E.N. and Upatnieks, J., JOSA 52, 1123 (1962)  
"Reconstructed Wavefronts and Communication Theory"
4. Korobkin, V.V. and Leontovich, A.J., Sov. Phys. JETP 17, 1242-45 (1963)  
"Coherence and Time Scanning of the Emission Spectrum of a Ruby Laser"
5. Bondarenko, N.G., Eremina, I.V. and Talanov, V.I., JETP 19, 1016 (1964)  
"The Phase Structure of the Output Beam of a Ruby Laser"
6. Davis, L.W., Appl. Phys. Letts., 10, 301 (1967)  
"Interferometric Investigation of the Wavefront of Laser Beams"
7. Miyamoto, T. and Yasuura, K., Appl. Opt. 10, 161 (1971)  
"Measurement of the Beam Parameters of a Laser Beam and Its Diffraction Field, Using a Hologram"
8. Cathey, W.T., in "Holography: State of the Art Review 1969", ed. Kallard, p.96, Optosonic Press.  
"Local Reference Beam Generation for Holography"  
Patent application Dec. 8, 1965: Patent granted Dec. 10, 1968.
9. Rosen, L. and Clark, W., Appl. Phys. Letts. 10, 140 (1967)  
"Film Plane Holograms Without External Source Reference Beam"
10. Caulfield, H.J., Harris, J.L. and Hemstreet, H.W. Jr., Proc. IEEE 55, 1758 (1967)  
"Local Reference Beam Generation in Holography"
11. Caulfield, H.J., Phys. Letts. 27A, 319 (1968)  
"Information Retrieval from Local Reference Beam Holograms"

## REFERENCES

12. Caulfield, H.J., Laser Focus, p 21, November 1967  
"Local Reference Beam Holography"
13. Lurie, M., JOSA 58, 614 (1968)  
" Fourier Transform Holograms with Partially Coherent Light: Holographic Measurement of Spatial Coherence"
14. Murata, K., Asakura, T. and Fujiwara, H., Optica Acta 17, 5 (1970)  
"Effects of Spatial Coherence on Holography"  
(First presented at the Symposium on Application of Coherent Light, Florence, 1968)
15. Fujiwara, H., Asakura, T., Murata, K.  
Optica Acta 17, 823 (1970)  
"Some Effects of Spatial and Temporal Coherence in Holography"
16. Ross, I.N., "Holographic Measurement of Coherence"  
paper 2-4, "Application of Holography: Proceedings of the Internatnl. Symposium of Holography 1970"  
eds: Vienot, Bulabois, Pasteur, Besançon, France
17. Aleksoff, C.C., Paper presented at the 1970 Spring Meeting of the Optical Society of America, JOSA 60, 74 (1970)  
"Holographic Determination of Spatial Coherence"
18. Aleksoff, C.C., JOSA 61, 1426 (1971)  
"Holographic Analysis and Display of Laser Modes"
19. Brandt, G.B., Appl. Opt. 8, 1421 (1969)  
"Image Plane Holography"
20. Patek, K., "Glass Lasers", London Illife Books, 1970.
21. Broude, V.L. et al, J. Exp. Theor. Phys. Lett. 2 (11), 324 (1965).
22. Snitzer, E., Appl. Opt. 5, 121 (1966)  
"Frequency Control of a  $\text{Nd}^{3+}$  Glass Laser"
23. Hercher, M., Appl. Opt. 8 (6), 1103 (1969)  
"Tunable Single Mode Operation of Gas Lasers Using Intracavity Tilted Etalon"

#### REFERENCES

24. Hercher, M., Appl. Opt. 7 (2), 39 (1965)  
"Single Mode Operation of a Q-Switched Ruby Laser"
25. Thompson, B.J. et al, Technical Report AFAL-TR-71-346,  
Advanced Research Project Agency, Air Force Avionics  
Laboratory, Wright-Patterson Air Force Base, Ohio,  
March 1972  
"Studies in Optics"

## SECTION III

THE DESIGN OF EFFICIENT SOLID STATE LASER SYSTEMS WITH  
HIGH AVERAGE POWER AND LOW BEAM DIVERGENCE  
The Measurement and Correction of Optical  
Distortion in Solid Laser Rods

by M. Hercher

1. INTRODUCTION

One of the most desirable characteristics of a laser is its capability to emit a beam whose angular divergence is limited only by diffraction. In order to realize this low beam divergence in practice, however, the laser resonator must be properly designed and the components of the laser must be of high optical quality. More specifically, a wavefront making a single traverse of the laser resonator should be distorted from a perfect plane or spherical wavefront by no more than a small fraction of a wavelength. In the case of solid lasers (either crystal or glass) this condition is often difficult to satisfy. To start with, most laser rods, particularly those whose length exceeds a few centimeters, are found to be optically imperfect even when their ends are polished plane and

parallel. Refined crystal growth and glass fabrication techniques have gone far to minimize this problem, but it still exists. In high quality solid laser materials typical passive optical distortions are on the order of one or two waves per centimeter of aperture for every ten or twenty centimeters of length. More difficult than these passive aberrations, however, are those distortions which are due to thermal effects during the operation of the laser. If a laser rod is optically pumped more or less uniformly across its cross-section, then it will be heated more or less uniformly. But if, as is typically the case, it is cooled by a fluid flow across its cylinder surface, then it will certainly be cooled nonuniformly. Any resultant thermal gradients within the laser rod will cause a corresponding optical distortion. These thermal distortions are of two types: those due to thermal expansion, and those due to a thermal variation in the refractive index of the laser material. In some instances these two effects have been used to balance one another, but in most cases this is not a viable approach.

The problem with which we are concerned in this section is this: given a laser rod which at the instant of laser emission has a reproducible optical distortion, how do we

(a) measure this distortion and (b) compensate for it. We will not be concerned with the question of avoiding these types of distortion either in the fabrication of materials or in the design of laser systems, although it is clear that significant improvements can be made in these areas.

In the following paragraphs we will describe a variety of techniques for accurately measuring the optical distortion in a laser rod at the instant of lasing, and we will describe some methods for using this data to correct for these distortions.

## 2. MEASUREMENT OF OPTICAL DISTORTION IN LASER RODS

It is fairly easy to measure the angular divergence of a laser beam, and with a little more trouble one can determine the radius of curvature of the sphere which most nearly matches the wavefront emitted by the laser. Unfortunately, this falls far short of the quantitative assessment of the laser beam which is required in order to make a correction plate for the laser. (A correction plate is a passive element which, placed inside the laser resonator, converts the distorted wavefront to a plane or spherical wavefront.) The adequate measurement of the distorted

wavefront must include both phase and amplitude information. The phase information is more important since when the phase distortion is corrected, the amplitude distribution will generally become uniform. In order to record the required phase information we must obtain an interferometric record of the wavefront. This can be in the form of a conventional interferogram, or it can be a hologram.

There are two somewhat different approaches that we can take in measuring the distortion of a laser rod. We can either directly record the wavefront emitted by the laser, or we can use the light from another laser -- preferably one emitting a plane wavefront -- to assess the interferometric quality of the laser rod under the conditions in which it is to be used. The first method has the advantage of directness, i.e. one obtains precisely the information that is desired, but this method is often inconvenient. For example, if the laser being tested has a broad spectral bandwidth then it may be very difficult to adequately equalize optical paths in the interferometer in order to obtain an interferogram of high visibility. The second method is less direct and may not precisely reproduce the operating conditions of the laser, but it



is often far more convenient.

Following are descriptions of a number of different techniques for obtaining interferometric measurements of distorted wavefronts from lasers. Each description is accompanied by an assessment of that particular method, and, in some instances, an example of a situation where it might prove particularly useful.

#### Mach-Zehnder Interferometer

The two versions of this interferometer which we have considered are shown in figs. 18 and 19. In the first case, shown in fig. 1, the laser rod under test is placed in one arm of the interferometer and a collimated beam from a gas laser is used as the light source. The camera is focused on the laser rod and the resultant interferogram is, in effect, a contour map of the aberrated wavefront which has made a single pass through the laser rod. We have used this arrangement extensively in measuring the thermal distortions in flashlamp-pumped ruby laser rods. A typical interferogram is shown in fig. 20, which is one frame from a 64 fps camera and was exposed approximately 1 msec after the flashlamp was fired. We have also used this arrangement with a Q-switched ruby laser as a light

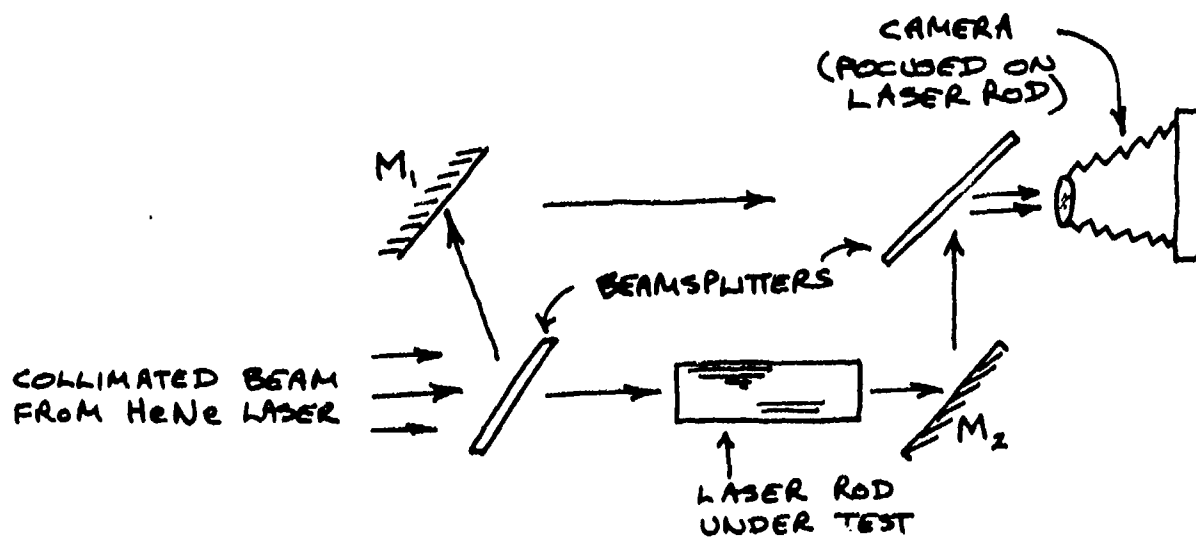


Figure 18. Mach-Zehnder interferometer arrangement for testing laser rods.

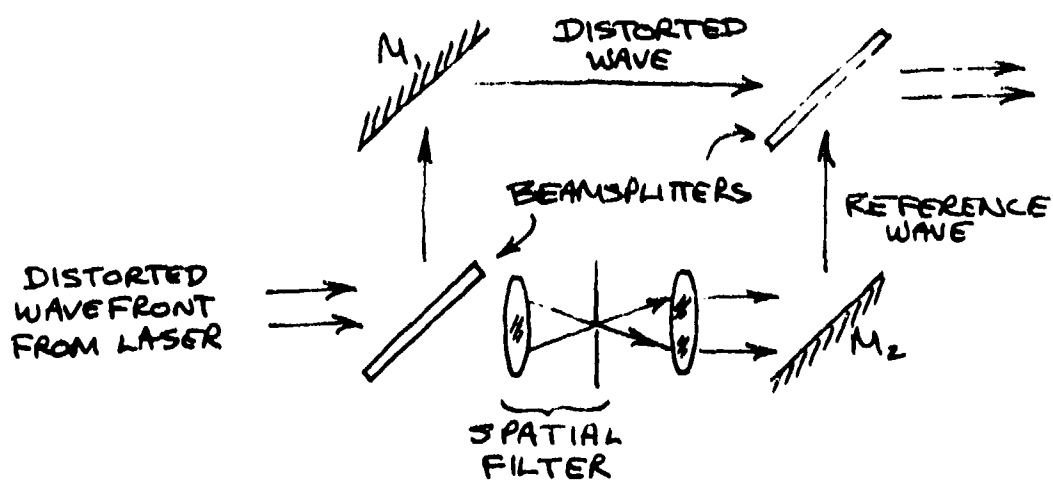


Figure 19. Mach-Zehnder interferometer arrangement for measuring distortion in laser wavefronts.



Figure 16. Interferogram of a pulsed laser rod in repetitive operation at 1 pulse per second. Exposure was made approximately 1 millisecond after flashing pulse.

source -- synchronizing the Q-switched laser pulse with the firing of the flashlamp so as to obtain an interferogram at the instant during the flashlamp pump pulse at which the laser rod under test was to be operated.

In the latter mode of operation, a helium-neon laser was used for aligning the interferometer and equalizing the optical path lengths in the two arms.

In the mode of operation shown in fig.19, it is not the laser rod which is examined interferometrically, but rather the wavefront which has emerged from the laser rod(s). As mentioned earlier, this method of assessment has the advantage of directly measuring the wavefront which is to be corrected. Also, this method is more suitable for measuring the wavefront distortion due to a number of laser rods in series. As shown in fig.19, the distorted wavefront passes through one arm of the interferometer, while a spatial filter is located in the other arm of the interferometer. This spatial filter is used to derive a diffraction-limited, undistorted plane wave from the aberrated incident wave. The more badly distorted the incident wave, the smaller the amount of energy in the spatially filtered wave. As a result, there is generally some difficulty in equalizing the energies in the two interfering wavefronts so as to

assure good contrast in the interferogram. One might expect that for a badly distorted wavefront, there might be a variation in wavelength across the beam; this would, of course, make it impossible to record interference fringes in the manner described above. To date we have not encountered this problem even though we have made measurements of laser rods so badly distorted that they tended to oscillate in filaments. The in-line hologram technique described below appears to be a far more convenient method for making the types of measurement described in this paragraph, and will be tested in the near future.

It should be noted that a Twyman-Green interferometer (fig.21) can be used in place of a Mach-Zehnder interferometer; since it is a double-pass interferometer, it is twice as sensitive as a Mach-Zehnder interferometer, but does not readily lend itself to the insertion of a spatial filter in one arm.

#### Holographic Wavefront Recording

Holographic techniques for recording laser wavefronts offer the significant advantage that they allow the distorted wavefront to be faithfully reproduced, so that interferometric assessment can be carried out afterwards

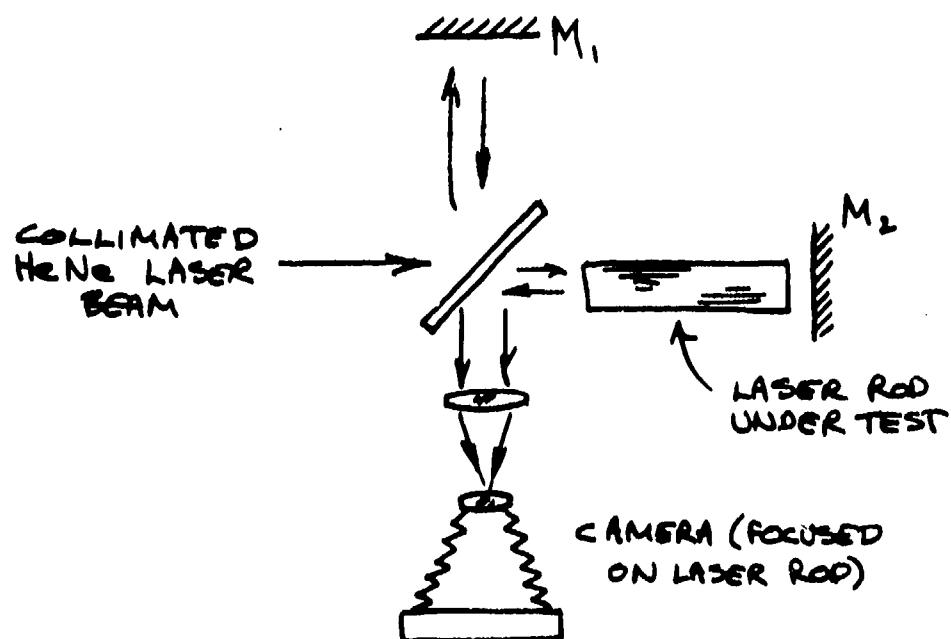


Figure 21. Twyman-Green interferometer arrangement for testing laser rods.

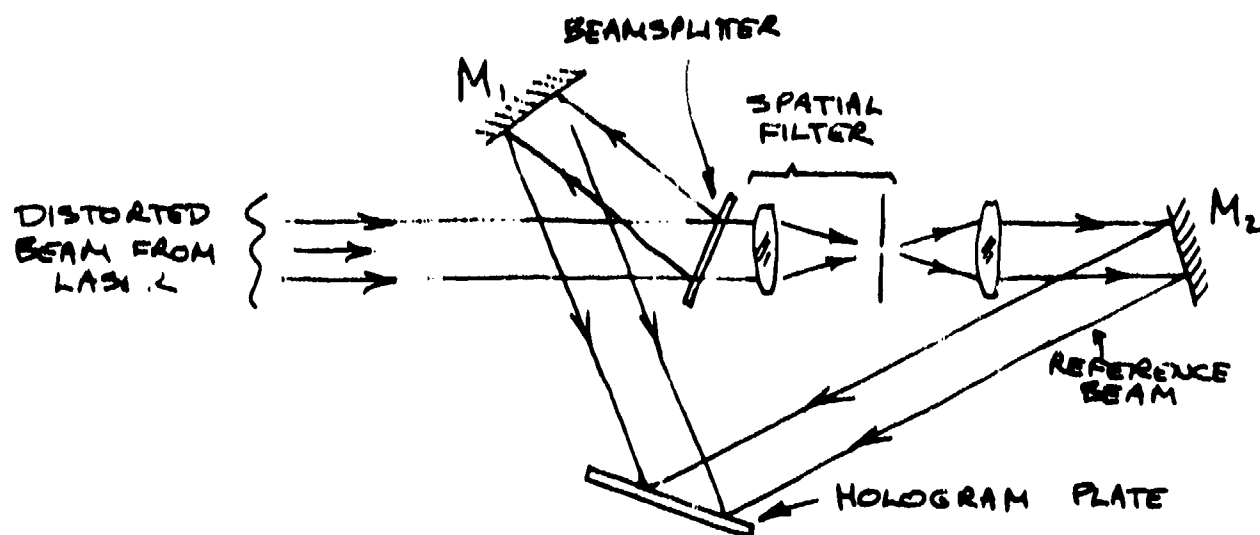


Figure 22. Method for obtaining holographic records of distorted wavefronts from lasers. Polarization of the laser beam should be perpendicular to the plane of the figure.

by a wide variety of techniques. The hologram itself, however, is an interferogram and requires careful equalization of optical paths, polarization orientation, high resolution film, etc. The basic optical arrangement is shown in fig. 22 (which closely resembles fig. 19). A major problem in using this technique is that the optical path lengths for the object and reference beams must be equal to within a single coherence length of the laser being tested. The coherence length is related to the spectral bandwidth of the laser by

$$L_c = \lambda^2 / \Delta\lambda,$$

where  $\Delta\lambda$  is the spectral bandwidth. For a ruby laser this may be as small as 5mm, and for an  $\text{Nd}^{+++}$  glass laser it is likely to be less than 1 mm. When the angle between the object and reference beams is appreciable, path equalization requires elaborate optical compensation and the use of this technique becomes questionable, particularly in view of the alternative techniques which can provide comparable data. (The elaborate path equalization techniques were developed in conjunction with the use of a Q-switched ruby laser for short exposure holography of non-luminous objects.) In the case of lasers operating at 1.06 microns, the very high resolution photographic materials generally

used for holography are not yet available.

After a hologram is obtained it can be bleached (which effectively increases the exposure latitude of the film at the expense of an increase in background noise) and "played back" by illuminating it with a beam (derived from a cw gas laser) whose orientation relative to the plate matches that of the reference beam during exposure. The reconstructed wavefront can then be assessed interferometrically (e.g., using the arrangement of fig.19) and, if desired, the effect of a correction plate can be directly observed.

#### In-Line Hologram

This technique, which we have only recently developed, is actually an interferometric as much as a holographic technique. That is to say, the resultant photograph can be either interpreted directly in terms of the wavefront distortions in the laser beam, or it can be used to holographically reconstruct the distorted laser beam. The optical system is simple, can tolerate reasonably large laser spectral bandwidths, and is well suited for on-line use in an operating laser system.

The optical arrangement for this system is shown in



fig.23: the distorted beam passes through a beam-splitter which, in practice, might only transmit a few percent of the incident energy. The "reference" beam is derived from a small portion of the incident wave and diverges to match the diameter of the object beam, at a distance  $L$ , either by diffraction or by the action of a small negative lens. The diameter,  $d$ , of the aperture used to select out a portion of the incident wave for use as a reference beam should match the maximum area in the incident beam over which the wavefront is essentially constant in phase. If necessary, this aperture may be small enough to guarantee a diffraction-limited spherical wave (i.e.  $d \sim \lambda D / 4D$ ), but this leads either to a very small amount of light in the reference beam, or else a large value for  $L$ . The maximum path difference between the reference beam and the object beam is approximately  $D^2/8L$ : this leads to the following inequality for  $L$  in order to ensure fringes of good contrast when the laser has a spectral bandwidth  $\Delta\lambda$ :

$$L \geq \frac{D^2 \Delta\lambda}{8 \lambda^2}$$

In the case of a beam from a  $\text{Nd}^{+++}$  glass laser with a beam diameter of 5cm and a  $20\text{\AA}$  bandwidth at a wavelength

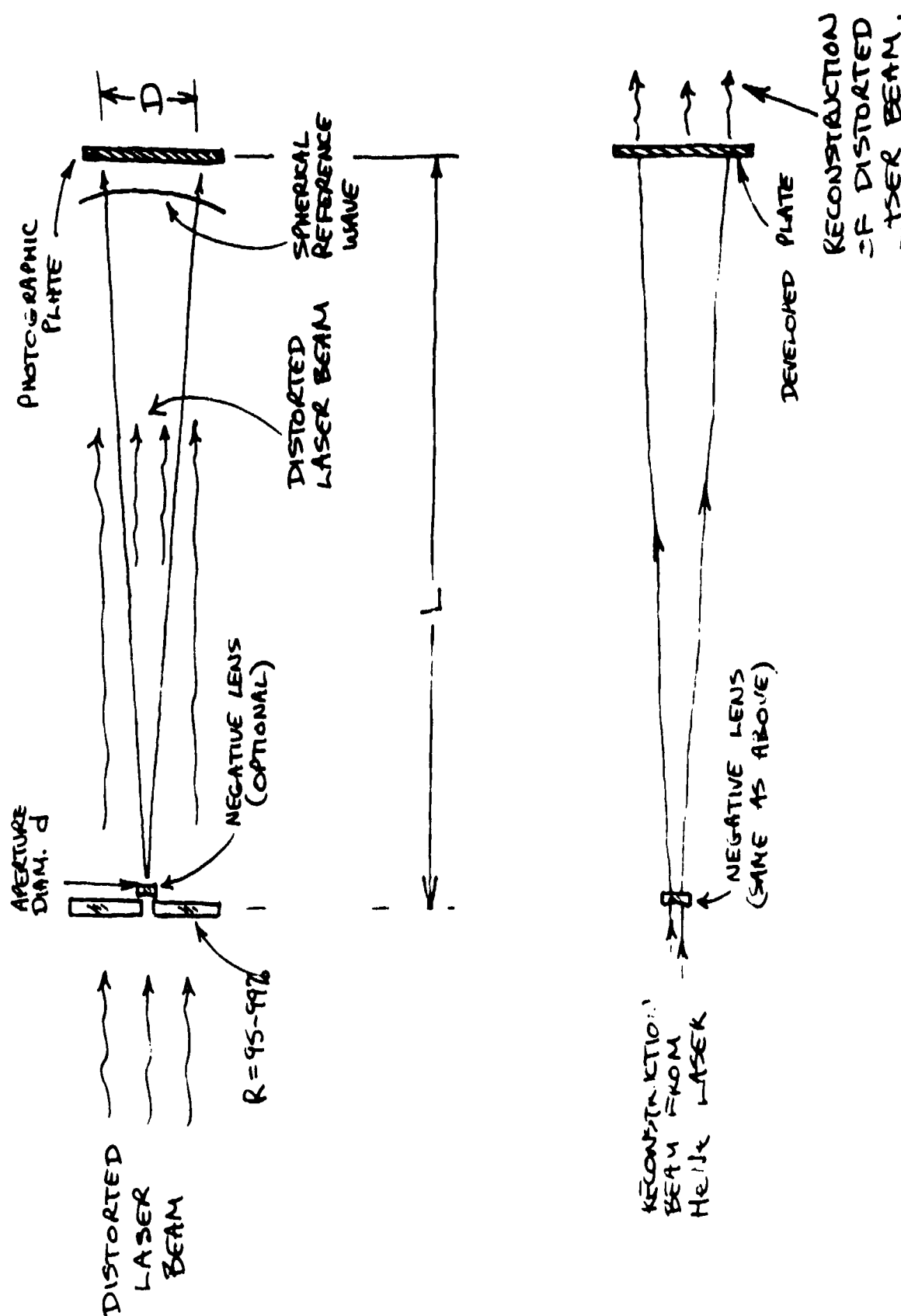


Figure 23. Method for obtaining in-line holograms of distorted laser wavefronts. This method is particularly suitable for high power, broad-band lasers.

of 1.06 microns,  $L$  would have to be greater than about 60 cm, which is certainly no problem. If we chose to be conservative in this case and worked with a 200 cm separation between the beam-splitter plate and the film, then the interferogram-hologram would have a total of approximately 150 roughly circular fringes. The precise shape of these fringes would contain the information from which the wavefront aberration could be calculated. Alternately, the developed photograph could be set back in place and illuminated by a point source (derived from a gas laser) located at the small aperture in the beamsplitter. (If a negative lens had been used to obtain the reference beam, the point source would be on the other side of the beamsplitter at a distance equal to the focal length of the negative lens.) This point source would, of course, appear in the center of the holographic reconstruction of the distorted wavefront -- but could easily be blocked out if desired. We are enthusiastic about this method of testing and are currently planning to use it in testing and ultimately correcting a number of large glass amplifier rods for use in the Laser Energetics Laboratory at the University of Rochester. The advantages of this technique over the earlier techniques which have been used are:

1. It offers the option of either holographic reconstruction or direct measurement from the interferogram.
2. It is cheap and simple and does not require elaborate optics or high resolution film.
3. It can easily be used on-line since it samples only a percent or so of the light and reflects the remainder from a plane mirror.
4. It allows measurements of laser beams with large spectral bandwidths.

### 3. CORRECTION OF OPTICAL DISTORTION IN LASER RODS

#### Introduction

The earliest attempts to optically correct laser rods at The Institute of Optics were made in 1962. The laser rods in question were 7.5cm long by 0.62cm diameter ruby rods whose mirrors were to be coated onto the ends of the rods. Prior to coating, the laser rods could be interferometrically assessed by illuminating the laser rod with a collimated beam from a HeNe laser and looking at the interference between the light reflected from the two ends of the rod -- being sure to illuminate the rod with the same linear polarization which it would emit as a laser.

Optical correction was accomplished by hand figuring of one of the ends of the laser rod; i.e. one end of the laser rod was polished by hand, using a Q-tip and diamond paste, until the desired degree of correction was attained -- with continuous interferometric monitoring. This process was extremely tedious, but was capable of excellent results -- particularly when the initial distortions were relatively smooth. The corrected laser rods had dramatically improved beam divergences, and spectra with well-defined axial modes. This method was used for correcting passive distortions (i.e. distortions existing in the unpumped laser rod), and would have been far more difficult to execute in correcting active distortions. Our present point of view is that this method has an air of desperation about it, and that by using the techniques described below comparable results can be achieved on a production scale and without the requirement for patient, highly skilled optical technicians.

#### Production of Scaled Correction Plates

We will define a correction plate as an optical component which is polished or otherwise fabricated so as to convert an incident wave with phase distortions

into a transmitted plane wave. In the correction procedure described in the previous paragraph, the correction plate was the laser rod itself. One end of the laser rod was figured by polishing so that its contour matched that of the incident-distorted wavefront. In this instance the correction plate had a 1 to 1 scale factor: that is to say, the figured correction surface had a contour just equal to the inverse of that of the distorted wavefront. In the technique which we will describe the surface contour of the correction plate will be scaled up to proportions more manageable by machine operation, and the surface of the correction plate will have a fine grind rather than a polish. The objective of these modifications is to replace the hand-figuring of correction plates by a tape-controlled machine operation.

Let us assume that the distorted wavefront to be corrected has been recorded in the form of an interferogram in which the fringes are contours of the distorted wavefront, having an interval of one wavelength. The desired correction plate is simply an optical element whose optical thickness contour map is the inverse of that of the distorted wavefront. That is to say, the contour map of the optical thickness of the correction plate would appear identical to the interferogram

of the distorted wavefront, except that peaks and valleys would be interchanged. Typical laser wavefront distortions are in the range of 10 to 100 wavelengths: the direct machining of a glass surface to achieve a polished surface contour on this scale is not feasible with presently available technology. If the scale of the desired correction could be increased, say by a factor of 100, and if the requirement for a polished surface could be relaxed, then the operation could be carried out by a tape-controlled milling machine.

The basic idea which we have proposed is to manufacture a scaled-up correction plate, as illustrated in fig.24, and then to scale it back down again for use by immersion in a liquid whose refractive index very nearly matches that of the plate. The scaling factor,  $M$ , can easily be shown to be given by:

$$M = \frac{n-1}{\Delta n} ,$$

where  $n$  is the refractive index of the glass correction plate, and  $\Delta n$  is the index difference between the correction plate and the immersion liquid. By scaling in this manner not only does mechanical fabrication become feasible, but the need to polish the surface of the correction plate is also removed. The intensity reflection coefficient at the

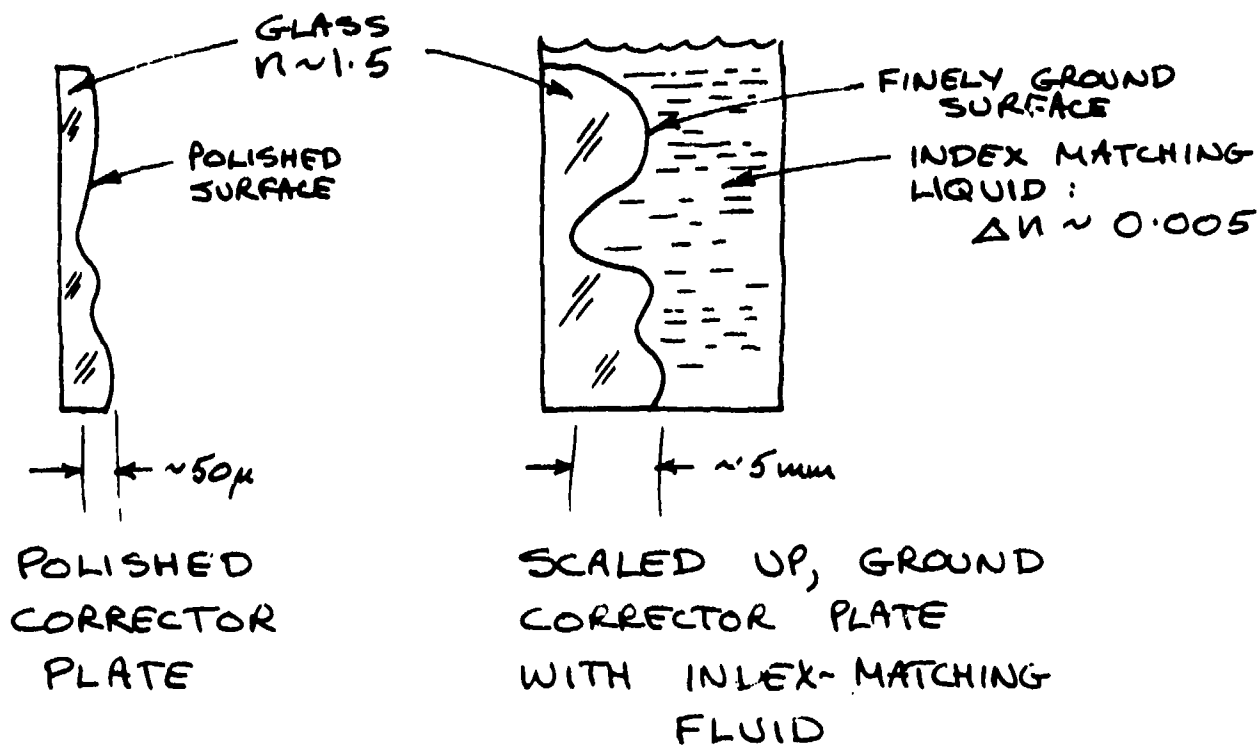


Figure 24. Illustration of a scaled-up correction plate.

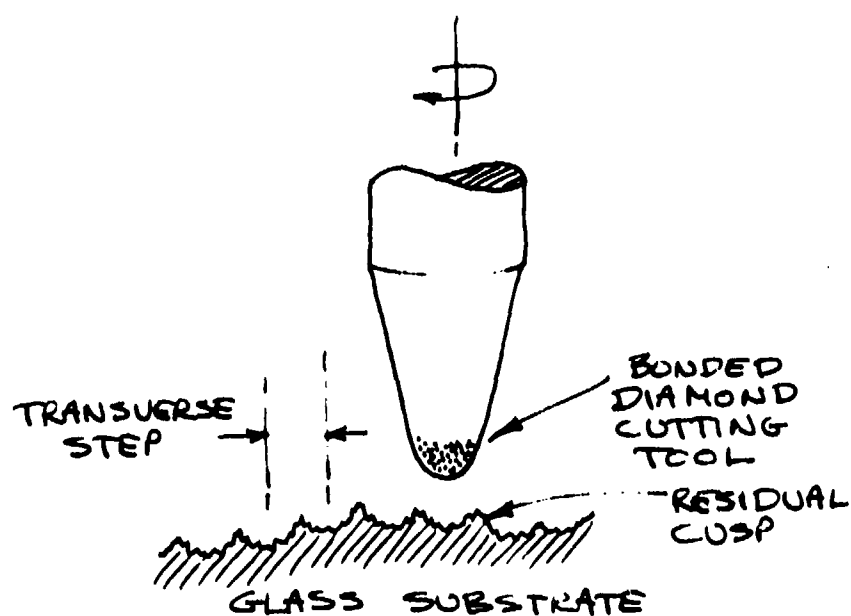


Figure 25. Machining of a scaled-up correction plate, using a spherical-tipped tool with bonded diamond grit.



glass-liquid interface is given by:

$$R = \frac{(\Delta n)^2}{4n^2}.$$

Thus if we are willing to tolerate a 1% reflection loss at the interface between the glass and liquid (which is reasonable for solid state laser systems) we should use an index mismatch no greater than approximately 0.3. This value is in fact far greater than any we would contemplate using in practice, so that the reflection loss at the interface can be neglected. The next question we should consider is the surface smoothness of the effective correction plate. An optical surface is generally considered to be smooth, or optically "polished", when its RMS surface roughness is less than an eighth of a wavelength. Thus, if we designate the RMS surface roughness by  $\bar{d}$ , and take into account the fact that the index immersion reduces the effective surface roughness by the scale factor M, we see that the following equation must be obeyed if the effective surface of the corrector plate is to be optically smooth:

$$\bar{d} < \frac{(n-1)\lambda}{8\Delta n} = \frac{\lambda M}{8}$$

To get an idea of what this means, consider an example in which the wavelength is  $6000\text{\AA}$  and the scale factor is 100: in this case the RMS surface roughness should be less

than  $7\frac{1}{2}$  microns, which could be attained by figuring with a diamond tool. The type of tape-controlled milling machine which we are going to use in making these scaled-up correction plates operates in a step-and-repeat mode. That is to say, the X and Y coordinates are set and then the tool comes down to a predetermined Z coordinate; the tool then goes up and a new XY coordinate is set whereupon the tool comes down to a new Z coordinate and so on. For the final operation we are planning to use a 1 millimeter diameter diamond tool with bonded 400 mesh diamond grit (a 400 mesh corresponds to a 10 micron particle size, which gives RMS surface finish of approximately 5 microns).

In a step-and-repeat operation of this sort, a small cusp of material is left between adjacent steps, as shown in fig.25. The height of this cusp should be made comparable to the RMS surface roughness: for a spherical diamond tool with a 1 millimeter diameter, the cusp height is reduced to seven microns when the sideways steps are approximately 170 microns. Taking steps of this size, approximately 3600 step-and-repeat operations would be required for each square centimeter of corrector plate surface. This would be tedious to do by hand but would present no

problems for a tape-controlled milling machine. To eliminate the interference pattern due to the regularity of the machining operation, it would probably be desirable to work the finished surface of the corrector plate with a loose slurry of 5 micron abrasive. The final machine operation described above would probably be preceded by a similar machine operation using a larger radius tool and a coarser diamond grit, but using the same control tape.

Let us consider how a correction plate would be manufactured in a specific instance. We will assume that the distorted wavefront to be corrected has been described in the form of an interferogram in which the fringe spacing corresponds to one wavelength contours. We will also assume the following: that the transverse section of the distorted wavefront is a square 2 centimeters on a side, the laser wavelength is 0.7 microns, and in scanning a cross-interferogram in a straight line one encounters no more than 40 fringes. We will proceed by making a tentative selection for the final grinding tool: let's say this is to be a 1 millimeter diameter tool with the 400 mesh diamond grit which we used in an earlier example. If, as in the earlier example, we take steps of 170 microns between machining operations, the RMS surface roughness (due both to the

selection of diamond grit size and the residual cusps on the surface) will be approximately 7 microns. We should now choose a scale factor such that this residual surface roughness can be reduced to less than an eighth of a wavelength, so that any scattering at the liquid-glass interface will be negligible. A reasonable scale factor would thus be 100. If the refractive index of the glass corrector plate is approximately 1.46, this scale factor can be attained within an index difference of approximately 0.005. This refractive index difference is certainly small enough so that reflection at the glass-liquid interface can be neglected. Now that we know what the scale factor must be, we can estimate what the general contour of the ground corrector plate will be. A 1-to-1 corrector plate made of polished glass would depart from a plane surface by about 60 microns, corresponding to the 40 wavelength distortion of the wavefront. With a scale factor of 100, the ground glass surface of the index-matched corrector plate would depart from a plane by about 6 millimeters. Note that the large scale factor is necessary primarily so that the index mismatch can be small enough to render surface scattering negligible. As mentioned earlier, the final machining run, made using a tool

1 millimeter in diameter with 400 mesh diamond, would be preceded by a machining run with a somewhat larger diamond tool having a coarser diamond grit.

The refractive index of 1.46 selected for the corrector plate (corresponding to fused quartz) was chosen because of the ready availability of index-matching liquids in the vicinity of this refractive index. In particular DMSO (dimethyl sulfoxide) has a refractive index of 1.46 at 20 degrees Centigrade and a  $dn/dt$  of  $4.27 \times 10^{-4}/^{\circ}\text{C}$ . Thus index-matching using quartz and DMSO can be achieved over a small range simply by varying the temperature of the DMSO. (One must, of course, also take into account the thermal variation of the refractive index for quartz.) DMSO has the added advantage that it is highly transparent at 1.06 microns, the wavelength of neodymium-doped lasers.

In order to obtain the approximately 15,000 instructions for the tape-controlled milling operation, the information contained in the interferogram of the distorted wavefront must be digitized. We plan to use a Hewlett-Packard model 9810 calculator in conjunction with a model 9864 graphical digitizer to accomplish this operation. There are many ways that this equipment can be used to provide the desired information, and we will describe just one such way.

Since a scan in either direction across the interferogram (see fig.26) is likely to encounter about 40 fringes, it would seem reasonable to perform an initial digitization by making 40 scans across the interferogram, say in the x-direction, and noting the location of the fringes crossed in each scan. This initial data, which would be obtained by a manual scan of the interferogram, would then be used as the computer input in calculating a least-squares mapping of the entire 2 centimeter by 2 centimeter area. This two-dimensional least-squares fit to the initial data would then be used to generate the approximately 15,000 z-coordinates for each point at which a machining operation is to be performed. Recall that these machining operations are to take place with 170 micron transverse spacings. The 15,000 sets of coordinates will then be coded onto paper or magnetic tape for use in controlling a milling machine. Happily, as mentioned before, this same set of instructions can be used for the initial machining operation to be carried out with a larger diameter tool and a coarser grit.

Although we have not yet carried out the complete procedure as described above, we have no doubt whatsoever that it will work and that it will take far fewer man hours

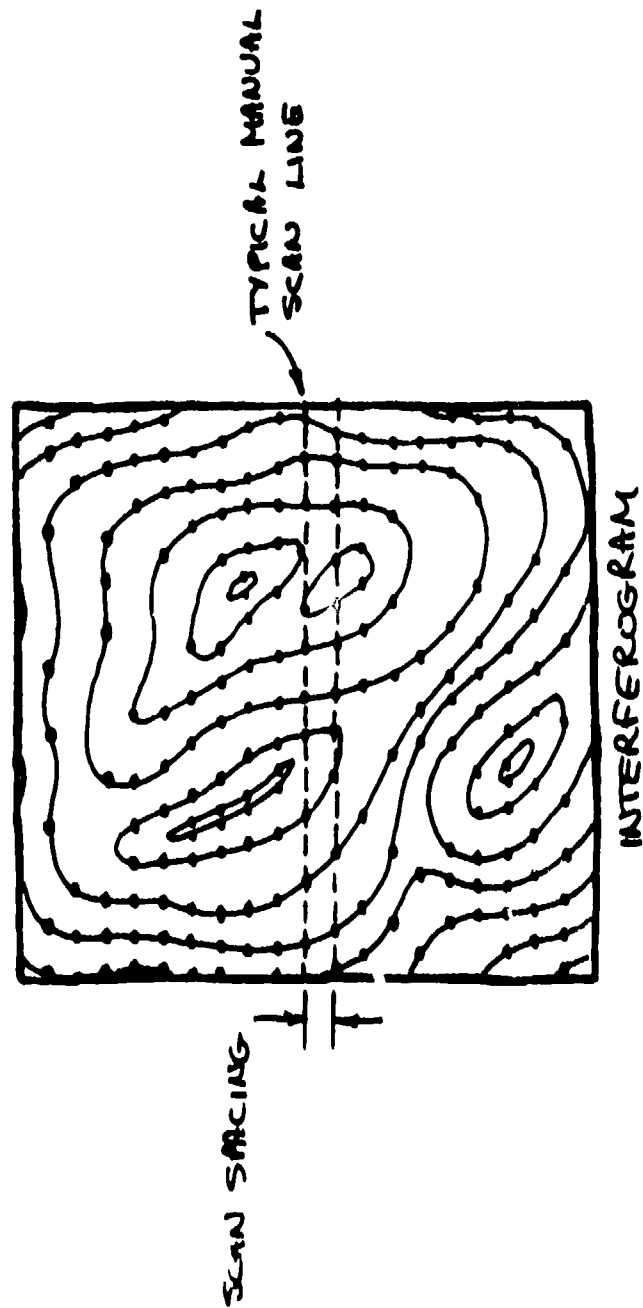


Figure 26. Digitization of data contained in a wavefront interferogram: the number of horizontal scans,  $M$ , is approximately equal to the number of fringes encountered in a single scan -- so that the total number of data points used to define the interferogram is  $M^2$ . These data are used to obtain a least squares mapping of the distorted wavefront.

than hand-figuring. By index-matching ground glass having a spherical figure, we have already confirmed the validity of the assumptions which we have made regarding reflection and scattering at the glass-liquid interface. Once the programs for computing the least squares fit and for generating the machine-control tapes have been written, the only labor involved in making a new correction plate will be that required to make the manual scan of the interferogram and to set up the milling machine. The whole operation, starting with an unknown laser rod and ending with a finished corrector plate, should take no longer than a day or two.

#### 4. SUMMARY

We have described what we believe to be a viable technique for (a) measuring the dynamic optical distortion in a laser rod, and (b) manufacturing a correction plate to compensate for this distortion. In our earlier work in this area we were able to demonstrate that a given laser rod and flashlamp-pumping configuration yielded distorted wavefronts which were reproducible as the operating conditions were kept constant. In particular, if the laser system is operated at an appreciable repetition rate, the



optical distortion of the laser wavefront is a sensitive function of the rep rate. We plan to put this measurement and correction scheme to use in the immediate future to correct large neodymium:glass laser rods which are being used as intermediate amplifiers in the laser fusion project currently being carried out at the University of Rochester's Laboratory for Laser Energetics.

A STUDY OF LASER BEAM-STEERING TECHNIQUES LEADING TO  
BEAM-STEERING DEVICES IN THE MULTI-MHz RANGE

J. M. Forsyth

1. INTRODUCTION

The principal objective of this research was to study a means for producing a high-speed, continuously scanning laser beam by appropriate use of an intra-cavity beam deflector to lock a set of transverse modes of the laser. The study was conducted primarily on an experimental basis since a simple theoretical model of the system had been given previously.<sup>(1)</sup> In this model, if a set of one-dimensional hermite-gaussian field distributions having the same longitudinal order number is locked in phase with a Poisson amplitude distribution, then a gaussian spot is formed in the output plane of the laser which translates with one-dimensional simple harmonic motion. The frequency of the spot motion is equal to the frequency separation of adjacent-order transverse-mode resonances of the cavity. The dimensions of the spot are identical to those of the lowest-order cavity mode.

Although this model is strictly valid only for a Poisson distribution, such a distribution is very nearly gaussian for systems of 10 or more modes and the Doppler-broadened gain profiles of many gas laser systems should tend to produce such mode amplitude distributions.

From the point of view of the construction of a practical system, a more important consideration is that of resolution, i.e. the number of spot diameters in a line of scan. The length of a scanned line is approximately equal to the effective width of the highest-order mode which will oscillate in the laser. The effective width of a high-order mode (measured by the distance between the  $1/e$  points of the distribution, say) is proportional to the square root of the order number of the mode. Thus, a large number of modes is required to achieve moderate resolution levels in this kind of operation.

These considerations dictate two requirements in the choice of laser for use in this system. First, the laser must have a large spectral bandwidth to support a large number of modes of large frequency separation. Secondly, the laser must be operable in a large aperture configuration. To meet these requirements and to insure good intra-cavity optical quality we constructed an argon-ion laser having a

1 cm bore diameter. Although this laser has been described in detail in a previous technical report<sup>(2)</sup>, we will append a brief description for completeness.

The use of an intra-cavity modulator to lock a small set of transverse modes was demonstrated previously.<sup>(3)</sup> The modulator action in this case consisted of mechanical tilting of a plane mirror which formed part of the laser cavity. Although this tilting action is not precisely equal to the wavefront dynamics of the mode-locked condition, it can be shown that if a hermite-gaussian field distribution is incident onto a tilting mirror, the reflected field contains sidebands which have the desired spectral frequencies and spatial distributions.<sup>(4)</sup> Strong transverse-mode coupling should result from the use of such a device. The strength of the coupling will, of course, depend on the sideband amplitude which, in turn, is proportional to the peak amplitude of the tilt.<sup>(4)</sup>

## 2. MODULATOR DESIGN

Active longitudinal mode-locking of homogeneously and inhomogeneously broadened lasers has been studied extensively.<sup>(5)</sup> It is well-known that the degree of mode-coupling produced by the modulator must be considerably higher for maintenance

of locking in homogeneous lasers than for inhomogeneous lasers. Since the argon-ion laser resembles a homogeneously broadened system unless the optical cavity is made impractically short, we felt that insufficient mode coupling would result from the use of mechanical mirror vibration in our system. We chose instead to introduce variable intracavity wavefront tilt by means of an electro-optic prism. Because the proper construction of the prism appears to play a pivotal role in the success of the locking experiments we will discuss our work to date in this area.

In addition to having a high electro-optic figure of merit, the most important characteristic of an electro-optic material in our application is good overall optical quality over a moderate aperture. The choice of materials is not a large one. Although lithium niobate has a high figure of merit and may be obtained in adequate sizes it is susceptible to partially reversible, optically-induced inhomogeneities, especially in the blue-green region of the spectrum. Operation of the material at elevated temperatures alleviates this difficulty to a large degree but one must then be careful to avoid intra-cavity air currents from the presence of the crystal oven. Large pieces of lithium niobate are rather expensive. The alternative is to use one of the

dihydrogen phosphates. While these materials are highly resistant to optically-induced damage at room temperature they suffer from a large solubility in water, making it difficult to prepare and maintain high-quality optical surfaces on the crystals. We choose ammonium dihydrogen phosphate (ADP) for our experiments because of (1) low cost and (2) the existence of an in-house optical surfacing facility.

### 3. MODULATOR CONSTRUCTION

Our best success to date in polishing ADP has come from the use of a standard pitch lap and cerium oxide abrasive but with a fluorocarbon fluid used instead of water. Even with this procedure we find it difficult to keep the surface free from numerous fine scratches and simultaneously maintain a high surface flatness. In any event, a good surface is soon degraded upon exposure to the generally humid air in Rochester. As a result we have spent considerable effort to develop a method of protecting the crystal surfaces.

It is not yet possible to significantly extend the service life of hygroscopic crystals by means of evaporated coatings. Therefore, we must bring the crystal faces into contact with "hard" optical windows either by use of cements

or by immersion in fluids. Because the absorption in optical cements is normally significant at laser power densities we began our experiments by contacting quartz windows to the crystal faces using a thin layer of (silicone) index matching fluid. While this arrangement yielded initially high optical quality, the optical homogeneity of the fluid quickly degraded in the presence of the RF (modulator) drive field. We reported on the transverse mode locking behavior observed with the crystal in this configuration and noted that the apparent resolution of the system was far below the theoretical expectation.<sup>(5)</sup> Since then we have investigated the properties of various optical cements in this application.

We have encountered either of two principal difficulties with most optical cements we have tried:

1. Bond rupture and/or bubble-like defects are produced in the film after a brief period of operation in close proximity to the laser discharge tube. (Although we have not confirmed it, we suspect that absorption of UV radiation from the discharge may be responsible). These defects initially prevent oscillation in well-structured transverse modes and eventually prevent oscillation altogether.
2. Severe light scattering prevents oscillation in well-

structured modes. In this case the cements exhibit a turbid appearance in laser light.

Very recently we have had some success with Kodak HE-S-1 optical cement which appears to be free of scattering problems and to have stable bonding properties. However, as of this report date we have not yet tested the cement under mode-locked conditions due to a malfunction in some electronics associated with proper alignment of the modulation equipment. We expect to make this test shortly.

#### 4. ADDITIONAL STUDIES

We are beginning a numerical analysis of the mode-locked field distributions which arise from a non-Poisson mode amplitude distribution. In our preliminary experimental observations we noted that under certain conditions we would sometimes observe stable amplitude distributions in which virtually all modes were equal in amplitude. We do not know what to expect in the output under these conditions, although we strongly suspect that if a scanning spot is obtained it will not exhibit a constant spot diameter across the field. This statement is made by analogy to the properties of the harmonic oscillator wave-functions in quantum mechanics.<sup>(6)</sup> In the latter case only the Poisson distribution



of modes results in a wavepacket with a stationary uncertainty product.

## 5. CONCLUSION

During the period of support we demonstrated transverse mode-locking in a large-bore argon ion laser. We confirmed that such operation leads to the production of a scanning beam from the output of the laser. However, the experimentally observed resolution of the scanning beam appears to have fallen short of the theoretically predicted performance level. The limitation appears to be in the poor optical quality of the intracavity modulators used in the experiments to date. Further work on this aspect of the problem is continuing.

## APPENDIX: Construction of Large-Bore Ion Laser

The basic construction details of the large-bore argon ion laser used in the transvers mode-locking experiments have been given previously.<sup>(2)</sup> Since that report we have modified the construction slightly to facilitate cleaning Brewster windows and to provide a more reliable water supply to the vacuum seals.

The discharge tube is made from a 12.5-inch long beryllium oxide tube with a 0.400 inch bore and an 0.078 inch wall thickness. A pair of brass assemblies are clamped to the outside wall of the BeO tube approximately 10 inches apart by means of O-rings. The plates which bear against these O-rings carry the pyrex tubes into which fused quartz Brewster windows are cemented. The inner side of each brass assembly is sealed (by means of O-rings) to the pyrex water jacket. Previously these brass assemblies were soldered or cemented to the BeO tube directly. However, we have found the O-ring seals more convenient to use when servicing the laser. To aid the vacuum tightness of the seal we used a fine optical abrasive on the outer BeO surface before final assembly.

Excitation of the discharge is by RF power supplied through a thirteen-turn cadmium plated coil closely wrapped around the pyrex water jacket. The excitation coil is water-cooled. Up to 11 KW plate input power at 5 MHz can be developed by the power supply. Nevertheless, due to the large active volume of gas excited, a rather low excitation density is achieved. At 11 KW input an output power of 100 mw is obtained. Virtually all of this energy is at  $\lambda = 4880\text{\AA}$ . (With an output mirror transmission of 2%, we are barely at threshold for oscillation on the  $5145\text{\AA}$  transition under these conditions.)

## REFERENCES

1. D. H. Auston, "Transverse Mode Locking," IEEE J. Quantum Electronics QE-4, 420 (1968).
2. B.J. Thompson et al., "Studies in Optics", Tech. Rept AFAL-TR-71-346, Air Force Avionics Laboratory, Wright-Patterson AFB, Ohio, 210pp, March, 1972.
3. D. H. Auston, "Forced and Spontaneous Phase Locking of the Transverse Modes of a He-Ne Laser," IEEE J. Quantum Electronics QE-4, 471 (1968).
4. P. Nebolsine, Ph.D. Thesis, University of Rochester, 1972.
5. D. J. Kuizenga & A.E. Siegman, "FM and AM Mode Locking of the Homogeneous Laser - Part I: Theory, " IEEE J. Quantum Electronics QE-6, 694 (1970).
6. L.I. Schiff, Quantum Mechanics, 2nd edition, McGraw-Hill, New York, 1955, pp 60-69.

## SECTION V

## FURTHER RESEARCH IN IMAGE-FORMING OPTICS

D. C. Sinclair, J. L. Meyzonnette, and N. Balasubramanian

## 1. INTRODUCTION

In this part of the research program we have investigated a number of interferometers which utilize moving fringe patterns to enable one to use ac detector circuitry rather than dc detector circuitry in the photoelectric readout for a testing interferometer. We formerly called such interferometers ac interferometers, but we now prefer to use the term heterodyne interferometers, since the generation of the moving fringe patterns can be interpreted as a beating together of two optical waveforms.

We have not yet been able to construct a laboratory model of a full heterodyne interferometer system, employing a detector array for readout. In anticipation of being able to build such a system in the future, we have studied a variety of interferometer configurations which we feel would be suitable candidates for the optical parts of such systems. In the early phases of the present investigation, we studied the use of mechanically moving grating systems as heterodyne interferometers. A complete report of this work was given in a previous quarterly progress report, and is included here as an appendix. More recently we have considered the use of heterodyne interferometry for vibration analysis, and have also built and studied a small heterodyne position-sensing interferometer.

In this report we detail the results of our recent theoretical investigations and describe some experiments that we have done on the position-sensing interferometer.

## 2. THEORY

Holographic interferometry allows one to compare a waveform originated at an object, while it is still, with the waveform given by the object after deformation, or in vibration. We consider here the case of real time analysis where the waveform corresponding to the still object is given by the hologram and the wavefront corresponding to the object in motion by the object itself.

We assume that the hologram records and reconstructs faithfully the wavefronts coming from the object and we do not take into account the shrinkage of the plate, or noise due to the photographic process.

Consider the arrangement shown in Figure 27. While the object is not in motion, the hologram will record:

$$I = [\Lambda_0(x,y,z) + R(x,y,z)]^2$$

During the reconstruction stage with the same reference beam, the hologram will give rise to  $\Lambda_0$  and  $\Lambda_1(x,y,z)$  corresponding to the deformed object.

Following Sten Waller's analysis we treat the diffusely reflected amplitudes  $\Lambda_0$  or  $\Lambda_1$  as realizations of a complex variable, such that: <sup>1,2</sup>

$$E[\Lambda_0] = E[\Lambda_1] = 0$$

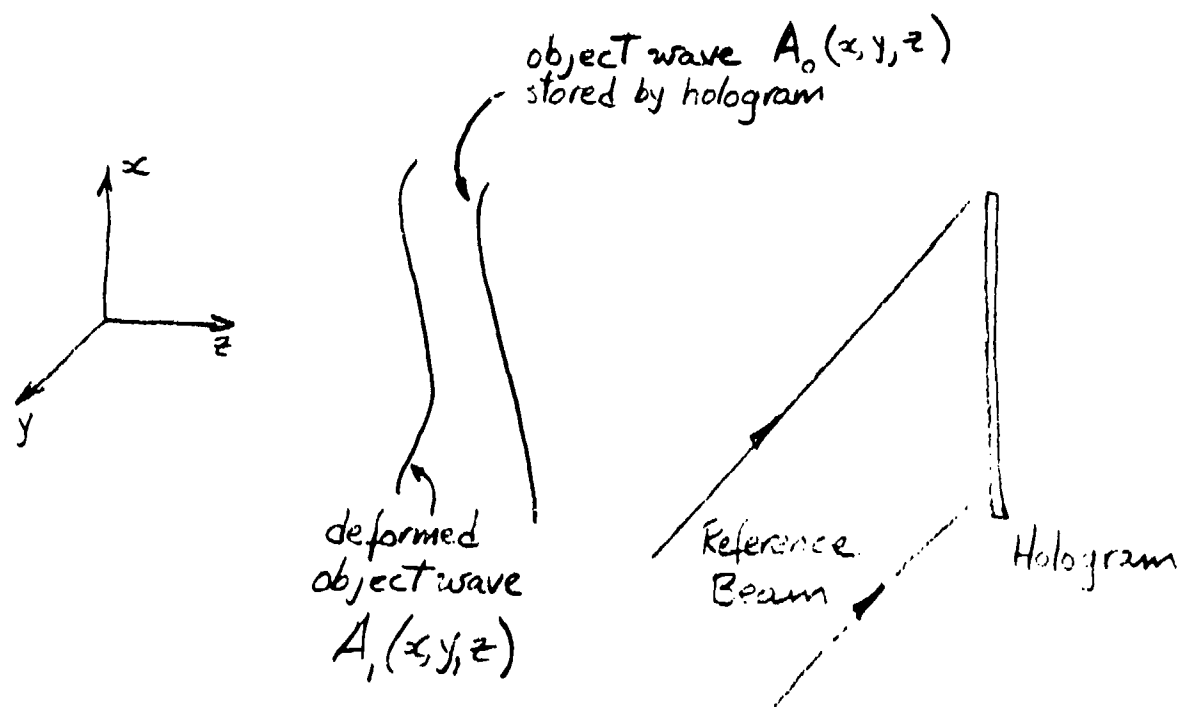


FIGURE 27

RELATION OF OBJECT WAVE AND DEFORMED  
OBJECT WAVE IN A HOLOGRAPHIC INTERFEROMETER

Hence, at any point in space, the total intensity is the result of a 2 wave-interference, so that if  $A = A_1 + A_2$ , then:

$$\begin{aligned} I &= AA^* \\ &= A_1^* A_1 + A_2^* A_2 + A_1^* A_2 + A_1 A_2^* \end{aligned}$$

The ensemble average of the intensity is:

$$E[I] = E[A_1^* A_1] + E[A_2^* A_2] + E[A_1^* A_2] + E[A_1 A_2^*]$$

Using the conventional notation:

$$I_1 = E[A_1 A_1^*]$$

$$I_2 = E[A_2 A_2^*]$$

$$\Gamma = E[A_1^* A_2]$$

$$\gamma = \frac{\Gamma}{\sqrt{I_1 I_2}} = |\gamma| e^{i\delta}$$

we get the expression for the total intensity:

$$I = I_1 + I_2 + 2\sqrt{I_1 I_2} |\gamma| \cos \delta$$

As usual in 2 beam interferometry, we define the visibility of fringes as follows:



$$V = \frac{I_{\max} - I_{\min}}{I_{\max} + I_{\min}} = \frac{2\sqrt{I_1 I_2}}{I_1 + I_2} |\gamma|$$

In order to evaluate the phase difference  $\delta$ , and to determine the areas of localization of the fringes, J. C. Vienot<sup>3</sup> has shown that one could use the concept of homologous rays with profit, in case of object motion. Karl Stetson<sup>4</sup> has extended the concept in order to include object deformation as well.

To introduce the concept of homologous rays or fields, one expands the field reflected from the object into its angular spectrum:

$$A_1(\underline{r}) = \int_{-\infty}^{+\infty} \Omega(\underline{k}) N_1(\underline{k}) e^{i\underline{k} \cdot \underline{r}} d\underline{k}$$

$\Omega(\underline{k})$  characterizes the aperture of the observation system, so that:

$$\Omega(\underline{k}) = \begin{cases} 1 & \text{when } \underline{k} \leq \Omega \\ 0 & \text{otherwise} \end{cases}$$

Hence, the previous equation can be written as:

$$A_1(x, y, z) = \int_{-\infty}^{+\infty} \Omega(k_x, k_y) N_1(k_x, k_y) e^{i(k_x x + k_y y + k_z z)} dk_x dk_y$$

In the same way, one considers the field diffraction by the object after deformation:

$$A_2(\underline{r}) = \iint \Omega(\underline{k}) e^{i\underline{k} \cdot \underline{r}} d\underline{k}$$

Provided some assumptions are made about the deformation,<sup>1</sup> one can write:

$$N_2(\underline{k}) = N_1(\underline{k}) e^{i\phi_1(\underline{k}, \underline{r})}$$

where  $\phi_1(\underline{k}, \underline{r})$  is given by:

$$\phi_1(\underline{k}, \underline{r}) = [\underline{k}_i(\underline{k}, \underline{r}) - \underline{k}] \cdot \underline{d}(\underline{k}_0, \underline{r})$$

$\underline{k}_i$  represents the incident wave propagation vector,  $\underline{d}$  represents the displacement of the surface at any given point, as shown in Figure 28.

The concept of homologous rays is valid only for small aperture systems, so that, inside  $\Omega$ , the vector  $\underline{k}$  can be written as:

$$\underline{k} = \underline{k}_0 + \underline{K}$$

where  $\underline{k}_0$  is directed along the line QP and  $\left\{ \begin{array}{l} \underline{K} \perp \underline{k}_0 \\ |\underline{K}| \ll |\underline{k}_0| \end{array} \right.$

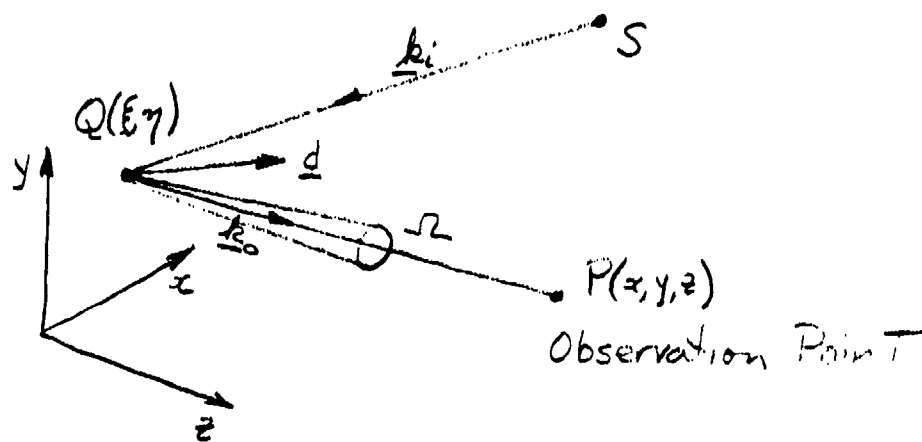


FIGURE 28

ILLUSTRATING VARIABLES USED TO  
DESCRIBE HOMOLOGOUS RAYS

Then, the phase difference in the direction  $\underline{k}$  is related to the phase difference along the main direction  $\underline{k}_0$  by:

$$\phi_L(\underline{k}, \underline{r}) = \phi_L(\underline{k}_0, \underline{r}) - [\underline{d}(\underline{k}_0, \underline{r}) + L \underline{\Delta \ell}(\underline{k}_0, \underline{r})] \cdot \underline{k}$$

where  $\underline{\Delta \ell}(\underline{k}_0, \underline{r}) = \frac{\Delta \underline{k}_0}{\underline{k}_0}$ , i.e., the change in the unit vector along the viewing direction introduced by the deformation of the object and  $L = z/k_{z0}$ .

Homologous rays are useful to help find the area of localization of the fringes, which is given by stating that the phase variation  $\delta\phi_L$  within the aperture be minimized inside the aperture,

$$\frac{d\phi_L}{dk} \approx 0$$

as shown in Figure 29.

Sten Waller shows that the area of localization is at the intersection of the bundle of homologous rays inside the aperture.

Considering that the illuminating source is at infinity so that  $\underline{k}_i$  is independent of the coordinates of Q, one may approximate the phase difference between two homologous rays as being:

$$\phi_L(x, y, k_0) = \underline{d} \cdot [\underline{k}_i - \underline{k}_0]$$

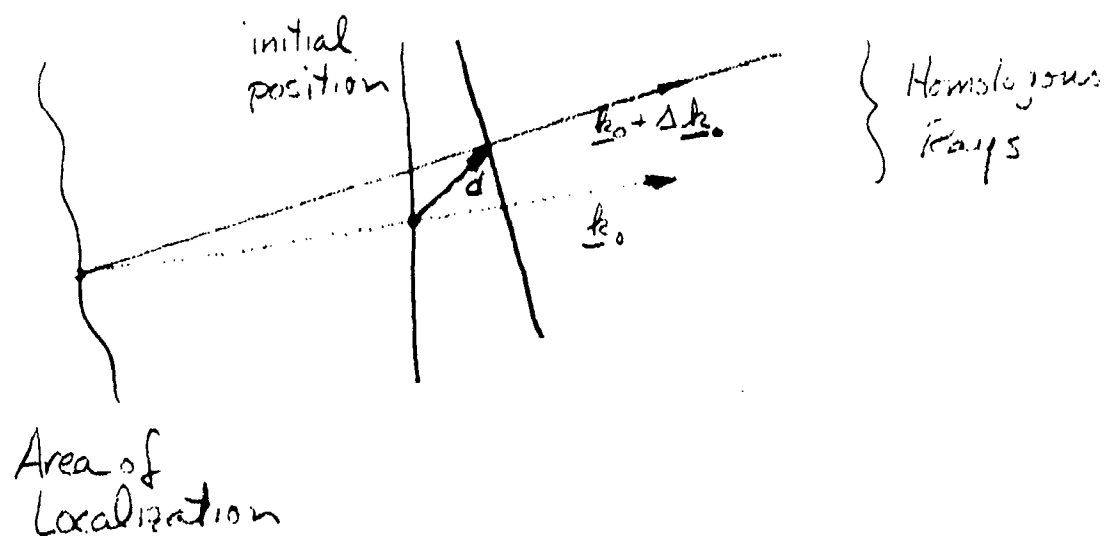


FIGURE 29

ILLUSTRATING HOMOLOGOUS RAYS

and the intensity in the area of localization is of the form:

$$I = I_0 [1 + \cos \phi_L]$$

If we want a unique determination of the displacement  $\underline{d}$ , we need its three components  $\Delta x$ ,  $\Delta y$ ,  $\Delta z$ . By choosing 3 different viewing directions, as shown in Figure 30, we get 3 equations:

$$\phi_{L1} = \underline{d} \cdot [\underline{k}_i - \underline{k}_{01}]$$

$$\phi_{L2} = \underline{d} \cdot [\underline{k}_i - \underline{k}_{02}]$$

$$\phi_{L3} = \underline{d} \cdot [\underline{k}_i - \underline{k}_{03}]$$

By counting how many fringes pass by when the direction changes, for example for  $\underline{k}_{01}$  to  $\underline{k}_{02}$ , then from  $\underline{k}_{02}$  to  $\underline{k}_{03}$  and from  $\underline{k}_{01}$  to  $\underline{k}_{03}$ , one can write:

$$\phi_{L1} - \phi_{L2} = \underline{d} \cdot [\underline{k}_{02} - \underline{k}_{01}]$$

$$\phi_{L1} - \phi_{L3} = \underline{d} \cdot [\underline{k}_{03} - \underline{k}_{01}]$$

$$\phi_{L2} - \phi_{L3} = \underline{d} \cdot [\underline{k}_{03} - \underline{k}_{02}]$$

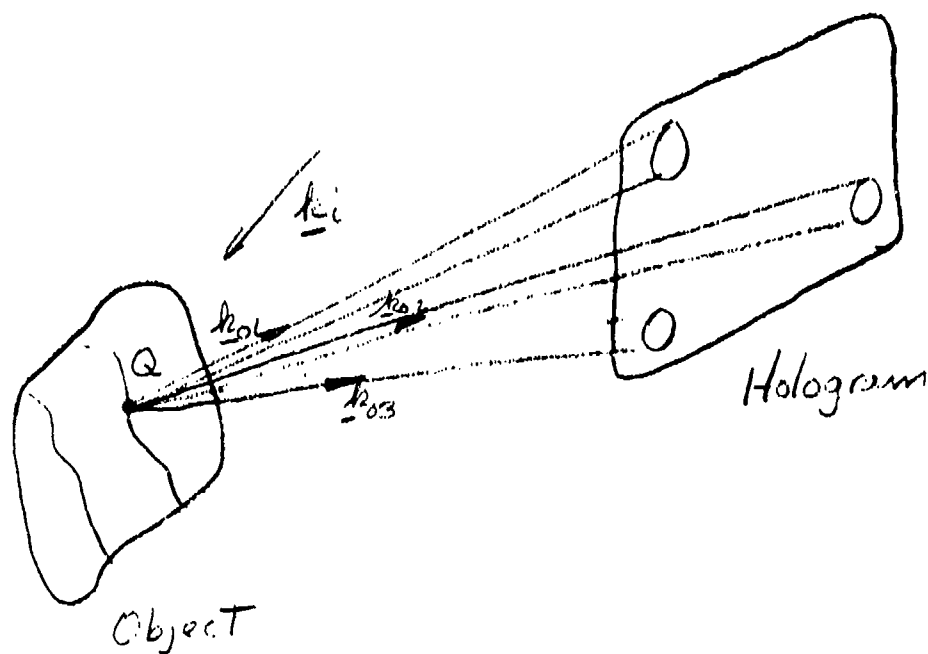


FIGURE 30

ILLUSTRATING THE WAVE VECTORS USED  
TO DESCRIBE OBJECT DISPLACEMENTS

One sees that it is impossible to determine uniquely a given displacement, since two deformations of equal amplitude, but of opposite directions would give the same result. The precision on the measurement depends upon the precision obtained on  $k_{12}$ ,  $k_{13}$ ,  $k_{23}$ . If the directions  $k_{01}$ ,  $k_{02}$ ,  $k_{03}$  are not very different from each other, the numbers  $k_{12}$ ,  $k_{13}$ ,  $k_{23}$  are usually small and the relative precision on them is poor.

One of the methods most often used in vibration analysis is to take the hologram of the object while in motion. Following Goodman, one can consider then the hologram as a temporal filter:

At each point of the plate, the exposure is

$$E(x,y) = \int_{-T/2}^{T/2} |H(x,y,t)|^2 dt$$

where  $|H(x,y,t)|^2$  = irradiance distribution

$T$  = exposure time

The luminous amplitude in the plane of the hologram is

$$H(x,y,t) = R(x,y) + O(x,y,t)$$

if  $R(x,y)$  is the reference wave, independent of time and  $O(x,y,t)$  is the wave scattered from the object in motion.



$$E(x,y) = E_R + E_S + R(x,y) \int_{-T/2}^{T/2} O^*(x,y,t) dt + R^*(x,y) \int_{-T/2}^{T/2} O(x,y,t) dt$$

Considering only the last term, giving the primary image, we get:

$$\begin{aligned} E_p &= R^*(x,y) \int_{-T/2}^{T/2} O(x,y,t) dt \\ &= R^*(x,y) \int_{-\infty}^{+\infty} \text{rect}(t/T) O(x,y,t) dt \end{aligned}$$

If

$$\tilde{O}(x,y,v) = \int_{-\infty}^{+\infty} O(x,y,t) e^{-2\pi i v t} dt,$$

we use Parseval's Theorem to get:

$$E_p = R^*(x,y) \int_{-\infty}^{+\infty} T \text{sinc}(\pi v T) \tilde{O}(x,y,v) dv$$

Hence, the hologram acts like a linear filter having a transfer function  $\text{sinc}(\pi v T)$ .

The use of time average holography is particularly useful for studying oscillatory motions. Considering the case of a sinusoidal time dependence, the object wave can be written as follows:

$$O(x,y,t) = O_0(x,y) e^{i\phi_0(x,y)} e^{i k \sin \omega t}$$

whose Fourier transform is:

$$\begin{aligned}
\tilde{O}(x,y,v) &= O_0(x,y) \int_{-\infty}^{+\infty} e^{i\phi_0} e^{ik \sin \omega t} e^{-2\pi i v t} dt \\
&= O_0(x,y) e^{i\phi_0} \int_{-\infty}^{+\infty} \cos(k \sin \omega t) e^{-2\pi i v t} dt \\
&\quad + i O_0(x,y) e^{i\phi_0} \int_{-\infty}^{+\infty} \sin(k \sin \omega t) e^{-2\pi i v t} dt
\end{aligned}$$

Using the expressions:

$$\cos(k \sin \omega t) = J_0(ka) + 2 \sum_{n=1}^{\infty} J_{2n}(ka) \sin 2n \omega t$$

$$\sin(k \sin \omega t) = 2 \sum_{n=0}^{\infty} J_{2n+1}(ka) \sin[(2n+1)\omega t]$$

we get:

$$\tilde{O}(x,y,v) = O_0(x,y) e^{i\phi_0(x,y)} \sum_{n=-\infty}^{+\infty} J_n(ka) \delta(v - \frac{n\omega}{2\pi})$$

which gives the following expression for the amplitude of the primary image:

$$\begin{aligned}
E_p &= R^* T O_0 e^{i\phi_0} \sum_{n=-\infty}^{+\infty} [J_n(ka) \int_{-\infty}^{+\infty} \text{sinc}(\pi v T) \delta(v - \frac{n\omega}{2\pi}) dv] \\
&= T R^* O_0(x,y) e^{i\phi_0} \sum_{n=-\infty}^{+\infty} J_n(ka) \text{sinc}(\frac{n\omega T}{2})
\end{aligned}$$

In the particular case where the exposure time  $T$  is much larger than the period of the vibration (i.e.,  $T \gg \frac{2\pi}{\omega}$ ),  $\text{sinc}(\frac{n\omega T}{2})$  is very small for all  $n$  except  $n = 0$ , and then

most of the contribution to  $E_p$  comes from the  $n = 0$  term:

$$E_p = TR^* O_0 e^{i\phi_0} J_0(ka)$$

The domain of application of the time average method as described above is limited to a certain range of vibrations amplitudes: because  $J_0(ka) > 0.9$  for  $ka < 0.6$ , the intensity will stay almost uniform across the image as long as the displacement is smaller than:

$$ka < 0.6 \Rightarrow a < \lambda/10$$

On the other hand, the method is not useful when the vibration gets larger than about  $10\lambda$ , because then the Bessel function has dropped down so much that it easily buried in the noise of the hologram and one sees only a uniform, gray image. Hence, one can conclude that the method is applicable only for displacements between these two limits

$$\lambda/10 < a < 10\lambda$$

looking at the expression for the intensity:

$$I = E_p E_p^* = T^2 R^2 O_0^2 J_0^2(ka)$$

one sees that the relative phase  $\phi_0(x,y)$  of the vibration at each point has disappeared, so that it is impossible to map the phase of the object in vibration.

One can extend the method to real time interferometry, by taking the hologram of the static object and replacing it at the same position. By reconstructing the object wave so that its amplitude is the same as the one from the object in vibration, one finds that the intensity in the fringe pattern is:

$$I(x,y,t) = 2[A(x,y)]^2 \left[ 1 - \cos[ka(x,y,t)] \right]$$

The - sign comes from the fact that there is a phase shift of  $\pi$  between actual and reconstructed waves [see Ref. (5) p. 442].

Hence observing the fringes with an averaging type of detector (eye, or camera) will yield the following intensity:

$$\begin{aligned} \langle I \rangle &= 2[A(x,y)]^2 \frac{1}{T} \int_0^T [1 - \cos ka(x,y,t)] dt \\ &= 2[A(x,y)]^2 [1 - J_0(ka)] \end{aligned}$$

This method presents the same disadvantage as the time average technique, i.e., it does not give any information about the relative phases of different points on the object, and the contrast of the fringes drops down as the amplitude of the vibrations gets larger than several wavelengths, as shown in Figure 31.

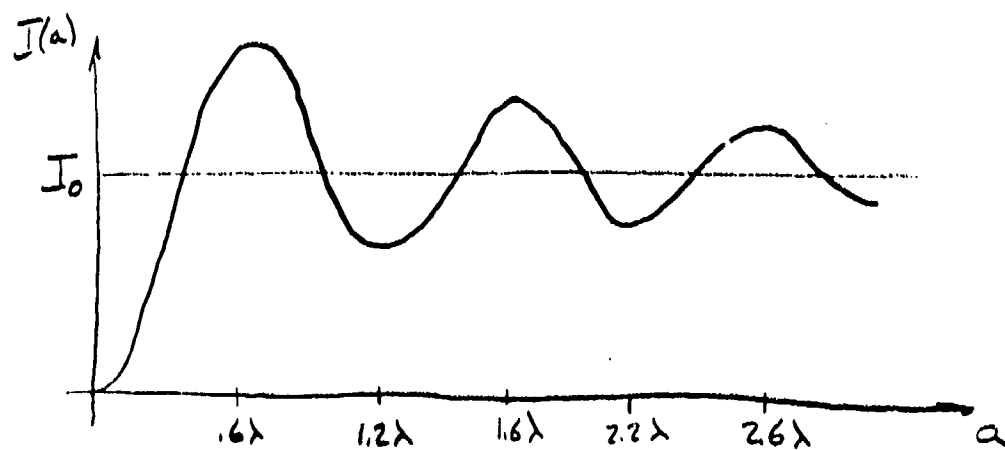


FIGURE 31

INTENSITY VARIATION VERSUS  
OBJECT DISPLACEMENT

In order to track precisely the motion of each area on the object, we consider the light reflected from the object as being Doppler shifted in frequency. By mixing this shifted signal with the carrier provided by the hologram of the static object, it is possible to map the amplitude and phase of a displaced or vibrating object.

Optical heterodyne detection is a very sensitive tool to determine object motions, and is widely used, for example in laser Doppler velocimetry. We can apply its principles to holographic interferometry in a "heterodyne holographic system."

We consider only the case of real time interferometry, in which we make the hologram of the static object with light of frequency  $\nu_0$ , as shown in Figure 32. After processing, we reconstruct the reference wave with a slightly different frequency  $\nu_1 = \nu_0 + \Delta\nu_0$  while the object is still illuminated with the same frequency  $\nu_0$ .

This method has been used by Neumann et al., and Aleksoff<sup>6,7</sup> for the study of vibrating objects. The phase of the reference beam is modulated during the reconstruction, after the hologram of the static object has been made. The frequency of modulation is the same as the frequency of the vibrating object, so that the reconstructed wave can be written as

$$E_r = A_r(x,y)e^{i[\omega t + \theta_r(t)]}$$

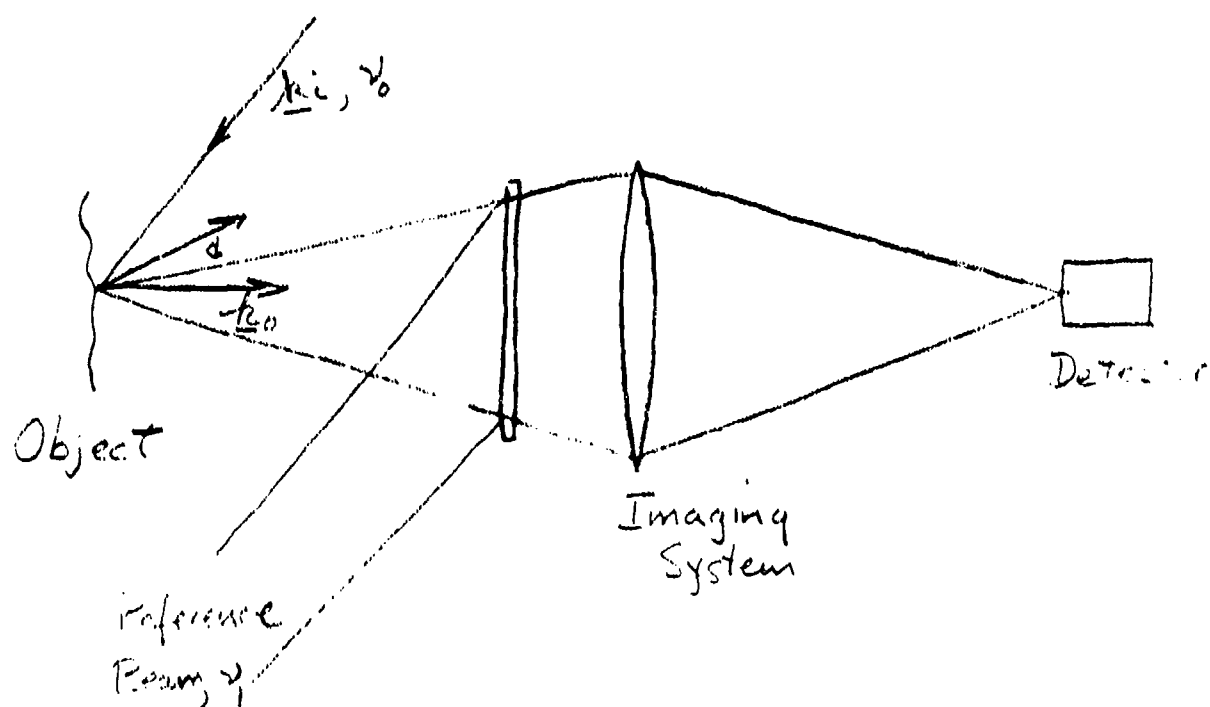


FIGURE 32

EXPERIMENTAL ARRANGEMENT FOR A  
HETERODYNE HOLOGRAPHIC SYSTEM

where

$$\theta_r = \theta_{r0} + k\Delta_r \cos(\Omega t + \phi_r)$$

The waveform originating at the object itself is

$$E_{\text{object}} = \Lambda_0(x,y) e^{i[\omega t + \theta_0(x,y,t)]}$$

$$\theta_0 = \theta_{00} + k\Delta_0(x,y) \cos[\Omega t + \phi_0(x,y)]$$

$\Delta_0(x,y)$  represents the amplitude of vibration of each point of the object, and  $\phi_0(x,y)$  is its phase. By adjusting the intensity of the reference beam, one can make  $a_r(x,y) \approx a_0(x,y)$  in order to get fringes having a maximum contrast.

Hence the total intensity in the fringe pattern can be written as

$$\begin{aligned} I(x,y,t) &= a_0^2 [1 + \cos(\theta_0 - \theta_r)] \\ &= a_0^2 \left[ 1 + \cos[\theta_{00} - \theta_{r0} + k\{\Delta_r \cos(\Omega t + \phi_r) \right. \\ &\quad \left. - \Delta_0 \cos(\Omega t + \phi_0)\}] \right] \end{aligned}$$



If we observe the fringe pattern with a detector having a large averaging time constant compared to the period of the vibration, we get the following average intensity:

$$\langle I(x,y) \rangle = 1/T \int_0^T I(x,y,t) dt$$

Since  $T \gg \frac{2\pi}{\omega}$ ,

$$\langle I(x,y) \rangle = a_0^2 |1 + J_0(k\Delta) \cos(\theta_{00} - \theta_{r0})|$$

where

$$k\Delta = k[\Delta_0^2 + \Delta_r^2 - 2\Delta_0\Delta_r \cos(\phi_0 - \phi_r)]^{1/2}$$

The intensity is at a peak, if:

$$k\Delta = 0$$

$$\theta_{00} = \theta_{r0}$$

That means that all the points vibrating in phase and with the same amplitude as the mirror in the reference beam will exhibit a maximum intensity. Everywhere else, the intensity will be given by:

$$I(x,y) = a_0^2 \left[ 1 + J_0\{k\Delta_0[1 - \cos(\phi_0 - \phi_r)]^{1/2}\} \cos(\theta_{00} - \theta_{r0}) \right]$$

By this means, one can draw a contour of all the points vibrating in phase and with the same amplitude. A precision of about  $5^\circ$  in determination of the phase has been reported.

The choice in the modulation of the reference beam is arbitrary and one is not limited to a sinusoidal one. In fact, one might choose a triangular, saw-tooth, or constant shift modulation.<sup>8</sup>

Let us consider that the reference beam is shifted in frequency by an amount  $\Delta\omega_0$  constant in time. Hence, the amplitude reconstructed by the hologram and corresponding to the virtual image is:

$$u_{\text{reconstructed}} = u_{\text{object}}(x,y)e^{i(\omega_0 + \Delta\omega_0)t}$$

If the object itself is displaced or in vibration, the light reflected from it is Doppler shifted by the amount:

$$\frac{\Delta\omega(x,y,t)}{\omega_0} = \frac{\underline{v}(x,y,t) \cdot \hat{n}}{c}$$

where

$$\hat{n} = \frac{\underline{k}}{k} \text{ is the unit vector along the viewing direction.}$$

If we use a detector fast enough to respond to signals of frequencies  $[\Delta\omega_0 - \Delta\omega]$ , we have to consider the characteristics

of heterodyne detection. The output of the detector is written as:

$$\begin{aligned}
 I_{\text{detector}} &= \iint_{\text{area of detector}} |u_1(x', y') e^{i(\omega_0 + \Delta\omega)t} \\
 &\quad + u_2(x', y') e^{i(\omega_0 + \Delta\omega)t}|^2 dx' dy' \\
 &= \iint_A \{|u_1(x', y')|^2 + |u_2(x', y')|^2\} dx' dy' \\
 &\quad + 2\text{Re} \iint_A u_1^* u_2 e^{i(\Delta\omega_0 - \Delta\omega)t} dx' dy'
 \end{aligned}$$

Considering only the term at frequency  $(\Delta\omega_0 - \Delta\omega)$ , we get:

$$i_{\text{het}}(t) = 2\text{Re} \iint_A u_1^* u_2 e^{i(\Delta\omega_0 - \Delta\omega)t} dx' dy'$$

Instead of integrating over the area of the detector, we integrate over the aperture of the hologram, and recall that:

$$u_2 = u_1 e^{i(\underline{k}_i - \underline{k}) \cdot \underline{d}}$$

where  $\underline{d}$  is the displacement of the object area imaged onto the detector.

$$i_{\text{het}}(t) \propto 2|u_1|^2 \text{Re} \int_{\text{area of hologram}} e^{i[(\underline{k}_i - \underline{k}) \cdot \underline{d} + (\Delta\omega_0 - \Delta\omega)t]} dA$$

One finds that the output intensity of the detector is proportional to:

$$i_{\text{het}}(t) \propto \text{sinc}\left(\frac{d_z}{4} \frac{\omega_{\text{max}}}{c}\right)^2 \cos[(\Delta\omega_0 - \Delta\omega)t + (\underline{k}_i - \underline{k}) \cdot \underline{d}]$$

for a given displacement  $d_z$  along the  $z$  axis. Hence, the instantaneous frequency of this signal depends only on the speed of the vibrating object, and its instantaneous phase depends only on its displacement.

By putting an array of detectors in the image plane of the object or of the localization area, as shown in Figure 33, we can sample the relative phases and displacements of small areas on the object comparing their frequencies and phases to those of a signal chosen as a reference. The double wavelength source could be obtained by Zeeman splitting of a laser light, or by electro-optical modulation [for example saw-tooth modulation] of a laser beam. The advantages of this method are the following:

- 1) Very precise phase measurement in the fringe pattern, compared to the case of photographic recording of still

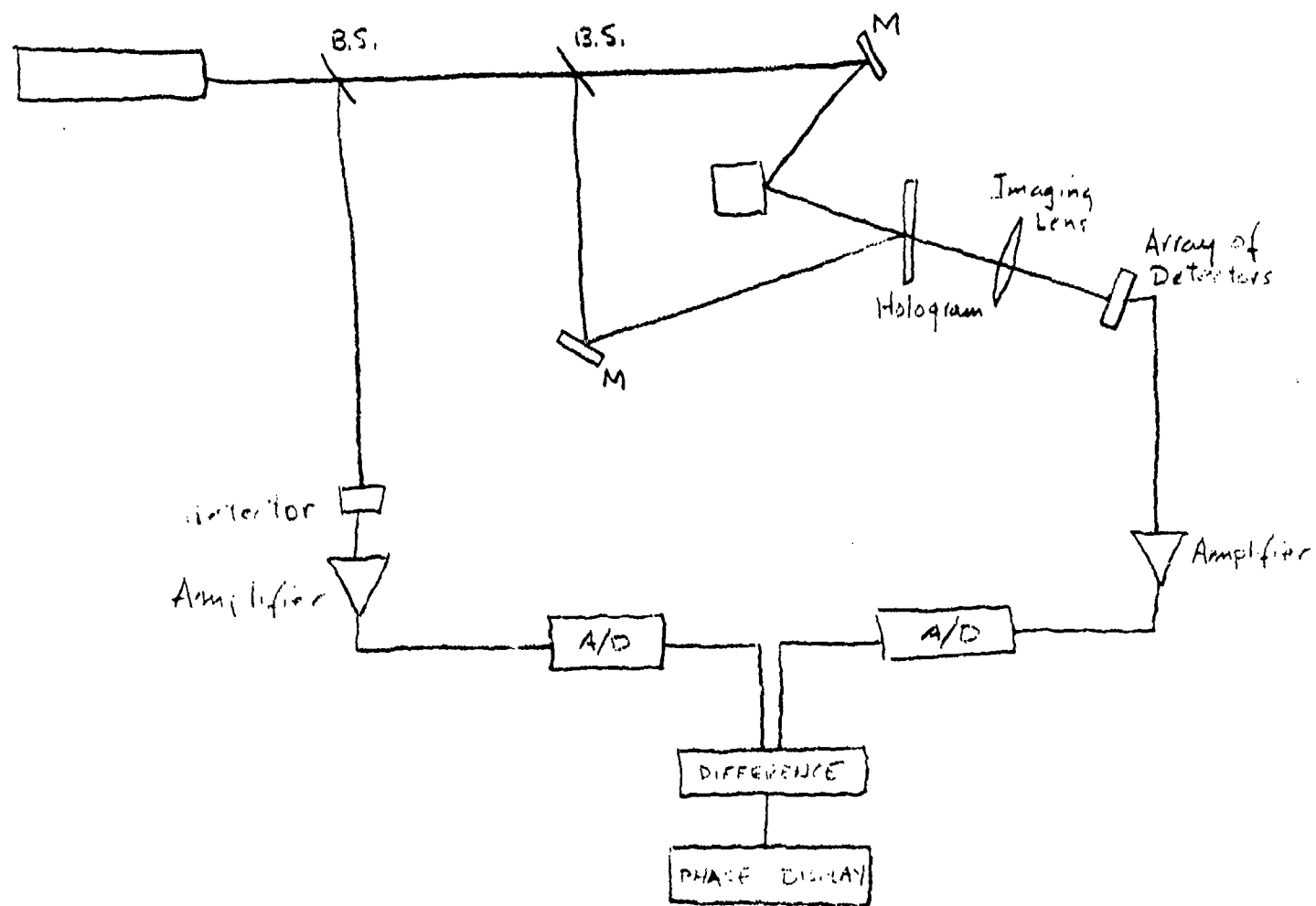


FIGURE 33

EXPERIMENTAL ARRANGEMENT FOR FULL-FIELD  
VIEWING OF A HETERODYNE INTERFEROGRAM

fringes, for example. This gives in turn a much better quantitative measurement of displacements and relative phases on the object.

2) The method is particularly valuable for very small displacements, where the sensitivity of usual methods gets very bad. This precision can be obtained by the use of the "coincidence logic circuits."

3) Easier information processing through the use of mini-computers.

### 3. EXPERIMENT

We have extended the insight that we have recently gained into holographic interferometry to develop a heterodyne position-sensing interferometer. This interferometer can be used to detect the position of a diffuse surface, by measuring the heterodyne signal generated when a holographically reconstructed spherical wave is interfered with a quasi-spherical wave reflected from a diffuse object.

The arrangement of the interferometer is illustrated in Figure 34, and a photograph of the apparatus used is shown in Figure 35. The hologram is made while the phase modulator PM is stationary. It is then developed and replaced approximately in position. If both arms of the interferometer are then illuminated, one sees, when looking through the hologram, two quasi-point sources of light. The alignment of these sources is comparatively easy. When the sources are close to being aligned, an interference pattern results behind the hologram which looks like that shown in Figure 36. However, when the two sources are exactly aligned, the pattern degenerates into one where the fringes have no preferred direction, such as shown in Figure 37. When the pattern shown in Figure 37 is observed, the phase modulator can be turned, on and the heterodyne signal arising from the beating of the Doppler-shifted reference wave and the direct signal wave can be observed. This signal is a maximum when the reconstruction of the holographic

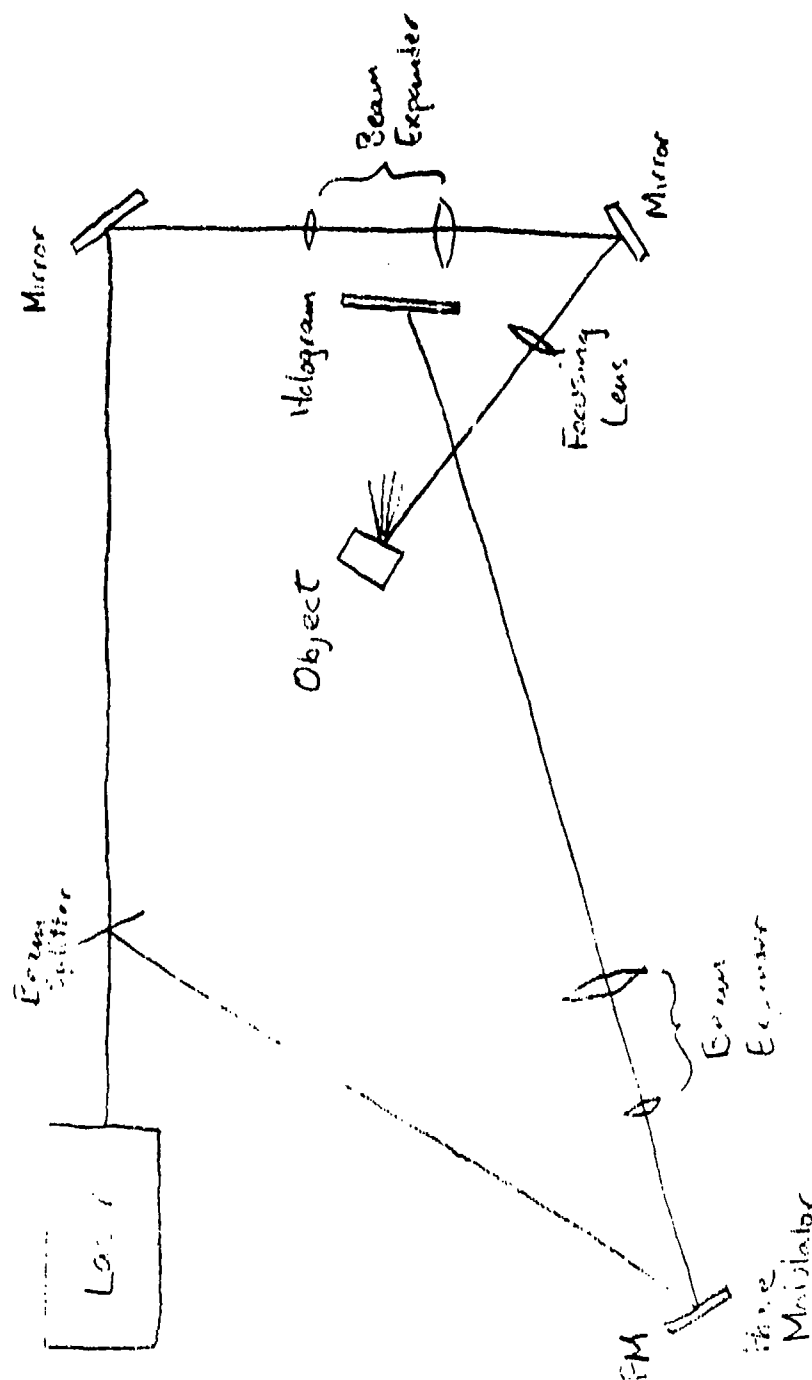


FIGURE 34  
EXPERIMENTAL ARRANGEMENT FOR THE  
POSITION SENSING HETERODYNE INTERFEROMETER



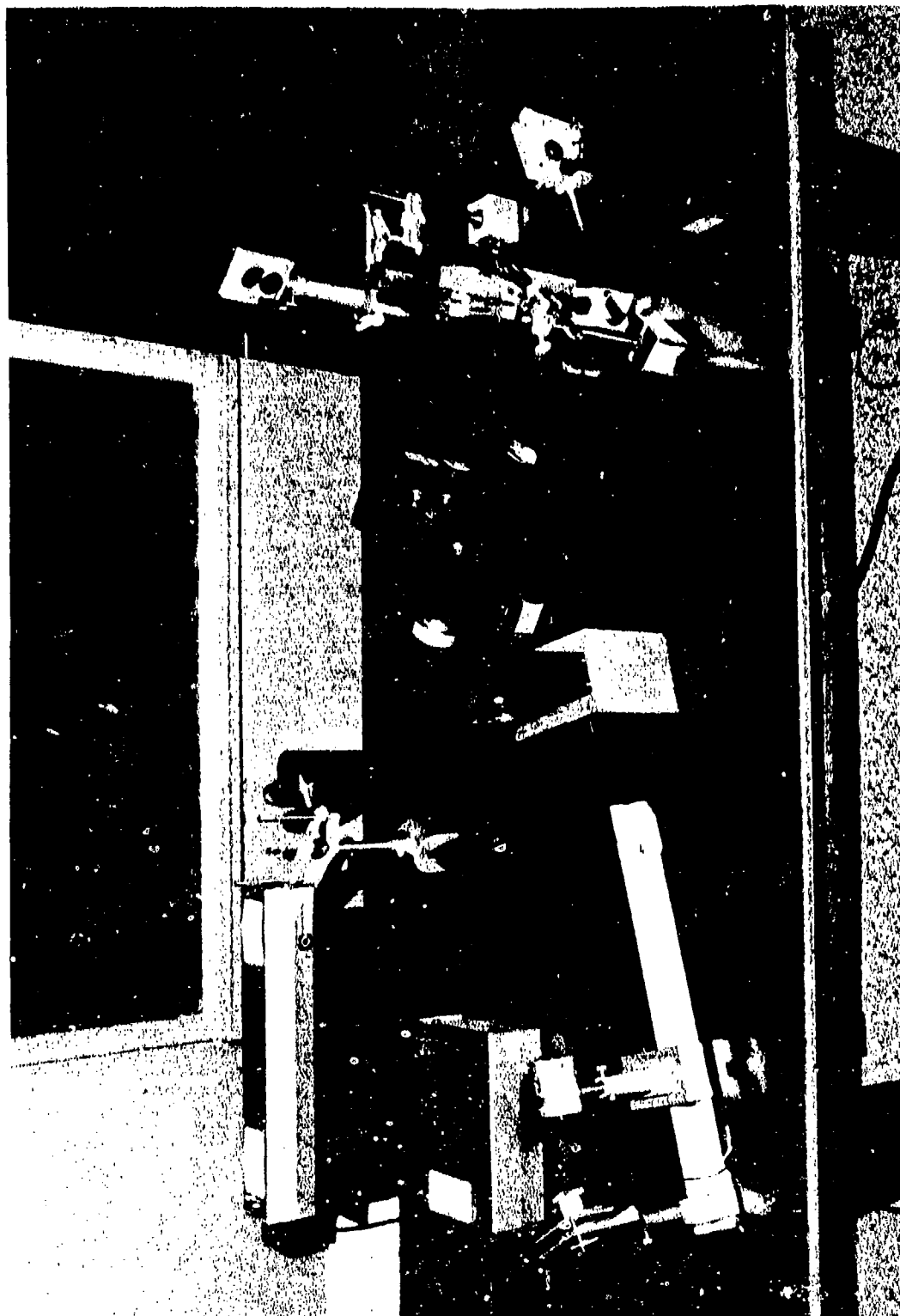


FIGURE 35

APPARATUS USED FOR THE POSITION  
SENSING HETERODYNE INTERFEROMETER

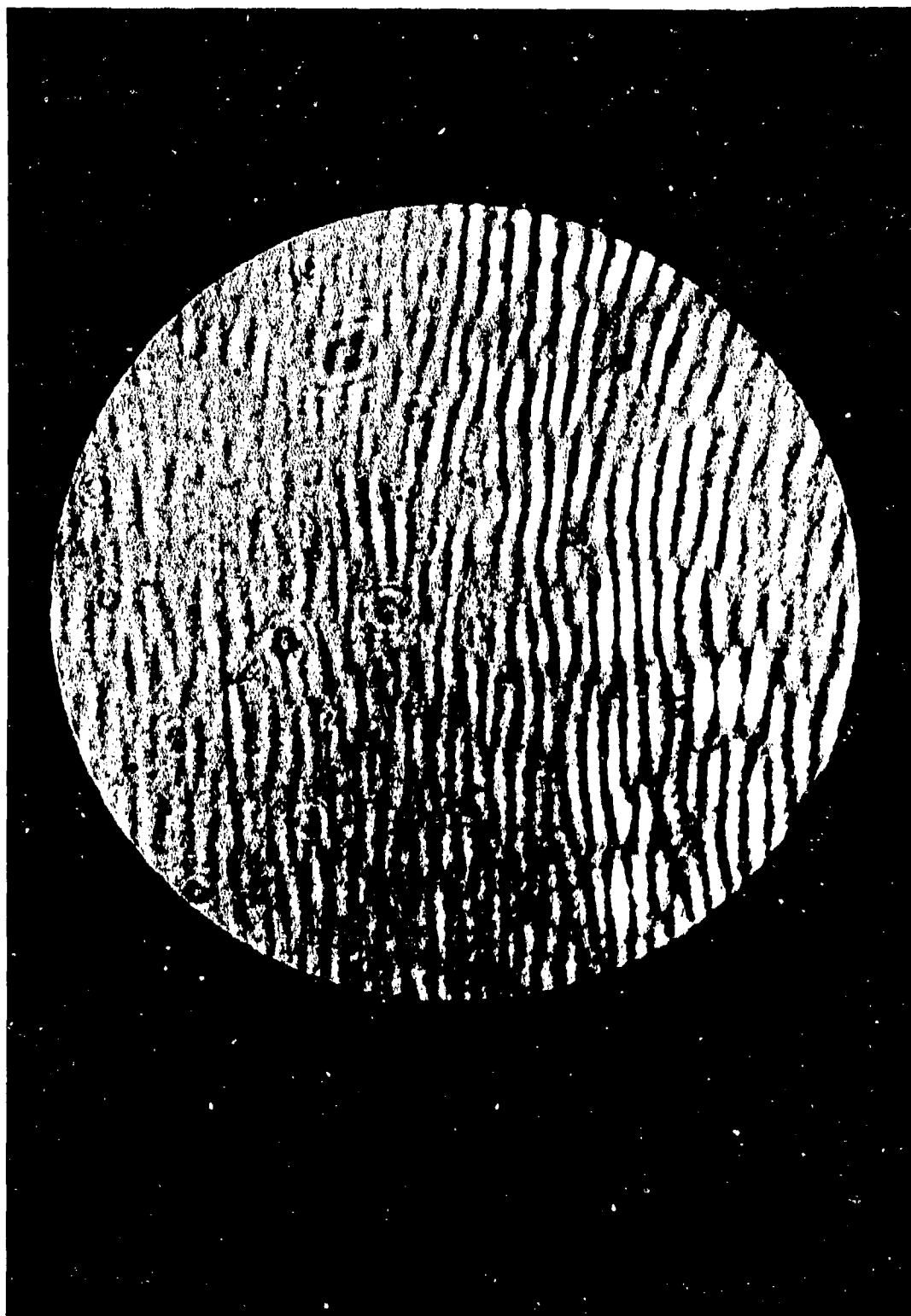


FIGURE 36  
INTERFEROGRAM CORRESPONDING TO  
PROBE BEAM DISPLACEMENT



FIGURE 37  
INTERFEROGRAM CORRESPONDING TO  
PROBE BEAM COINCIDENCE

point source falls exactly on the illuminated point on the diffused surface.

The accuracy of this device as an interferometer is lower than that of conventional optical interferometers, because it is limited effectively by the focal depth of the hologram. It is thus expected that the interferometer will be used for sensing the position of diffuse objects to an accuracy of from 1 to 10 micrometers. We are currently in the process of studying the characteristics and limitations of this interferometer, and hope to report the details shortly.

## References

- 1 Sten Walles, Arkiv för Fysik, B 40, nr 26, 300, (1969).
- 2 Sten Walles, Optica Acta, 17, 899, (1970).
- 3 J. Ch. Vienot, Cl. Frochly, J. Monneret, & J. Pasteur, p. 133, in "The Engineering Uses of Holography," Robertson & Harvey, eds., published by Cambridge University Press (1970).
- 4 K. A. Stetson, p. 307, in "The Engineering Uses of Holography," Robertson & Harvey, eds., published by Cambridge University Press (1970).
- 5 Collier, Burchardt, & Lin, "Optical Holography," Academic Press, New York (1971).
- 6 D. B. Neumann, C. F. Jacobson, G. M. Brown, Applied Optics, 9, 1357, (1970).
- 7 C. C. Aleksoff, Applied Optics, 10, 1329, (1971).
- 8 F. M. Mottier, Applied Physics Letters 15, 285, (1969).

## AC INTERFEROMETER STUDIES

During the past quarter, we have investigated several procedures for constructing an AC grating interferometer. Most of our work has been concentrated on the optical-mechanical design of a moving-grating system, particularly on the production of low-frequency gratings suitable for such systems.

The AC grating interferometer is based upon the Classical Ronchi Test, but in a way that would allow a more rapid treatment of the data by means of a minicomputer.

As seen in Figure 38, the Ronchi test gives rise to a fixed fringe pattern which is usually recorded photographically, then analyzed.

In our experiment, the ruling is translated uniformly across the axis  $zz'$ , which causes the fringes to sweep along the image plane, where they can be recorded by a photoelectric imaging device, such as silicon diode array, vidicon tube, etc.

As a first approach to the problem, consider that the receiver is an array of detectors feeding their electrical output into a selective amplifier tuned to the frequency  $f_0$  (for example,  $f_0=1000\text{Hz}$ ). The linear speed of the ruling

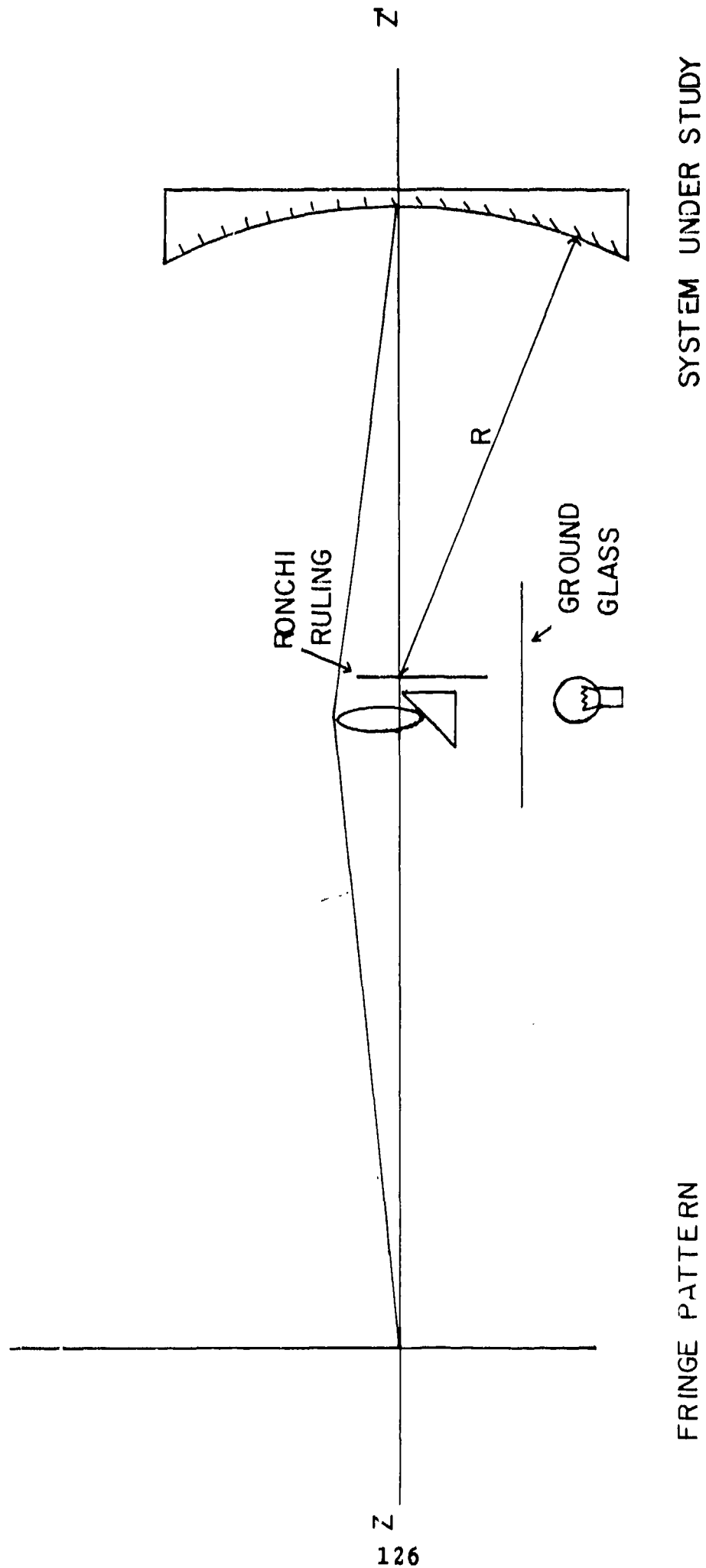


FIGURE 38  
AC INTERFEROMETER CONFIGURATION

will have to be such that:

$$v = \frac{f_o}{f_x} \text{ mm/s}$$

if  $f_x$  is the spatial frequency of the ruling in  $\text{mm}^{-1}$ .

Each detector of the array gives an electrical output, the relative phase of which depends only on the position of the detector and the aberrations of the systems S. What we have to do is to measure the phases of all these detectors as accurately as possible in order to reconstruct the fringe pattern from which we can deduce the characteristics of the optical system.

## I. Possible Means of Translating the Ruling

### A. Radial grating

The first means we have thought of has been to use a radial grating centered on a rotating disc. This would be the simplest way, but presents the disadvantage that the spatial frequency is not constant over the aperture, which introduces additional fringes from the beating of the variable frequencies.

For example, taking the following data:

aperture	5mm x 5mm	}	50 fringes
ruling	10 lines/mm		

we would get a beat fringe if:

$$\frac{\Delta f}{f} = \frac{1}{50} = \frac{\Delta R}{R} \quad R_{\min} = 250\text{mm}.$$



In order to avoid this, the radius of the disc should be several times  $R_{\min}$ ; it would be enormous.

#### B. Translation of linear ruling

The ruling could be translated back and forth by some kind of cam (large displacements, corresponding to coarse rulings) or piezoelectric crystals (very fine rulings).

But in order to get a precise measurement of phases, we feel that we should register the sinusoidal outputs of the detectors over a relatively large number of periods. This rules out the PZ crystal and also the mechanical cam; for example: ruling 2 lines/mm the linear speed should be around 50 cm/s.

#### C. Rotation of linear ruling

In this method, which we have chosen as a starting point, the ruling is set on uniform rotation by a drum. In order to get a large number of periods, even with gratings having spatial frequencies of 1 line/mm, we make its circumference as long as 40cm (which would allow us to measure the phase of each point over 400 periods per revolution for such a ruling). This method introduces some curvature of field in the direction perpendicular to the axis of rotation of the ruling. It is not important, though, as long as the aperture of the imaging lens L is kept very small (for example, a square of 5mm x 5mm).

See Figure 39 for general description of the interferometer.

## 11. Making of the Rulings

We have attempted several methods to make gratings about 40 to 50 cm long, and from 7 to 15 mm wide.

### A. Stroboscope and drum camera

This has been used to make low frequency rulings (about 2 lines/mm).

Set up: See Figure 40.

The object slit (10cm x 4mm) is imaged onto the film after a reduction in magnification by 15x. This method could give good results if the series motor on the drum camera was replaced by a synchronous motor.

Another drawback comes from the fact that the output of the Strobotac is not constant in time. There is an intensity modulation of about 10 to 20% which appears on the film after processing, even though it is a high contrast film.

### B. Michelson Interferometer and drum camera

Set up: See Figure 41.

By adjusting the voltage of the generator such that the total displacement of  $M_2$  is  $\frac{\lambda}{2}$ , the power output varies as:

$$I(t) = 4 I_0 \cos^2 \frac{4\pi \Delta}{\lambda}$$

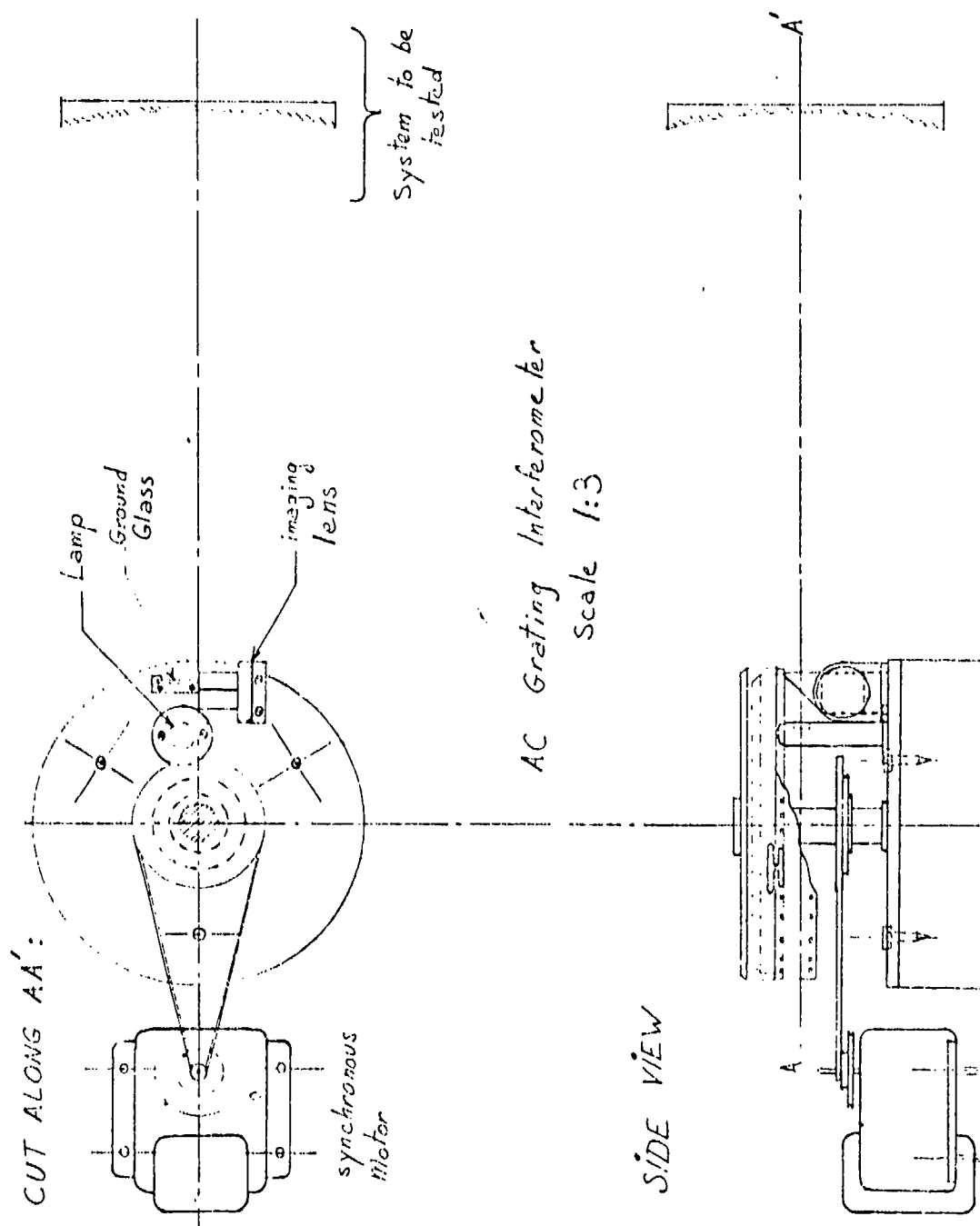


FIGURE 39  
MECHANICAL DESIGN FOR AN  
AC GRATING INTERFEROMETER

SET UP:

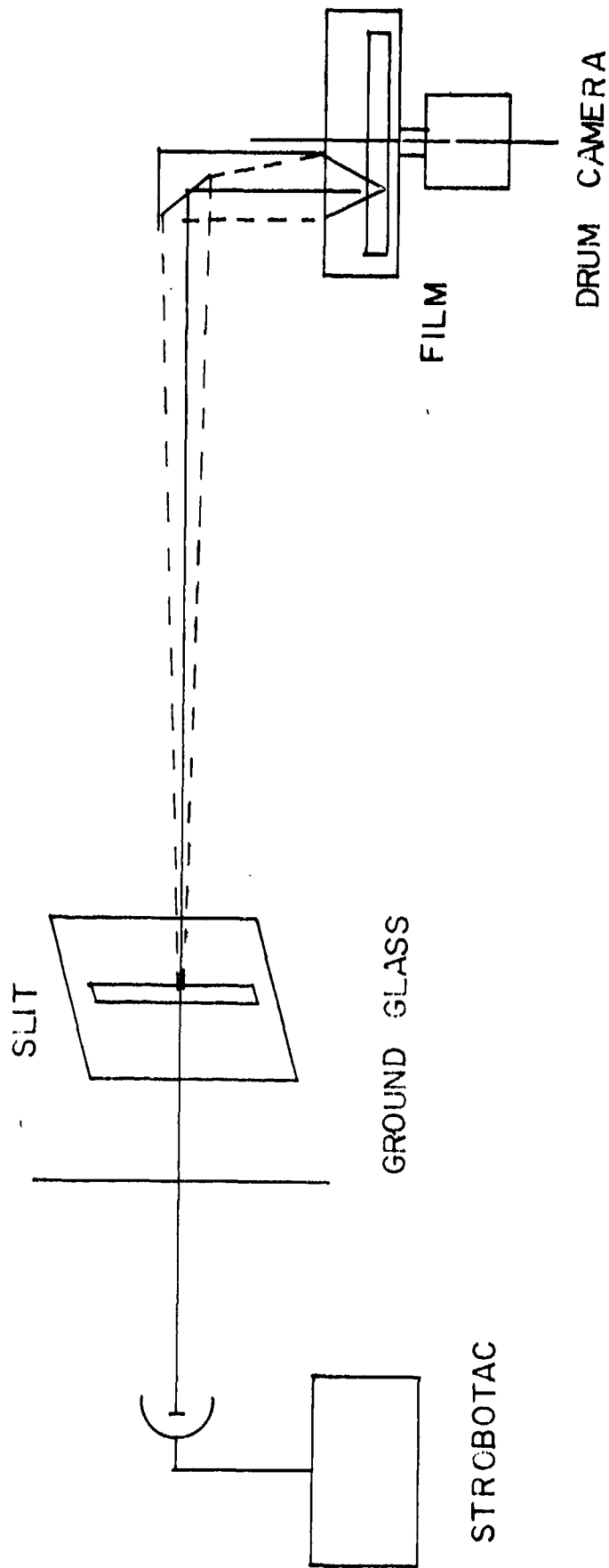


FIGURE 40  
ARRANGEMENT FOR MAKING PHOTOGRAPHIC  
GRATINGS USING A STROBOTAC

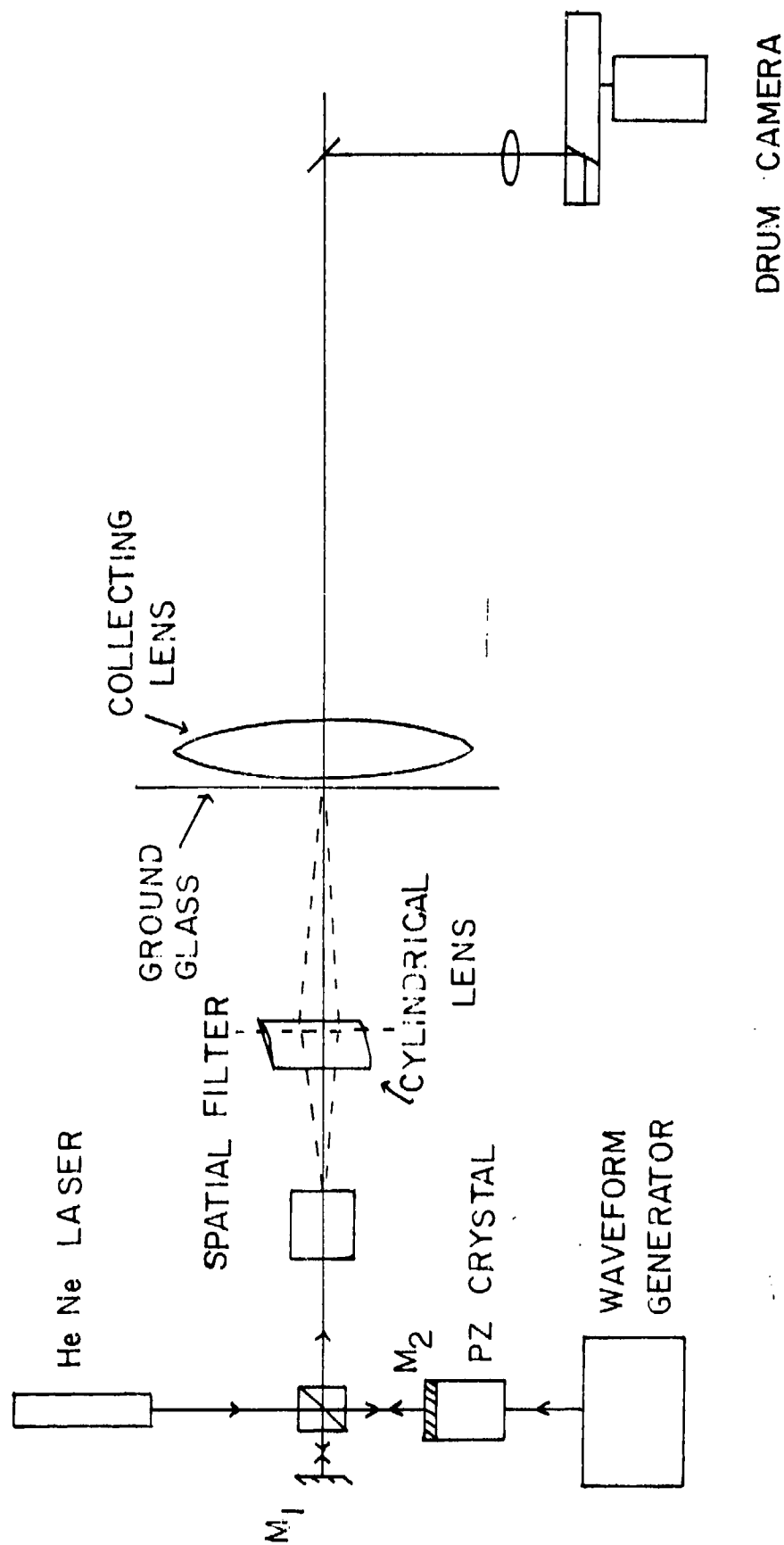


FIGURE 41  
ARRANGEMENT FOR MAKING PHOTOGRAPHIC  
GRATINGS USING A MODULATED LASER

The line given by the cylindrical lens was 10cm x 0.1mm and was imaged through the same demagnification of 15x as before.

This method could have given much higher spatial frequencies than the first one, since we could drive the piezoelectric crystal up to 20 times faster than the strobotac. The results were not satisfactory, though, because of the unstability of the mirror  $M_2$ , which resulted in a non-uniform modulation of the beam.

### C. Interference

Finally we have used the interference from 2 point sources. See Figure 42.

In space, the equi-phase surfaces are hyperboloids whose intersection with the plane of the film gives hyperbolas. See Figure 43.

The distance between two consecutive fringes is:

$$d = \frac{\lambda}{\sin \theta}$$

if  $d_0$  is the spacing at  $P_0$ , the spacing at any point P is:

$$d = d_0 / \cos^3 \phi \cos \psi$$

if  $\phi$  and  $\psi$  are two of the spherical coordinates of P with respect to O. In our case,  $P_0P \ll OP_0$ , so:

$$d \approx d_0 \left(1 + \frac{3\phi^2}{2}\right) \left(1 + \frac{\psi^2}{2}\right)$$

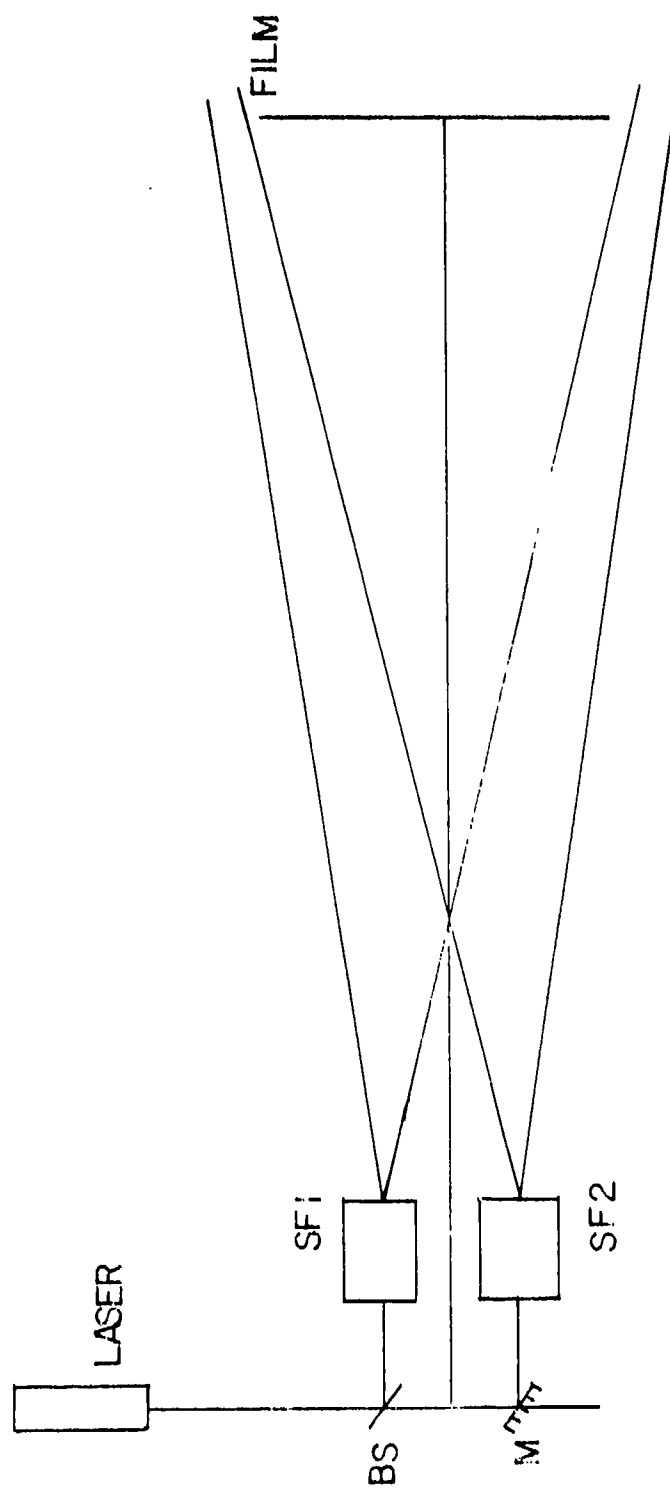


FIGURE 42  
ARRANGEMENT FOR MAKING PHOTOGRAPHIC  
GRATINGS USING AN INTERFEROMETER

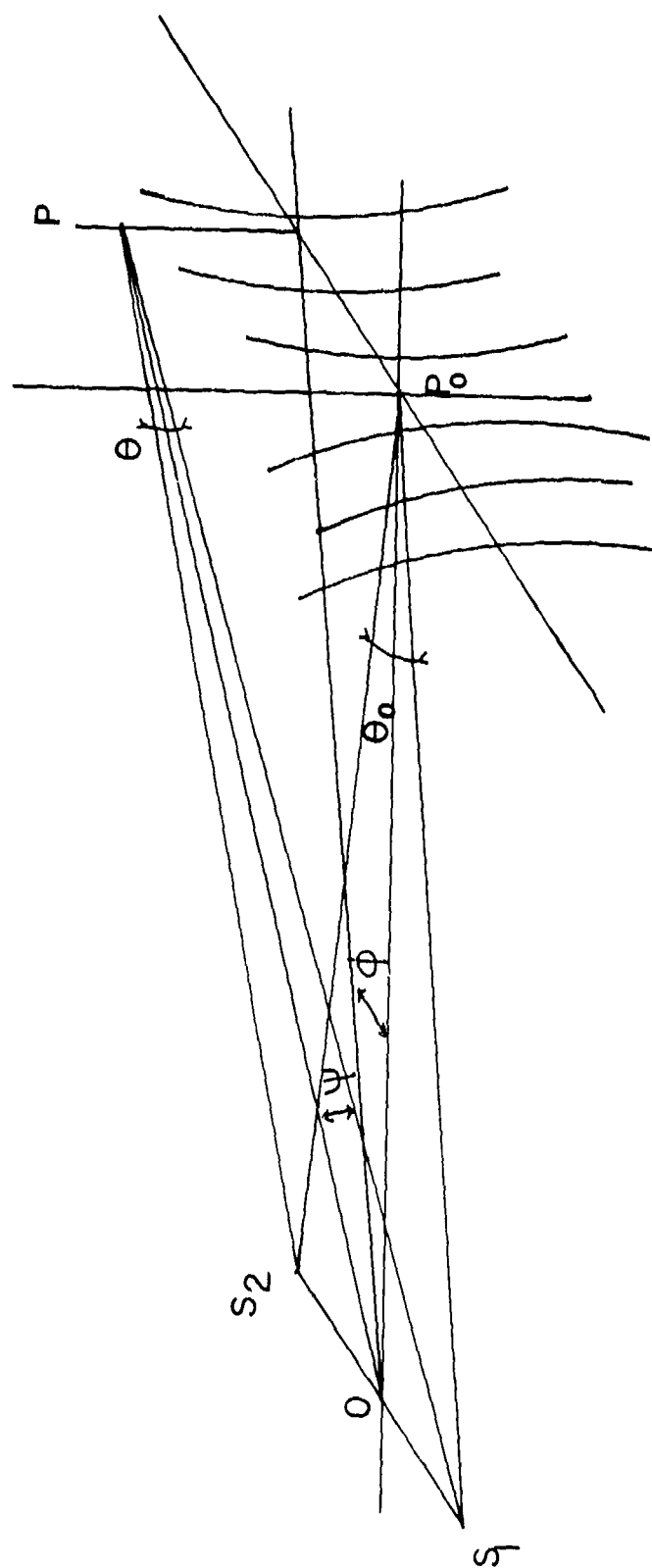


FIGURE 43  
FRINGE GEOMETRY WITH THE  
ARRANGEMENT OF FIGURE 42



The length of the ruling being not more than 50cm and its width not more than 1cm,

$$\frac{d - d_0}{d_0} \leq \frac{3}{2} \left( \frac{25}{400} \right)^2 \approx \frac{3}{500}$$

### Conclusion

In Figures 44, 45, and 46, we show three contact prints of the rulings we have made originally on 16mm high contrast films (Kodak Tri-X). Their spatial frequencies are 1.8, 5, and 18 lines/mm. Even for the lower spatial frequency the maximum transmission is not higher than 0.5 because the density of the base itself in such a film is between 0.1 and 0.2.

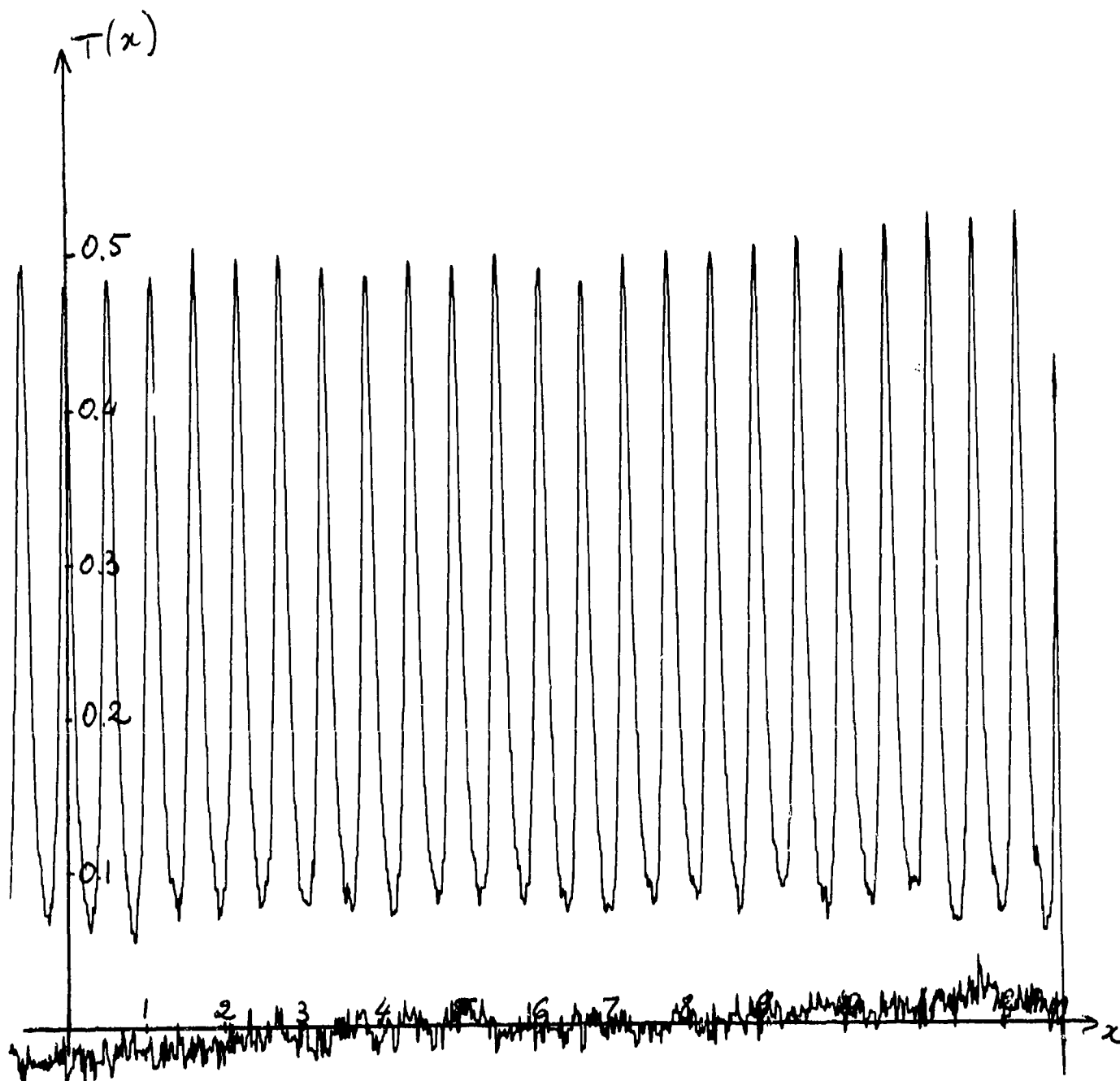


FIGURE 44  
1.8 LINES/MM GRATING

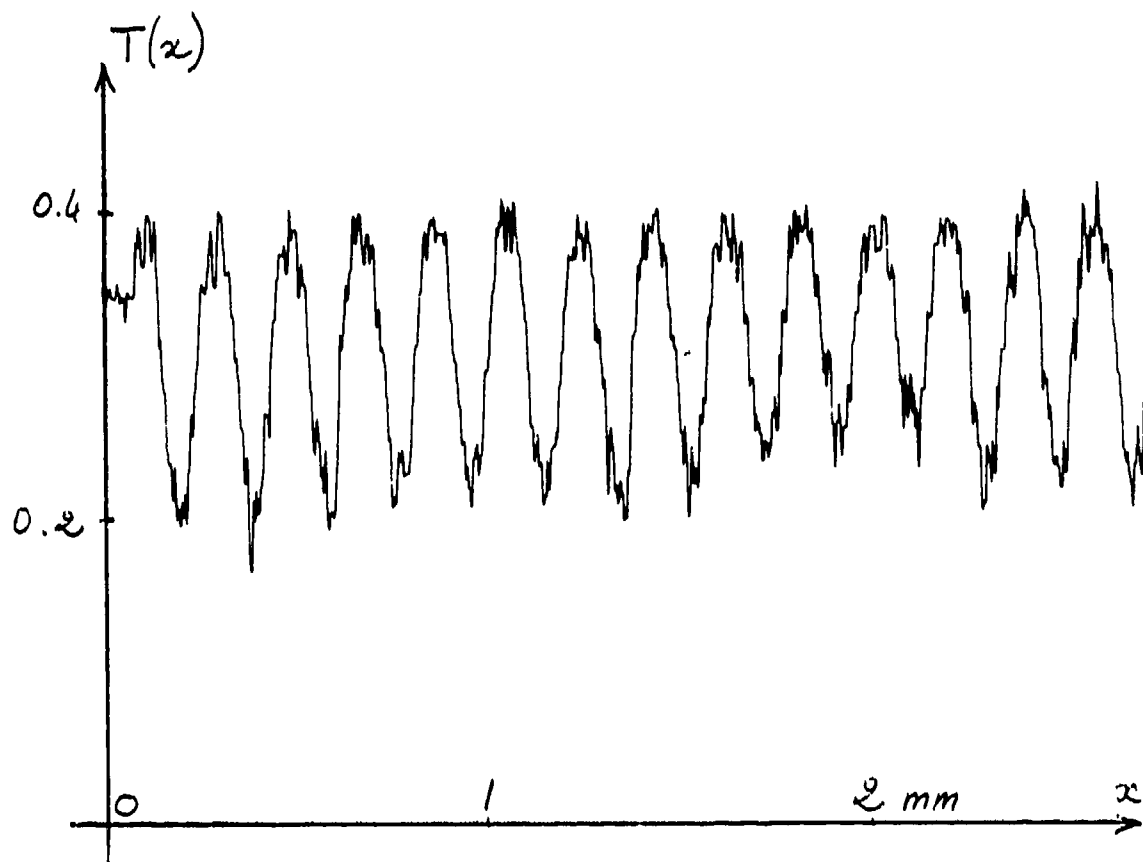


FIGURE 45  
5 LINES/MM GRATING

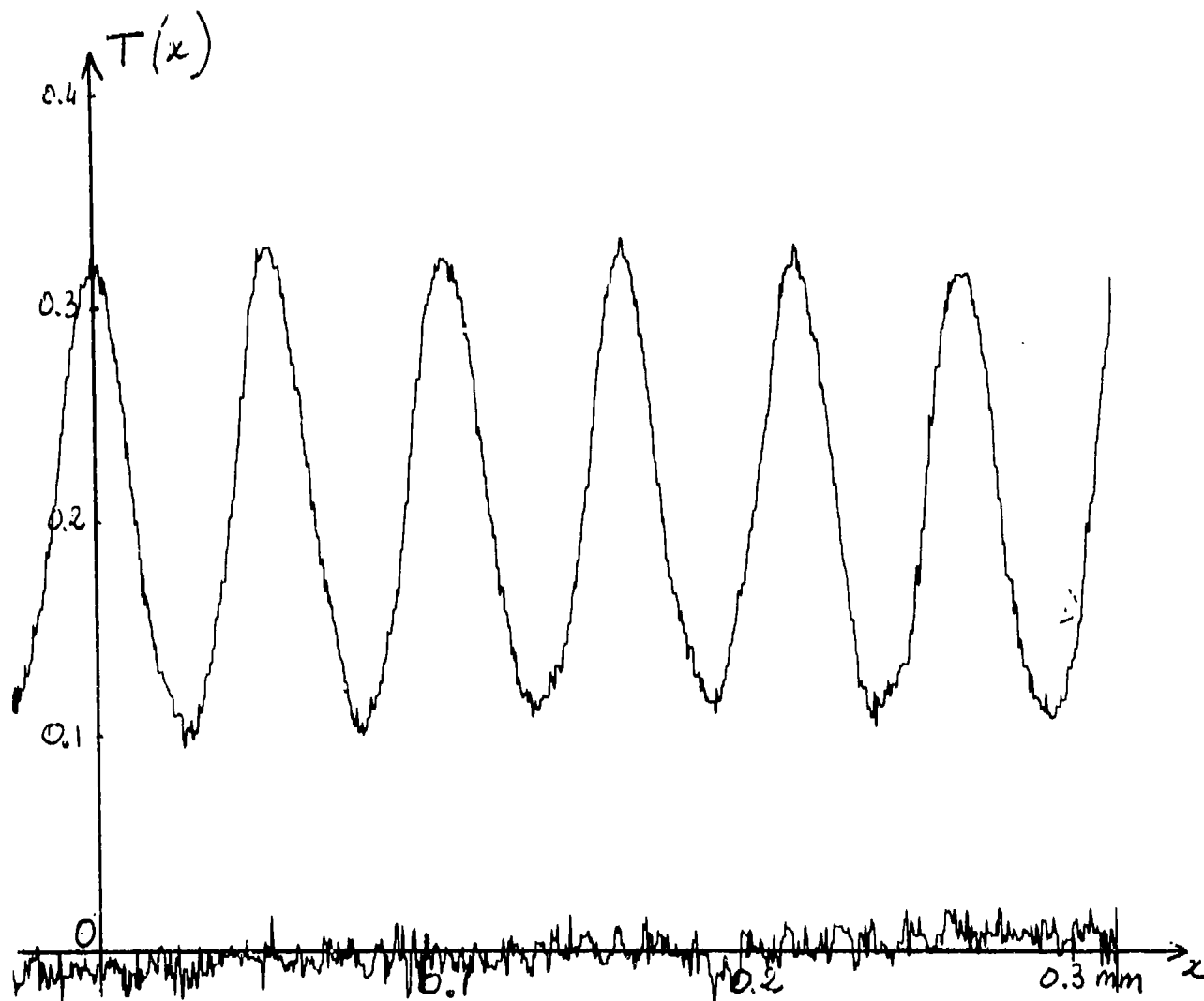


FIGURE 46  
18 LINES/MM GRATING

DOCUMENT CONTROL DATA - R & D

(Security classification of title, body of abstract and indexing annotation must be entered when the overall report is classified)

1. ORIGINATING ACTIVITY (Corporate author) The Institute of Optics The University of Rochester Rochester, New York 14627		2a. REPORT SECURITY CLASSIFICATION unclassified	
		2b. GROUP	
3. REPORT TITLE STUDIES IN OPTICS			
4. DESCRIPTIVE NOTES (Type of report and inclusive dates) Technical. 1970 Feb 13 to 1972 Dec 15			
5. AUTHOR(S) (First name, middle initial, last name) Brian J. Thompson; Michael Hercher; James M. Forsyth; Douglas C. Sinclair; N. Balasubramanian			
6. REPORT DATE April 1973		7a. TOTAL NO. OF PAGES 150	7b. NO. OF REFS 39
8a. CONTRACT OR GRANT NO. F33615-70-C-1151-P00006		9a. ORIGINATOR'S REPORT NUMBER(S) none	
b. PROJECT NO. 745, Amend. 6			
c. Program Code No. 62703-D		9b. OTHER REPORT NO(S) (Any other numbers that may be assigned this report) AFAL-TR- 73-112	
d.			
10. DISTRIBUTION STATEMENT This document is subject to special export controls and each transmittal to foreign governments or foreign nationals may be made only by prior approval of the Air Force Avionics Laboratory, AFAL/TEO.			
11. SUPPLEMENTARY NOTES		12. SPONSORING MILITARY ACTIVITY Advanced Research Projects Agency, Air Force Avionics Laboratory, Air Force Systems Command, Wright-Patterson AFB, Ohio	
13. ABSTRACT These studies in optics relate to a variety of interconnected problems in the evaluation and controlled improvement of the output characteristics of lasers and the design of laser systems. Four major areas of endeavor are focussed upon in the sections of this report. Section II is a study of techniques for assessing laser beam propagation characteristics for both cw and pulsed lasers using holography in conjunction with interferometry. Section III concerns itself with some design problems of efficient solid state laser systems with high average power and low beam divergence with particular reference to the measurement and correction of optical distortion in solid laser rods. Section IV has as its objective a means of producing high-speed continuously scanning laser beams by use of intra-cavity beam deflection. The final portion is an evaluation of the technique of ac interferometry.			

14 KEY WORDS	LINK A		LINK B		LINK C	
	ROLE	WT	ROLE	WT	ROLE	WT
Coherence						
Holography						
Optics						
Lasers						
Interferometry						
Systems, optical						

**THIS REPORT HAS BEEN DELIMITED  
AND CLEARED FOR PUBLIC RELEASE  
UNDER DOD DIRECTIVE 5200.20 AND  
NO RESTRICTIONS ARE IMPOSED UPON  
ITS USE AND DISCLOSURE.**

**DISTRIBUTION STATEMENT A**

**APPROVED FOR PUBLIC RELEASE;  
DISTRIBUTION UNLIMITED.**